To the Graduate Council:

I am submitting herewith a dissertation written by Moon Kyu Ko entitled "Modeling and Control of a Fixed Bed Reactor." I have examined the final copy of this dissertation for form and content and recommend that it be accepted in partial fulfillment of the requirements for the degree of Doctor of Philosophy, with a major in Chemical Engineering.

Duane D. Bruns, Major Professor

We have read this dissertation
and recommend its acceptance:

Accepted for the Council:

Associate Vice Chancellor
and Dean of The Graduate School

MODELING AND CONTROL OF A FIXED BED REACTOR

A Dissertation

Presented for the

Doctor of Philosophy

Degree

The University of Tennessee, Knoxville

Moon Kyu Ko

August 1991

This dissertation is dedicated

to the memory of my dear brother, Young Ho.

ACKNOWLEDGEMENTS

I wish to thank Dr. Duane D. Bruns for his help and support throughout the course of this work. I wish to thank Dr. Charles F. Moore, Dr. Steven M. Serbin, Dr. James J. Downs, and Dr. Tse-Wei Wang for their valuable discussion. I also wish to thank Vinod Shah and my colleagues for their help and friendship.

The Computing Center of the University of Tennessee deserves special thanks for its timely assistance, especially Virginia Patterson, Don Broach, and Sue Smith.

Finally, I wish to thank my parents for their endless support and Jung-Sook for her support and encouragement during the course of this work.

ABSTRACT

A comprehensive study of a fixed bed reactor carrying out the water-gas shift reaction, from the mathematical modeling to controller applications, is presented. The development of the mathematical model for a distributed parameter system in this disseration is oriented toward assisting control system development. It represented a major part of the work in this research. A mathematical model based on mass and energy balances of the reactor system is developed in detail. This partial differential equation model is then discretized by the orthogonal collocation procedure. Dynamic and steady state simulations show the effects of changes in input variables on the reactor output variables and the sensitivity of the state variables to such changes, and thus guides to effective control system configurations.

The development of effective multivariable control strategies depends on the choice of manipulated and controlled variables. Since fixed bed reactors are distributed parameter systems, the selection of sensor locations is a complicated problem associated with sensor sensitivity and interaction. A strategy based on Singular Value Analysis is used to determine the selection of sensor locations and control loop pairing for SISO designs.

In order to deal with the complex behavior of a fixed bed reactor, i.e. nonlinearity, large time delays, and inverse response, the Dynamic Matrix Control or Quadratic Dynamic Matrix Control (DMC/QDMC) algorithm is implemented. A technique is included in the algorithm that allows the controller to predict the future outputs based on the response of the past inputs within the time horizon required to reach a steady state. The QDMC algorithm is a extended version of the DMC algorithm which provides for rigorous handling of process constraints. By using the solution of a quadratic

program, the algorithm calculates required moves for the manipulated variables which minimize the sum of squared differences between the controlled variable projections from set points while maintaining the constrained variables within bounds.

Control of a fixed bed reactor, using the single-input single-output (SISO) DMC or QDMC algorithm, is demonstrated. The control algorithm seems to be very effective in dealing with difficult dynamic process characteristics; nonlinearity, large time delays, and inverse response. DMC or QDMC algorithm shows excellent control system performances when the reactor is subjected to changes in set point or faces a disturbance.

The multi-input multi-output (MIMO) QDMC algorithm is successfully implemented on the reactor. The QDMC algorithm yields excellent preformances in set point tracking and disturbance rejection. The results show the loop interaction handling capability of the MIMO QDMC algorithm, as well as its ability to deal with the inverse response, and large time delays.

TABLE OF CONTENTS

CHAPTER PAGE

CHAPTER PAGE

LIST OF FIGURES

FIGURE PAGE

FIGURE PAGE

FIGURE PAGE

LIST OF TABLES

TABLE PAGE

CHAPTER 1

Introduction

Design of fixed bed reactors and their control presents many exciting areas of research, for example, catalyst development, reactor configuration, numerical methods for solving partial differential equations, ..., onto developing new control strategies. Even considering only process control aspects, a host of topics could be listed, as the need for sensor development, sensor location selection, ..., through robustness issues.

Fixed bed reactor control has been a challenging problem in the chemical industry [13,16,48,58,64,73,74]. These systems are distributed in nature, highly nonlinear, multivariable and complicated due to interaction between temperature and concentration caused by chemical reactions. Such reactors are key elements in many industrial processes so they are constantly subjected to evaluations with emerging new control techniques to enhance their performance.

In general, the primary control objective is to operate within product quality specifications. For a fixed bed reactor, the specifications are typically placed on the exit stream composition. Therefore, it is necessary that the reactor is operated near the design concentration profile. When the reactor is subjected to process disturbances, such as changes in heat input, feed temperature, feed composition and flow rate, a control scheme is require to maintain the profile. Since reliable real time concentration sensors are not available, the control strategy is directed at sustaining the reactor's temperature profile. By controlling the temperature profile it is hoped that the concentration profile

and exit composition are indirectly maintained.

Often secondary control objectives have to be met. In the case of tubular reactors carrying out exothermic reactions controlling the hot spot temperature can be a major concern. Additional complicating factors which must be dealt with in the control of these types of reactors are the inverse response (often referred to as wrong-way behavior) and large dead times.

The major part of this research is devoted to developing a rigorous dynamic model for the water-gas shift reactor. One motivation for this undertaking is to establish a distributed parameter process model that can be utilized in the control studies. Previous work in the department has dealt with lumped parameter models. Thus the modeling effort was initiated with no software available for the dynamic simulation of partial differential equations.

During the past thirty years, a lot of modeling studies have been undertaken ranging from simple to complex using various numerical techniques and different approaches to verify the assumptions used. The fixed bed reactor dynamic model developed here uses major assumptions from previous modeling studies with the intent to provide a rigorous dynamic model for control studies. Thus, the mathematical model is based on the mass, component and energy balances for the reactor. These partial differential equations are then discretized by the orthogonal collocation procedure as the underlying numerical solution procedure. Steady state and dynamic simulations show the effects of changes in input variables on the reactor output variables and their sensitivity to such changes and, thus allow the design of effective control structures.

The success of a control structure for a distributed parameter process depends on the analysis tools available and their use in understanding the process structure and

dynamics. The development of effective control strategies depends on the choice of the controlled and manipulated variables. In the case of single-input single-output (SISO) control, the effectiveness largely depends on the sensitivity between the input and output along with the dynamics between the input and output pair. In the case of multi-input multi-output (MIMO) control, additional complexity is added due to interaction. In this work, these issues are investigated using Singular Value Analysis (SVA) and Relative Gain Array (RGA) based on the reactor temperature steady state gain matrix. This matrix is defined by simulating the steady state changes in the reactor temperatures at the collocation points for step changes in the inputs. The control structures are further evaluated by implementing them on the reactor simulation.

The DMC or QDMC algorithm is an important class of model predictive controller. It is easy to implement and applicable to processes with difficult dynamic characteristics, such as nonlinearities, large time delays, and inverse response behavior. As water-gas shift reactor exhibits all of these troublesome characteristics, some initial studies using the DMC and QDMC algorithms are presented to illustrate the utility of the dynamic model.

The DMC or QDMC algorithm is derived from a technique of representing the dynamics of a process with a set of numerical coefficients. This process description is called the dynamic vector which is derived from a step response of a process output to a manipulated variable. Then, the algorithm assembles the dynamic matrix and applies a least squares formulation to minimized the sum of the squares of error over a time horizon. Implementation of the DMC or QDMC algorithm to this distributed parameter reactor system is based on SVA and RGA steady state studies and on open loop dynamic simulation.

1.1 Research Outline

This dissertation research is organized by chapter in the following manner: Chapter 2 first presents an introduction and brief literature review on modeling and design aspects of packed bed reactors. The development of the distributed water-gas shift reactor models, both steady state and dynamic, are then given. These rigorous models are generated from first principles utilizing established simplifications and assumptions from the literature. Collecting model parameters, model construction, algorithm development, testing and verification of the simulation represent the major part of the present research. Simulation testing and verification included studies on the number of collocation points needed and what error criteria (and thus what integration time step size) was required to yield an accurate simulation. In addition, initial thoughts about a heat integrated system which utilizes the reaction energy in the exit gas from the reactor to heat the feed gas employing a heat exchanger is presented. Finally, steady state and dynamic simulations of the reactor are given. Both the steady state and dynamic simulations show the response of the temperature and conversion profiles to step changes in feed temperature, feed composition and feed flow rate, as well as, in reactor temperature. These simulations provide the information needed to build the steady state gain matrix. They also illustrate the inverse response behavior and dead time characteristics.

Chapter 3 presents a literature survey on control studies of fixed bed reactors. In view of this literature survey, the control problem and objectives of this study are given. Operation of this type of reactor is a regulator control problem. When the reactor is subjected to process disturbances, a control system is required to maintain a specified

concentration profile. Since reliable on-line concentration sensors are not available, the control strategy becomes that of maintaining the reactor temperature profile. By controlling the temperature profile, it is felt that the concentration profile and exit conversion are indirectly maintained.

Chapter 4 address the control problem in terms of maintaining the desired reactor temperature profile. It utilizes analysis of the steady state gain matrix using SVA and RGA to identify the best manipulated variables to use for both SISO and MIMO (2 $\times$ 2) control. It also treats the problem of sensor location in terms of both process conditioning and process interaction.

Chapter 5 contains some initial control studies which evaluate two SISO control strategies and two MIMO control structures. The control schemes are formulated to control specific temperatures in the temperature profile. The success of indirectly maintaining the desired concentration profile by temperature control is addressed. The controller applications focus on the DMC and QDMC algorithms with limited comparison to the classical PI algorithm.

Finally, Chapter 6 discusses conclusions drawn from this research and lists recommendations for future work.

CHAPTER 2

Mathematical Model Development of a Water-Gas Shift Reactor

2.1 Introduction

Dynamic and steady state models have played a central role in the design and optimization of chemical processes and in the development of control strategies. The area of fixed bed reactor modeling has been a subject receiving considerable effort during the past thirty years and is still a challenging problem due to its complexity. Advances in numerical techniques for the solution of partial differential equations have accelerated the development of fixed bed reactor models. These dynamic models of chemical reactors are used for various objectives: i) to describe the steady state and dynamic behavior of chemical reactors for process design and optimization, ii) to investigate the proper start-up procedures, iii) to aid the design of reactor control systems to stabilize the reactor from disturbances, iv) to speed-up reactor recovery from input changes in an optimal way, and v) to aid the determination of the best manipulated and controlled variables for a given control objective.

Fixed bed reactors are used to carry out catalyzed gas-phase, exothermic reactions. The interaction between heat and mass transfer processes have required considerable effort in mathematical modeling. As the temperature and concentration in these chemical reactors are distributed, depending both on time and location, partial differential equations (PDEs) are used to describe their dynamic behavior. Detailed mathematical

models of fixed bed reactors consist of material and energy balances along with descriptions of the reaction kinetics. Direct solutions of these detailed nonlinear PDEs are impossible and numerical approximations are employed where one is faced with many difficulties.

In developing a model one should be concerned about the effects of the model structure, operating conditions, parameters and their sensitivity on the steady-state and dynamic behavior of the reactor model. One way to develop mathematical models is to start from a detailed description of the reactor system and then reduce them to relatively simpler models by retaining essential elements and eliminating or approximating those which are not. To establish a numerical solution methodology a discretization procedure is required to convert the set of PDEs into a set of ODEs. The resulting ODEs are usually of high order (here order refers to the number of first order ODEs in the set of equations) to retain the properties of the original PDEs, but there are no general rules to guide in selecting the order of the model. This relatively high order model makes direct application of modern control theories difficult. As a result, low-order models are often desired for controller design, on-line multivariable control and process optimization. One method, which is often used to determine the model order needed for a good simulation, is eigenvalue analysis associated with modal techniques [14]. In general, some key decisions have to made before pursuing controller design. These include an appropriate order for the model, the dominant modes of the original model and the optimum set of retained state variables.

Advances in the area of numerical techniques for the solution of partial differential equations, such as the orthogonal collocation technique [37,112] , have brought considerable changes in fixed bed reactor modeling. Thus, the formulation and solution of

dynamic models become more accurate even with only a small number of grid points and can be easily extended to its control applications. The following discussions are based on pseudo-homogeneous reactor models and orthogonal collocation techniques for discretization of the PDE model. However the modeling approach and analysis described below should be applicable to any fixed bed reactor system. As a basis for continuing effort in the development of control systems after a brief literature review, the current study presents a mathematical model and analysis of a fixed bed reactor that contains detailed studies of mathematical modeling techniques and aspects of the model development. In addition, common assumptions and numerical solution techniques are discussed.

2.2 Review of Fixed Bed Reactor Modeling

The area of fixed bed reactor modeling has progressed along with numerical techniques for the solution of partial differential equations due to a considerable amount of research effort. In the early stages of a modeling study, steady state analysis is mainly done to provide necessary information for a reactor design. Many aspects of the model are investigated and validated which lead to model simplification. This thesis does not attempt to present a full detailed review of fixed bed reactor modeling since major portions of reaction engineering books [23,39] are devoted to this subject. Instead, this thesis uses some of the major advances in this area as guidelines in its model development procedure.

In general the model can be classified into two categories depending on a distinction between the solid and fluid phases. In the first category, psuedo-homogeneous

models [14,48,58,65] assume that temperature and concentration are identical in both phases at any given position in the reactor. On the other hand, heterogeneous models [27,32,64] describe temperature and concentration profiles in both phases separately. Futhermore in either category of model, additional terms may be introduced to get better descriptions of mass and energy behavior. In a one dimensional model, temperature and concentration profiles are assumed uniform throughout the cross section, while in a two dimensional model these profiles change radially.

Advances in numerical techniques for the solution of partial differential equations have made considerable changes in the area of fixed bed reactor modeling. Application of the orthogonal collocational technique [111,112], which adapts well to split boundary value problems in fixed bed reactor models, has brought major improvement not only in steady state analysis but also in dynamic analysis. The method uses the roots of the Legendre polynomials as collocation points and the Lagrangian polynomials as expansion functions.

Finlayson [37,38] initiated the application of the orthogonal collocation method to steady state packed bed reactor analysis. The method was shown to be faster and more accurate than finite difference techniques. The method was also easily applied to the two dimensional models when radial temperature and concentration profiles were needed. But still the finite difference technique was widely used in the analysis of packed bed reactor models until Jutan et al. [58] presented the application of the orthogonal collocation method in dynamic analysis of a two dimensional packed bed reactor model. The development of a model by this method showed desirable aspects for control studies when the partial differential equations of a nonadiabatic packed bed reactor model were converted to a low order state space model using this method.

Bonvin et al.[14] presented steady state and dynamic analysis of an autothermal fixed bed reactor model carrying out the water-gas shift reaction which uses the heat from exthothermic reaction to preheat the incoming feed gas. A two dimensional homogeneous PDE reactor model was converted to a linear state-variable form suitable for dynamic analysis by using the orthogonal collocational method and the assumption of quasi-steady state for the coolant temperature and concentration profile.

Khanna and Seinfeld [64] presented a dynamic analysis of a fixed bed methanation reactor. A two dimensional heterogeneous model which included axial and radial dispersion of mass and energy, accounted for the axial thermal well which is located in the center of the reactor and used to measure temperatures, and incorporated multiple reactions was discretized by an orthogonal collocation procedure. Their dynamic analysis investigated the effects of reactor operating conditions, and axial and radial diffusion of mass and energy. They also studied the validities of the psudo-homogeneous and quasi-steady state assumptions.

The model developed presented here is based on these past studies in order to develop a more rigorous model for fixed bed reactor control. Dynamic and steady state analysis of a fixed bed reactor will show details of the mathematical modeling techniques used and aspects of the model development.

2.3 Reactor System

Many factors, besides the obvious ones of the desired rate of conversion and composition of the raw and converted gases, have to be considered in the designed and operation of industrial shift reactors [2,3,4,19,76]. Some of these factors are: i) operating charac-

teristics of the catalyst used, such as their chemical and physical characteristics, and temperature limits on their operation, ii) the kinetics of the catalyzed shift reaction, iii) the equipment and proper strategies required to operate normally, as well as, to shut down and start up in a safe manner, and iv) some consideration of construction materials and problems of corrosion.

The heat generation along the reactor is uneven and at the beginning of the reactor it can be so large that an uncontrollable temperature rise can occur. Due to this heat generation by the exothermic reaction, the tubes containing the catalyst have a small inside diameter to ensure a high surface/volume ratio for radial heat transfer through the tube wall. Various types of reactor designs have been used to remove excessive heat due to exothermic reaction. One approach is to use multiple adiabatic reactors in series with a quench feed stream injected between the reactors [40,113,114]. In such a case, control action is done by manipulation of the temperature and feed flow rate of the quench stream injected between the beds. Another approach is to use the autothermal reactor [14,109,110] which is designed so the feed gas passes countercurrently over the outside wall of the reactor tube before it enters the reactor. Therefore part of the heat from exothermic reaction is transferred radially through the reactor wall to preheat the incoming feed stream. Thermal coupling between the incoming feed stream and reactor section creates a unique heat feedback situation which can cause multiple steady states and reactor stability problems. Thus the main concern for this design is focused on the local stability of the reactor. It may even be desirable to operate the reactor at an unstable state. A third approach is to remove the heat of reaction through the reactor walls into an outer jacket filled with a cooling fluid [64]. Such a cooling system is especially useful for highly exothermic reactions and can also be used for heating

up the reactor during start-up to prevent undesired side reactions at low operating temperatures.

A nonadiabatic tubular fixed bed reactor in which the water-gas shift reaction proceeds on an iron-oxide catalyst is selected for model development in this work. The fixed bed reactor under consideration is sketched in Figure 2.1. It consists of a reaction section packed with catalyst and inner wall surrounded by a cooling section. The reactor chamber is approximately 60 cm long, with an inside diameter of 3 cm and is packed with high temperature iron-oxide catalyst. Temperature sensors are located at various axial locations to measure temperature.

2.3.1 Water-Gas Shift Reaction

The reaction considered in this study is the water-gas shift reaction which is a source of commercial hydrogen production. With growing demand for hydrogen in the production of ammonia, processing of petroleum, and other industrial applications, the importance of this reaction continues to grow. The reaction of carbon monoxide with steam to produce hydrogen and carbon dioxide is the water-gas shift reaction.

$$CO + H_2O \rightleftharpoons CO_2 + H_2, \quad \triangle H_o = -9838 \; cal \; gmole^{-1} \tag{2.1}$$

The heat of reaction for the water-gas shift reaction [19] is taken as a linear function of temperature between 400 K and 900 K (see Figure 2.2), where T is in K. The heat of reaction is given by

$$\triangle H^* = -10644 + 2.254T^* \quad cal \; gmole^{-1} \tag{2.2}$$

The reaction is an exothermic reaction governed by thermodynamic equilibrium and promoted by catalyst. The equilibrium constant is reported [11,12] to be independent of

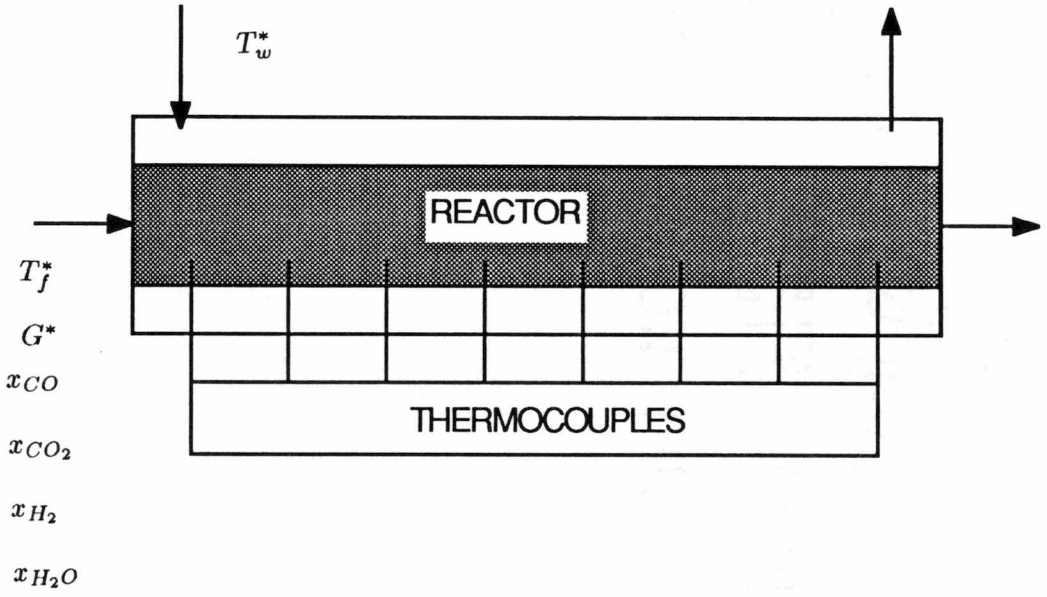

Figure 2.1: Fixed Bed Reactor.

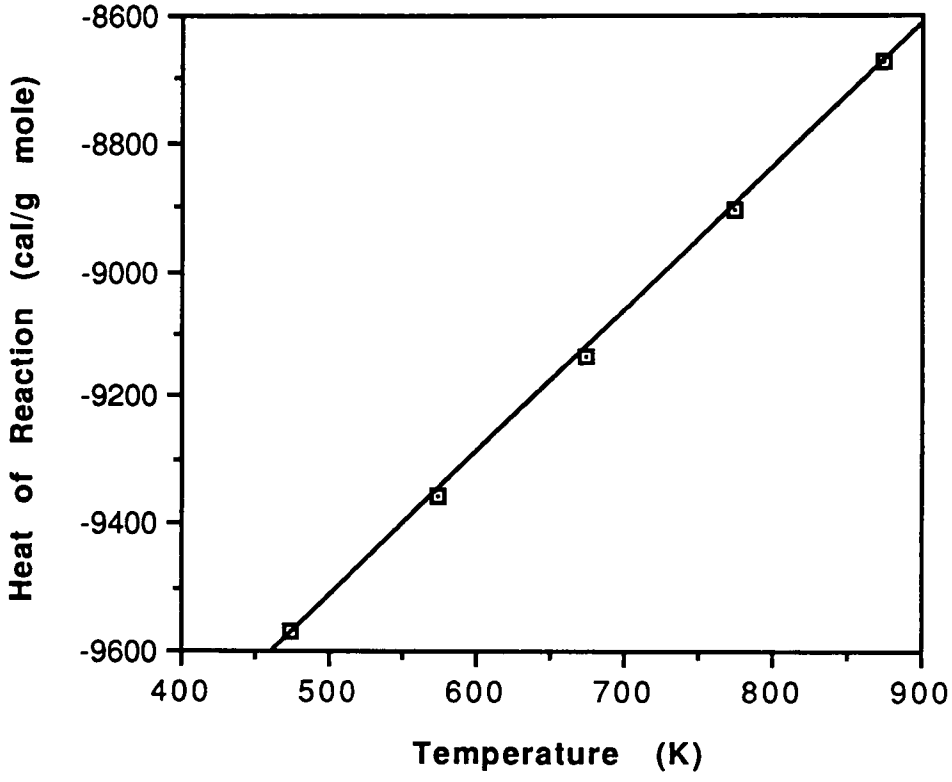

Figure 2.2: Temperature dependence of heat of reaction.

pressure and decreases as the temperature is raised. Thus, high conversions are favored by low temperature. As gas passes through the catalyst bed, the reactor temperature is raised by the heat of reaction and thus the equilibrium conversion becomes less. Typical reactors operate at pressures from 1 to 80 atm, the raw gas may vary from 75% CO to 3% CO, the composition required of the product gas may be down to 0.2% CO and the gas may contain impurities which poison the catalyst.

There are two types of catalysts commercially available [19]:

- High Temperature (HT) catalyst.

    1. Composition: $75-90\%\ Fe_2O_3,\ 5-15\%\ CR_2O_3$
    2. Active temperature range : $330-550°C$

- Low Temperature (LT) catalyst.

    1. Composition: Copper Oxide and Zinc Oxide, plus Aluminum Oxide or Chromium Oxide.
    2. Active temperature range: $200-260°C$.

Reactors are normally designed such that the exit gas composition is close to equilibrium [19]. The cost of this overdesign is accepted so major fluctuations in gas flow rate or modest changes in inlet gas temperature have little impact on the CO conversion and the adiabatic reactor temperature rise. The desired inlet gas temperature is usually determined by calculating the maximum adiabatic temperature assuming equilibrium is reached in the exit gas. The temperature rise should not exceed a $200°C$ range ($300-500°C$) for HT catalysts or a $50°C$ range ($200-250°C$) for LT catalysts. The adiabatic temperature rise in a reactor for each percent (wet basis) of CO converted is

typically $10 - 11°C$. Despite the heat of reaction, the temperature of the catalyst is close to the gas phase temperature. The reported temperature difference between gas and catalyst is only 1 to $2°C$ [19].

There are three main factors that decide the rate equations: reaction kinetics, diffusion of reactants into the catalyst, and diffusion of products back to the gas stream. For moderate pressures (up to 50 atm) when the overall rate of reaction is controlled by bulk diffusion in the HT catalyst pores, the rate equation expressed in terms of mole fractions is as follows [19]

$$\text{Rate of reaction} = P^{1/2} k x_{CO} (1 - \frac{x_{CO_2} x_{H_2}}{x_{H_2O} x_{CO} K_p}) \tag{2.3}$$

where

$$k = k_o exp(\frac{E}{R_g}(\frac{1}{T_{HS}} - \frac{1}{T^*})) \tag{2.4}$$

$$lnK_p = -4.3229 + 4568.3\frac{1}{T^*}, \quad T^* \text{ in K} \tag{2.5}$$

Equilibrium constant data for the water-gas shift reaction [19] is fit as shown in Figure 2.3 for temperatures between 493 K and 783 K to provide Equation 2.5.

This rate equation for the HT catalyst indicates that:

- The forward reaction rate is first order with respect to CO concentration.
- The forward reaction rate is zero order with respect to water vapor.
- The forward reaction rate is retarded as equilibrium conditions are approached.
- The forward reaction is proportional to the 0.5th power of the total pressure.

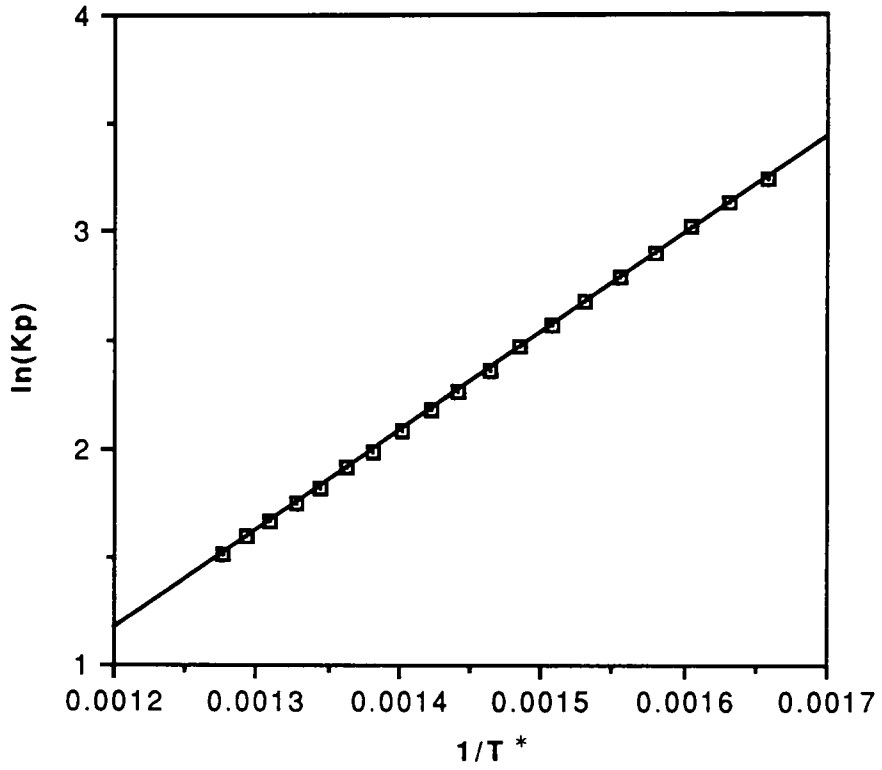

Figure 2.3: Temperature dependence of equilibrium constant.

2.4 Fixed Bed Reactor Model Development

2.4.1 Formulation of a Two Dimensional Dynamic Model

The two dimensional mathematical representation of the fixed bed reactor is fully developed in this section. The common assumptions used in previous studies are considered and their validities are discussed.

The reactor volume is treated as a homogeneous phase based on the assumption that the difference between the catalyst and gas temperatures is negligible in high velocity tubular reactors. Experimental studies [14,55,58] have proved that there is not much difference between the catalyst and the gas temperatures with this difference being only 1 to $2°C$.

Major assumptions which are well established in the literature and used in this study are:

- The velocity profiles in the reactor are uniform, with no radial variation [14,64]. With the radial aspect ratio (tube-to-particle diameters) about 50, experimental observations [55] show radial variations in fluid velocity occur only close to the wall. It appears that a large radial aspect ratio is desirable in many cases, but it can lead to excessive temperature rise due to the highly exothermic reaction.

- The term, $(\rho_s c_{ps}(1-\epsilon) + \rho_g^* c_{pg}^* \epsilon)$, appears in the energy accumulation term of the energy balance. Since $(\rho_s c_{ps}(1-\epsilon))$, associated with the solid phase, is about four orders-of-magnitude larger than $(\rho_g^* c_{pg}^* \epsilon)$, associated with the gas phase, the term, $(\rho_s c_{ps}(1-\epsilon) + \rho_g^* c_{pg}^* \epsilon)$, is reduced to $(\rho_s c_{ps}(1-\epsilon))$ in the PDE energy balance [64,14]. With this simplification and the fact that the temperature of the catalyst

and gas phase are essentially the same (within $2°C$ [19]), a homogeneous model will be used in this study in which the energy accumulation in the gas phase is neglected.

- The axial and radial dispersion of mass in the reaction section are neglected. This is due to the large L/d_p ratio and the large Peclet numbers which are well justified by previous studies [14,64].

- The response of the concentration in the reactor is very fast with respect to the reactor temperature changes. Some studies [14,48] show the time scale between these two differ by about 3 orders-of-magnitude. Therefore, the pseudo-steady state assumption is used for the concentration.

- The reactor wall temperature is the same as the cooling fluid temperature and is uniform over the reactor length [58,64]. This assumption is based on the high thermal conductivity of the reactor wall and on the high convection in the cooling jacket.

- The gas phase density and heat capacity are governed by the ideal gas law.

- The physical properties of the solid catalyst are taken as constants [14,64].

- The pressure drop across the reactor is neglected [14,64].

The effect of temperature on the equilibrium constant, heat of reaction, gas density and velocity is taken into account. The heat capacity of the gas could be treated as a function of temperature throughout the reactor. However, in this study the heat

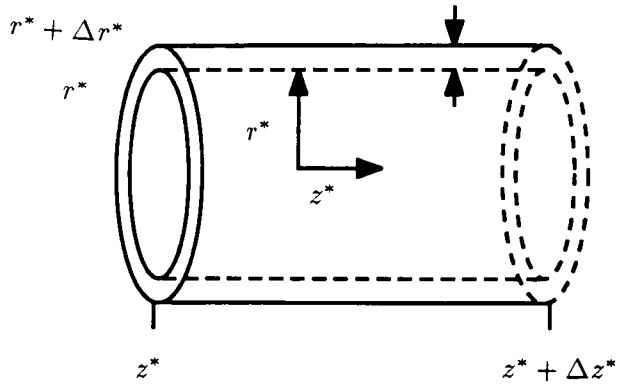

Figure 2.4: Volume element $2\pi r^* \Delta r^* \Delta z^*$ with coordinate system indicating the direction in which mass and thermal energy are transported through the surface.

capacity is calculated based on the feed gas composition averaged over the operating temperature range of 300 to 500°C. This heat capacity is used throughout the reactor.

The full description of the reactor model consists of the energy and component balances with boundary conditions. The following equations are written in general format, but in the development of the dimensionless model in the next section some of the terms will be deleted based on previously discussed assumptions. Note a superscript $*$ is used on all variables that will be made dimensionless for the dimensionless model. The variables not marked with a $*$ are treated as constants. The differential energy and component balances for the reactor can be written in the following form (see Figure 2.4):

Energy Balance in the Reaction Section:

$$\begin{pmatrix} accumulation \\ term \end{pmatrix} = \begin{pmatrix} axial \\ convective \\ term \end{pmatrix} + \begin{pmatrix} axial \\ dispersive \\ term \end{pmatrix} + \begin{pmatrix} radial \\ dispersive \\ term \end{pmatrix} + \begin{pmatrix} reaction \\ term \end{pmatrix}$$

$$2\pi r^*\Delta r^*\Delta z^*\frac{\partial}{\partial t^*}((\rho_s c_{ps}(1-\varepsilon)+\rho_g^* c_{pg}^*\varepsilon)T^*) = \varepsilon 2\pi r^*\Delta r^*(\rho_g^* c_{pg}^* u^* T^*|_{z^*} - \rho_g^* c_{pg}^* u^* T^*|_{z^*+\Delta z^*})$$
$$+2\pi r^*\Delta r^*(-k_z\frac{\partial T^*}{\partial z^*}|_{z^*} + k_z\frac{\partial T^*}{\partial z^*}|_{z^*+\Delta z^*}) + 2\pi r^*\Delta z^*(-k_r\frac{\partial T^*}{\partial r^*}|_{z^*} + k_r\frac{\partial T^*}{\partial r^*}|_{z^*+\Delta z^*})$$
$$+ 2\pi r^*\Delta r^*\Delta z^*(-\Delta H)^* R^* \qquad (2.6)$$

Component Balance on CO in the Reaction Section:

$$\begin{pmatrix} accumulation \\ term \end{pmatrix} = \begin{pmatrix} axial \\ convective \\ term \end{pmatrix} + \begin{pmatrix} axial \\ dispersive \\ term \end{pmatrix} + \begin{pmatrix} reaction \\ term \end{pmatrix}$$

$$\varepsilon 2\pi r^*\Delta r^*\Delta z^*\frac{\partial c_{CO}}{\partial t^*} = \varepsilon 2\pi r^*\Delta r^*(c_{CO}u^*|_{z^*} - c_{CO}u^*|_{z^*+\Delta z^*})$$
$$+ \varepsilon 2\pi r^*\Delta r^*(-D_e\frac{\partial c_{CO}}{\partial z^*}|_{z^*} + D_e\frac{\partial c_{CO}}{\partial z^*}|_{z^*+\Delta z^*}) - 2\pi r^*\Delta r^*\Delta z^* R^* \qquad (2.7)$$

where

$$R^* = P^{1/2}x_{CO}k_o exp(\frac{E}{R_g}(\frac{1}{T_{HS}} - \frac{1}{T^*}))(1 - \frac{x_{CO_2}x_{H_2}}{x_{H_2O}x_{CO}K_p}) \qquad (2.8)$$

Since the boundary has no volume, it can not accumulate energy or mass. Therefore, the axial boundary condition for temperature can be found from an energy balance on a small section at the entrance of the reactor and then let the volume go to zero. The

boundary condition obtained is:

at $z^* = 0$

$$-\pi R^2 k_z \frac{\partial T^*}{\partial z^*} = \pi R^2 \rho_g^* u^* c_{pg}^* (T_f^* - T^*) \tag{2.9}$$

At the end of the reactor, the temperature gradient is generally different from zero but the standard condition of zero gradient is used here [13,64]:

at $z^* = L$

$$k_z \frac{\partial T^*}{\partial z^*} = 0 \tag{2.10}$$

The boundary condition for concentration of CO can be obtained from a mass balance at the entrance of the reactor yielding:

at $z^* = 0$

$$-\varepsilon\pi R_i^2 D_e \frac{\partial c_{CO}}{\partial z^*} = \varepsilon\pi R^2 u^* (c_{CO_o} - c_{CO}) \tag{2.11}$$

Again, the zero gradient condition is assumed for concentration at the end of the reactor:

at $z^* = L$

$$\frac{\partial c_{CO}}{\partial z^*} = 0 \tag{2.12}$$

The radial boundary condition at the wall is obtained from the equal heat flux condition for heat conduction and heat transfer:

at $r^* = R_i$

$$-\pi R_i L k_r \frac{\partial T^*}{\partial r^*} = \pi R_i L h_w (T_w^* - T^*) \tag{2.13}$$

The symmetry condition at the center of the reactor gives:

at $r^* = 0$

$$k_r \frac{\partial T^*}{\partial r^*} = 0 \tag{2.14}$$

Referring to Equation 2.6, since $\rho_g^* c_{pg}^* \varepsilon$ is much smaller than $\rho_s c_{ps}(1-\varepsilon)$, the energy accumulation in the reactant gases phase is much smaller than the energy accumulation in the catalyst phase, so it can be neglected. Introducing the mass flow rate defined as $G^* = \rho_g^* u^*$, the product $\rho_g^* u^*$ is replaced. Recall that using G^* provides some advantages, since it is independent of temperature while ρ_g^* and u^* are functions of temperature.

When Δz^* and Δr^* approach zero, Equations 2.6 to 2.14 give the PDE description of the reactor as follows:

Energy Balance in the Reaction Section:

$$(\rho_s c_{ps}(1-\varepsilon))\frac{\partial T^*}{\partial t^*} = \frac{-\varepsilon G^* c_{pg}^*}{M}\frac{\partial T^*}{\partial z^*} + k_z \frac{\partial^2 T^*}{\partial z^{*2}} + k_r \frac{1}{r^*}\frac{\partial}{\partial r^*}(r^* \frac{\partial T^*}{\partial r^*}) + (-\Delta H)^* R^* \tag{2.15}$$

Component Balance on CO in the Reaction Section:

$$\frac{\partial c_{CO}}{\partial t^*} = -\frac{\partial c_{CO} u^*}{\partial z^*} + D_e \frac{\partial}{\partial z^*}(\frac{\partial c_{CO}}{\partial z^*}) - \frac{R^*}{\varepsilon} \tag{2.16}$$

where

$$R^* = P^{1/2} x_{CO} k_o exp(\frac{E}{R_g}(\frac{1}{T_{HS}} - \frac{1}{T^*}))(1 - \frac{x_{CO_2} x_{H_2}}{x_{H_2O} x_{CO} K_p}) \tag{2.17}$$

with boundary conditions

at $z^* = 0$

$$-k_z \frac{\partial T^*}{\partial z^*} = \frac{G^* c_{pg}^*}{M}(T_f^* - T^*) \tag{2.18}$$

$$-D_e \frac{\partial c_{CO}}{\partial z^*} = u^*(c_{CO_o} - c_{CO}) \tag{2.19}$$

at $z^* = L$

$$k_z \frac{\partial T^*}{\partial z^*} = 0 \tag{2.20}$$

$$\frac{\partial c_{CO}}{\partial z^*} = 0 \tag{2.21}$$

at $r^* = 0$

$$k_r \frac{\partial T^*}{\partial r^*} = 0 \tag{2.22}$$

at $r^* = R_i$

$$-k_r \frac{\partial T^*}{\partial r^*} = h_w(T_w^* - T^*) \tag{2.23}$$

2.4.2 Dimensionless Model

The dynamic behavior in this study is similar to cases presented in the literature [14,48,49]. The response of the concentration in the reactor is very fast with respect to temperature changes. The changes in CO conversion take place much faster than changes in the catalyst bed temperature. Some studies [14,48] show the time scale between these two differ by about 3 orders-of-magnitude. Therefore, this allows the use of the pseudo steady state form of the component mass balance equation in the reaction section, that is, the time derivative, c'_{CO} of Equation 2.16, can be set equal to zero.

The model can be cast into dimensionless form by introducing the dimensionless variables and parameters shown in Table 2.1. The reference time, t_{ref}, which is used to make time dimensionless needs some description. A reference thermal velocity, u_o, with units of cm/sec is introduced. It is approximately the velocity of the thermal wave that moves through the reactor bed in response to feed temperature changes. It is used to define a reference time, t_{ref}, as L/u_o. Thus, t_{ref} is approximately the time that it takes for the thermal wave to propagate from the entrance to the exit of the reactor. For the sake of convenience in notation all variables used in the remainder of this study are dimensionless, unless it is specified otherwise. Note the dimensionless variables do not have the superscript $*$. The energy and component mass balances given by Equation 2.15 to 2.23 stated in dimensionless form are:

$$\frac{\partial T}{\partial t} = v_a \frac{\partial^2 T}{\partial z^2} - c_{pg} G \xi \frac{\partial T}{\partial z} + v_r \frac{1}{r} \frac{\partial}{\partial r}(r \frac{\partial T}{\partial r}) + (-\Delta H)\beta_a R \tag{2.24}$$

$$0 = \frac{\partial x}{\partial z} - G\beta_b R \tag{2.25}$$

Note that the quasi-steady state assumption has been incorporated with into Equa-

Table 2.1: Dimensionless Variables and Parameters

Dimensionless Variables		
$r = \frac{r^*}{R_i}$	$t = \frac{t^*}{t_{ref}}$	$T = \frac{T^*}{T_{ref}}$
$T_f = \frac{T_f^*}{T_{ref}}$	$T_w = \frac{T_w^*}{T_{ref}}$	$G = \frac{G^*}{G_{ref}}$
$x = \frac{c_{CO_o} - c_{CO}}{c_{CO_o}}$	$z = \frac{z^*}{L}$	$c_{pg} = \frac{c_{pg}^*}{c_{pg_{ref}}}$
$\Delta H = \frac{\Delta H^*}{\Delta H_{ref}}$		
Dimensionless Parameters		
$\gamma = \frac{E}{R_g T_{ref}}$	$\beta_a = \frac{P^{1/2} L k_o \Delta H_{ref}}{\rho_s c_{ps}(1-\epsilon) u_o T_{ref}}$	$\beta_b = \frac{P^{1/2} L k_o}{\epsilon G_{ref}}$
$\xi = \frac{G_{ref} c_{pg_{ref}} \epsilon}{\rho_s c_{ps}(1-\epsilon) u_o}$	$\upsilon_a = \frac{k_z}{\rho_s c_{ps}(1-\epsilon) u_o L}$	$\upsilon_m = \frac{G_{ref} L}{M_{ref} c_o D_e}$
$\upsilon_r = \frac{k_r L}{\rho_s c_{ps}(1-\epsilon) u_o R_i^2}$	$\upsilon_w = \frac{G_{ref} c_{pg_{ref}} \epsilon L}{k_r}$	$\psi = \frac{8 \upsilon_r B_i}{4 + B_i}$
$B_i = \frac{h_w R_i}{k_r}$		

tion 2.25. The dimensionless reaction rate is expressed as:

$$R = x_{CO_o}(1-x)exp(\gamma(\frac{T_{ref}}{T_{HS}} - \frac{1}{T}))(1 - \frac{(x_{CO_{2_o}} + x_{CO_o}x)(x_{H_{2_o}} + x_{CO_o}x)}{(x_{H_2O_o} - x_{CO_o}x)x_{CO_o}(1-x)K_p}) \quad (2.26)$$

with boundary conditions

at $z = 0$

$$\frac{\partial T}{\partial z} = Gv_w(T - T_f) \quad (2.27)$$

$$\frac{\partial x}{\partial z} = Gv_m x \quad (2.28)$$

at $z = 1$

$$\frac{\partial T}{\partial z} = 0 \quad (2.29)$$

$$\frac{\partial x}{\partial z} = 0 \quad (2.30)$$

at $r = 0$

$$\frac{\partial T}{\partial r} = 0 \quad (2.31)$$

at $r = 1$

$$\frac{\partial T}{\partial r} = Bi(T - T_w) \quad (2.32)$$

2.4.3 Orthogonal Collocation Method

The chemical reactor system of coupled nonlinear partial differential equations with split boundary conditions is too complex to solve analytically. Therefore a considerable amount of effort has been put into numerical solution techniques for complex nonlinear chemical reactors during the past twenty years [37,112]. Application of the orthogonal collocation method has proven to be very effective in the area of nonlinear chemical reactor systems. Thus, the following formulation is based on the fundamentals of the

method given by Villadsen and Stewart [112]. This section describes how the technique is applied to the fixed bed reactor model. For a more detailed description the reader is referred to their book.

Expansions of trial functions are widely used in solving boundary-value problems. The coefficients of the expansions are typically determined by the weighted residual method or variational principles. The unknown solution is expanded in a set of trial functions which are chosen to produce the approximate solution of the differential equation and satisfy the boundary conditions. When this trial function is substitued into the differential equation, the residual is formed. The residual will become zero when this trial function is the exact solution. In this method the coefficients of the trial function are chosen such the the residual is forced to be zero in an average sense. The weighted integrals of the residual are set to zero:

$$\int_V w_j R dV = 0, j = 1, ..., N \tag{2.33}$$

One method of weighted residuals is the collocation method. In this method, the weighting functions are chosen to be the Dirac delta function.

$$w_j = \delta(z - z_j) \tag{2.34}$$

Thus the residuals, R,

$$\int_V w_j R dV = R \mid_{z_j} \tag{2.35}$$

become zero except at the specified collocation points. Then the technique forces the residual to be zero at the specified collocation points. As the number of collocation points increases, the residual is zero at more and more points and presumably approaches zero everywhere.

In other techniques, difficulties often arise due to the evaluation of Equation 2.35 when the integrals involves complex nonlinear terms, but the collocation method is only required to evaluate the residual at the collocation points due to the weighting function being the Dirac delta. The orthogonal collocation method, which is a collocation method with collocation points chosen to be the zeros of any Jacobi polynomial, was fully developed by Villadsen and Stewart [111] for boundary value problems. The collocation points are chosen optimally and the error decreases faster as the number of collocation points increase. The trial functions are chosen as orthogonal polynomials which satisfy the boundary conditions and the roots of the polynomial are selected as collocation points. The collocation points are calculated using a program given by Villadsen and Michelsen [112] where the roots of Jacobi polynomial satisfy the orthogonal relationship. Furthermore this approach can be simplified such the solution can be derived in terms of its value at the collocation points, instead of the coefficients of the trial functions. Compared to finite difference schemes, where derivatives are expressed in terms of the neighboring grid points, the collocation method expresses derivatives in terms of the solutions at each collocation point in the collocation scheme. Thus the orthogonal collocation method can be relatively easy to program and the numerical solution requires a small number of collocation points compared to the number of grid points necessary for a finite difference scheme [37,38].

2.4.4 Discretization by Orthogonal Collocation

The orthogonal collocation procedure with a single interior collocation point in the radial direction treats the radial temperature profile as parabolic. A single interior collocation point in the radial direction was successfully used by Jutan [58] and Bonvin [14] in order

to keep the size of the resulting set of PDEs manageable. The same type of application of the orthogonal collocation procedure in the radial direction for the water-gas shift reactor model is based on the assumption of a parabolic radial temperature profile which can be expressed as a function of the radius. The assumed temperature profile can be presented in the following form:

$$T(z,r,t) = d_0(z,t) + d_1(z,t)r + d_2(z,t)r^2 \tag{2.36}$$

where d_0, d_1 and d_2 are functions of the z coordinate and time. Since the assumed profile should satisfy the boundary conditions 2.31 and 2.32, the second term, $d_1(z,t)$, drops out and Equation 2.36 becomes:

$$T(z,r,t) = d_0(z,t) + d_2(z,t)r^2 \tag{2.37}$$

where

$$d_2(z,t) = \frac{Bi}{2}(T(z,1,t) - T_w(z,t)) \tag{2.38}$$

The single interior collocation point is chosen from the root of the first shifted Legendre orthogonal polynomial (r=0.707). At r=0.707 the temperature represents the reactor bed temperature at each axial cross section. Now the reactor temperature can be expresssed at each collocation point in the following form:

$$T(z,0,t) = d_0 \tag{2.39}$$

$$T(z,.707,t) = d_0 + d_2/2 \tag{2.40}$$

$$T(z,1,t) = d_0 + d_2 \tag{2.41}$$

Equations 2.39 through 2.41 can be used to express temperatures T(z,0,t) and T(z,1,t) in terms of the temperatures T(z,.707,t) and T_w. Therefore, Equation 2.36 becomes:

$$T(z,r,t) = \frac{1}{4+Bi}((4+2Bi)T(z,.707,t) - BiT_w(z,t) - 2Bi(T(z,.707,t) - T_w(z,t))r^2) \tag{2.42}$$

This equation is used to evaluate the first and second derivatives of the reactor temperature T in the radial direction:

$$r\frac{\partial T}{\partial r} = -\frac{4Bi}{4+Bi}(T(z,.707,t) - T_w(z,t))r^2 \tag{2.43}$$

$$\frac{1}{r}\frac{\partial}{\partial r}(r\frac{\partial T}{\partial r}) = -\frac{8Bi}{4+Bi}(T(z,.707,t) - T_w(z,t)) \tag{2.44}$$

Then, Equation 2.24 and 2.25 become:

$$\frac{\partial T}{\partial t} = v_a\frac{\partial^2 T}{\partial z^2} - Gc_{pg}\xi\frac{\partial T}{\partial z} - \psi(T - T_w) + (-\Delta H)\beta_a R \tag{2.45}$$

$$0 = \frac{\partial x}{\partial z} - G\beta_b R \tag{2.46}$$

where the boundary conditions in the radial directions, Equation 2.27 and 2.28, are imbeded by the collocation procedure into the resulting equations. Note that with a single interior point in the radial direction, the number of PDEs has not been increased.

The resulting radially lumped model still consists of coupled, nonlinear PDEs. Since it is still too complex to solve analytically, discretization in the axial coordinate is done by the method of orthogonal collocation with N interior collocation points. Although orthogonal collocation in the axial direction transforms the equations into a large set of ordinary differential equations, they can be solved using conventional techniques. The collocation points are chosen as the roots of the Nth order shifted Legendre polynomial. There are N interior collocation points and 2 boundary condition points for the reactor temperatures and conversions. The assumed axial profiles of temperature and conversion

are expressed as follows:

$$T(z,t) = \sum_{i=1}^{N+2} T_i(t)\iota_i(z) \tag{2.47}$$

$$x(z,t) = \sum_{i=1}^{N+2} x_i(t)\iota_i(z) \tag{2.48}$$

where T_i and z_i are the values of the dependent variables at ith collocation point. The polynomials, $\iota_i(z)$ are (N+1)st-order Lagrange polynomials for the ith collocation point:

$$\iota_i(z) = \sum_{j=1,i\neq j}^{N+2} \frac{(z - z_j)}{(z_i - zj)} \tag{2.49}$$

Since only one Lagrangian is not zero at each collocation point and the residual is forced to zero at that point, the coefficient of Lagrangian term is the solution at that point.

The remainder of the derivation is straightforward but requires lengthy algebraic manipulations. Therefore it is not included here, instead each step is described below.

1. Since the $\iota_i(z)$ are known functions based on the collocation points, evaluate the axial derivatives $\frac{\partial T}{\partial z}, \frac{\partial^2 T}{\partial z^2}, \frac{\partial x}{\partial z}, \frac{\partial^2 x}{\partial z^2}$ and then substitue back into the PDEs (Equations 2.45– 2.46) and the corresponding boundary conditions (Equations 2.27– 2.30).

2. The assumed solution must satisfy the boundary conditions. By combining Equations 2.45– 2.46 with the corresponding boundary conditions (Equations 2.27– 2.30), the unknowns at each end point $(T_1, T_{N+2}, x_1, x_{N+2})$ can be expressed as functions of the dependent variables at the N interior collocation points.

The resulting equations are N coupled, nonlinear ODEs, and N coupled nonlinear algebraic equations as following:

$$
\begin{aligned}
T_j' = \quad & v_a \textstyle\sum_{i=2}^{N+1}(B_{j,i} + H1(-B_{j,1}A_{N+2,N+2} + B_{j,N+2}A_{N+2,1})A_{1,i} \\
& + H1(B_{j,1}A_{1,N+2} + B_{j,N+2}(A_{1,1} - Gv_w)A_{N+2,i})T_i \\
& - Gc_{pg}\xi \textstyle\sum_{i=2}^{N+1}(A_{j,i} + H1(-A_{j,1}A_{N+2,N+2} + A_{j,N+2}A_{N+2,1})A_{1,i} \\
& + H1(A_{j,1}A_{1,N+2} + A_{j,N+2}(A_{1,1} - Gv_w)A_{N+2,i})T_i \\
& + H1(v_a(-B_{j,1}A_{N+2,N+2} + B_{j,N+2}A_{N+2,1}) \\
& - Gc_{pg}\xi(-A_{j,1}A_{N+2,N+2} + A_{j,N+2}A_{N+2,1}))Gv_wT_f \\
& - \psi(T_j - T_w) + (-\Delta H)\beta_a R \qquad (2.50) \\
0 = \quad & \textstyle\sum_{i=2}^{N+1} A_{j,i}x_i + H2(-A_{j,1}A_{N+2,N+2} + A_{j,N+2}A_{N+2,1}) \textstyle\sum_{i=2}^{N+1}(-A_{1,i}x_i) \\
& + H2(A_{j,1}A_{1,N+2} + A_{j,N+2}(A_{1,1} + Gv_m)) \textstyle\sum_{i=2}^{N+1} A_{N+2,i}x_i \\
& + G\beta_b R \qquad (2.51)
\end{aligned}
$$

where $B_{i,j}$ and $A_{i,j}$ are collocation matrices, H1 and H2 are collocation quantities, and T, T_w, T_f, and x are the vectors.

This nonlinear ODE model is mathematically much more tractable than the original nonlinear PDEs. The nonlinear ODE model is used to simulated the dynamic behavior of the fixed bed reactor and evaluate controller performance in this study.

However, the model could be transformed into a linear state-variable model for Linear Control Theory to evaluate or design control structures [13,60]. In such a case, the inputs are mass flow rate (G), feed temperature (T_f), wall temperature (T_w) and feed composition (CO, CO_2, H_2, and H_2O concentrations). This transformation is made by linearizing around the steady state operating conditions which leads to equations that could be written in the following form:

$$T' = A_{11}T + A_{12}x + A_{13}G + A_{14}T_f + A_{15}x_{CO_o} + A_{16}x_{CO_{2_o}} + A_{17}x_{H_{2_o}} + A_{18}x_{H_2O_o} + A_{19}T_w \quad (2.52)$$

$$0 = A_{21}T + A_{22}x + A_{23}G + A_{24}x_{CO_o} + A_{25}x_{CO_{2_o}} + A_{26}x_{H_{2_o}} + A_{27}x_{H_2O_o} \quad (2.53)$$

The linearized form of Equation 2.53 could be solved for x in terms of T and substitution made back into Equation 2.52. Then Equation 2.52 would be in the state space form where T' are the state variables and G, T_f, T_w, x_{CO_o}, $x_{CO_{2_o}}$, $x_{H_{2_o}}$, $x_{H_2O_o}$ are the manipulated variables.

It should be noted that the proposed control studies for conventional PI controllers and DMC do not require the development of such a linearized model. Examples of DMC algorithm implementation show that it can handle difficult dynamic characteristics, such as nonlinear behavior, inverse response, and nonminimum phase. This is an often listed advantage of DMC. Thus, this study will not develop a linearized ODE model.

2.5 Heat Exchanger Model

In order to consider a heat integrated system which utilizes the reaction energy in the exit gas from the reactor to heat the feed gas, a heat exchanger could be used (see Figure 2.5). The type of heat exchanger (gas-to-gas) needed requires a larger heat transfer area. For initial study purposes, the model of the Economizer (the heat exchanger) should be as simple as possible since it is a secondary unit, then depending on the results the model could be modified. Ideally the simulation should be compared with experiment. In that sense, three different types of models are described.

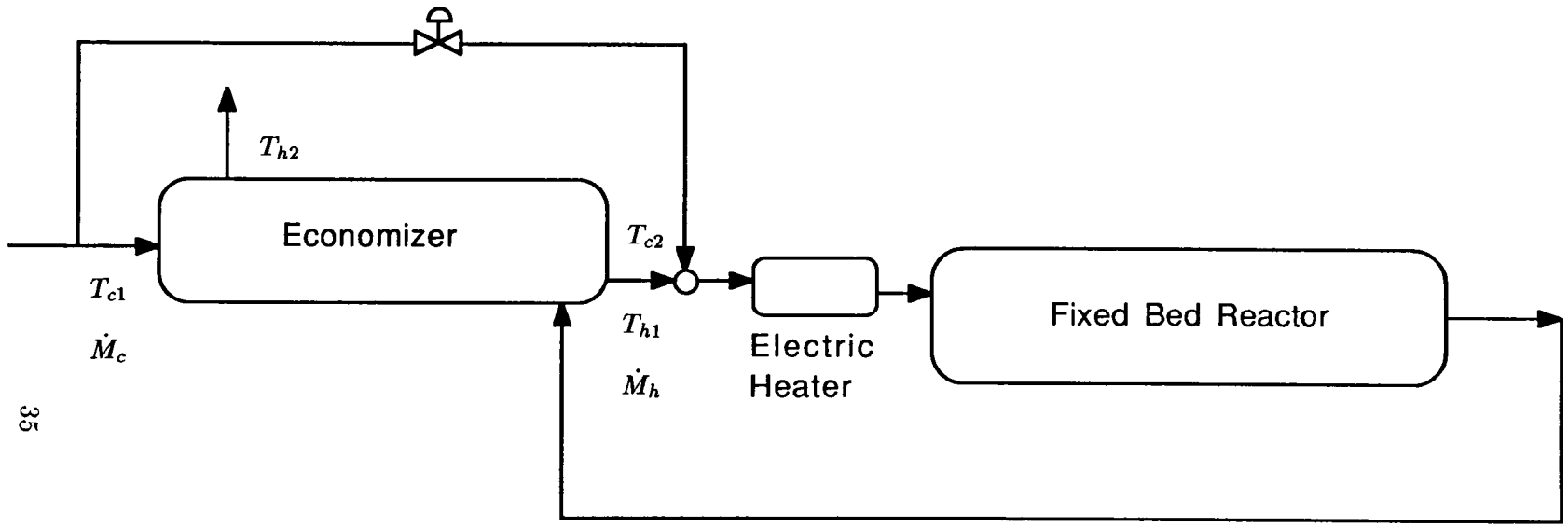

Figure 2.5: Fixed Bed Reactor with Economizer System(Heat Exchanger).

Case A) Nonlinear Steady State Model

A nonlinear steady state model based on the overall heat transfer coefficient and log mean temperature driving force is easily formulated. The rate of heat transfer is:

$$Q_{HT} = U_o A_o (\Delta T)_{LM} \tag{2.54}$$

where for counter current flow

$$\Delta T_{LM} = \frac{(T_{h1} - T_{c2}) - (T_{h2} - T_{c1})}{ln\frac{T_{h1}-T_{c2}}{T_{h2}-T_{c1}}} \tag{2.55}$$

Incorporating the energy balances gives:

$$Q^h_{EB} = \dot{M}_h c_{pg} (T_{h1} - T_{h2}) \tag{2.56}$$

$$Q^c_{EB} = \dot{M}_c c_{pg} (T_{c2} - T_{c1}) \tag{2.57}$$

If heat loss to the ambient air is neglected, then Equations 2.54- 2.57 can be written as

$$Q^c_{EB} = Q^h_{EB} = Q_{HT} \tag{2.58}$$

In this case, the unknown variables and parameters which are either to be solved for or defined, are

Unknown variables: T_{h2}, T_{c2}, Q_{HT}, Q^c_{EB}, Q^h_{EB}

Unknown parameters: U_o, A_o

This set of equations can be solved iteratively by the Newton-Raphson method.

Case B) Transfer Function Model with Variable Dead Times

In general, the response of heat exchangers can be fit with first order with dead time transfer functions. Since the transportation lags vary significantly with the flow rates

the dead times should be expressed as functions of the two gas flow rates. This leads to a transfer function description as follows:

$$\begin{bmatrix} T_{c2} \\ T_{h2} \end{bmatrix} = \begin{bmatrix} G_{11}, G_{12}, G_{13}, G_{14} \\ G_{21}, G_{22}, G_{23}, G_{24} \end{bmatrix} \begin{bmatrix} T_{c1} \\ T_{h1} \\ \dot{M}_c \\ \dot{M}_h \end{bmatrix} \tag{2.59}$$

where

$$G_{i,j}(s) = \frac{K_{i,j} e^{-t_{d_{i,j}} s}}{\tau_{i,j} s + 1} \tag{2.60}$$

$$t_{d_{i,j}} = f(\dot{M}_c, \dot{M}_h) \tag{2.61}$$

In this case, the unknown variables and parameters to be defined are

Unknown parameters: $K_{i,j}$, $\tau_{i,j}$,

Unknown functions: $t_{d_{i,j}}$

Case C) Transfer Function Model with Variable Dead Times, Time Constants and Gains

This model also assumes that the heat exchanger response can be fit with first order with dead time transfer functions in more general form. In this case, the gain, time constant and dead time may be functions of temperature and mass flow rate. Thus, the

transfer function for model formulation would be

$$\begin{bmatrix} T_{c2} \\ T_{h2} \end{bmatrix} = \begin{bmatrix} G_{11}, G_{12}, G_{13}, G_{14} \\ G_{21}, G_{22}, G_{23}, G_{24} \end{bmatrix} \begin{bmatrix} T_{c1} \\ T_{h1} \\ \dot{M}_c \\ \dot{M}_h \end{bmatrix} \tag{2.62}$$

where

$$G_{i,j}(s) = \frac{K_{i,j} e^{-t_{d_{i,j}} s}}{\tau_{i,j} s + 1} \tag{2.63}$$

where

$$t_{d_{i,j}} = f(\dot{M}_c, \dot{M}_h) \tag{2.64}$$

$$K_{i,j} = f(\dot{M}_c, \dot{M}_h, T) \tag{2.65}$$

$$\tau_{i,j} = f(\dot{M}_c, \dot{M}_h, T) \tag{2.66}$$

In this case, the unknown functions to be defined are $K_{i,j}$, $\tau_{i,j}$, and $t_{d_{i,j}}$.

The incorporation of an economizer model with the reactor simulation is suggested as a topic for continuing the research beyond the present dissertation. It is anticipated

that such an addition will make the control study more applicable to some industrial operations. In this regard a study found in the literature includes a heat exchanger. It is directed at the development of a dynamic model for control studies [71] which are concerned with system stability. Adding a heat exchanger to the present simulation will add the aspect of stability problems due to the inherent heat feedback added to the process operation. In many respects this is similar to the autothermal reactor [14] where heat transfer between the reactor section and feed stream takes place in a countercurrent flow arrangement. This type of heat feedback is responsible for multiple steady states found in this autothermal reactor. Thus control of this type of system also is concerned with system stability.

The goals of the present research agenda are to establish the dynamic reactor simulation and to initiate evaluation of some new control strategies based on the dynamic simulation. The attractive problem of reactor operation heat integrated with the heat exchanger is left as an enticement to future use of the reactor simulation.

2.6 Numerical Simulation

Steady state profiles can be obtained from the dynamic nonlinear collocation model. When the time derivatives of Equations 2.52 and 2.53 are set equal to zero, the resulting 2N+4 nonlinear algebraic equations can be solved iteratively by the Newton-Raphson method. They can also be obtained from the dynamic simulation by integrating until the steady state solution is reached. In some extreme cases where solution for steep axial profiles causes numerical convergence problems, it may be necessary to use the dynamic simulation results as an initial guess to obtain a solution from the steady state

algorithm.

The steady state solution also can be used as the expansion point in a linearization procedure to generate a linear model. It also can help in finding the region of steady-state multiplicity for reactors such as the autothermal reactor or the reactor with economizer.

Dynamic solutions of the fixed bed reactor model requires numerical techniques for a high order set of nonlinear ODEs. Many techniques are available for the solution of initial value problems with nonlinear ODEs. In this study, the method of Gear from ODEPACK [54] is used which solves the initial value problem for a stiff system of nonlinear ODEs.

The numerical values of the model parameters used in this study are based on information and results found in the literature for other fixed bed reactors [14,64]. The parameter values, base case operating conditions, and reference values are collected in Tables 2.2 and 2.3. The heat of reaction and the equilibrium constant are shown in Figures 2.2 and 2.3 over the expected temperature range of operation. The present model will use the heat of reaction and the equilibrium constant as expressed in Equations 2.2 and 2.5. Reference values for ΔH, G, and M are the values of these functions at T_{ref}. The reference value for $c_{pg_{ref}}$ is based on the feed mole fractions averaged over the operating temperature range of $300 - 500°C$.

2.6.1 Steady State Simulation Results and Discussions

The following steady state simulation results are obtained from solving the $2N + 4$ nonlinear algebraic equations iteratively by the Newton-Raphson algorithm where N is the number of interior collocation points. The steady state equations are obtained from

Table 2.2: Nominal Parameter Values

Reactor Dimensions	
reactor length L, cm	60.0
inside diameter of reactor $2R_i$, cm	3.0
Reaction Parameters	
pre-exponential factor k_o, gmoles/$atm^{1/2}cm^3$sec	3.787e-5
standard temperature T_{HS}, K	706.15
activation energy E, cal/gmole	11500
heat of reaction ΔH_o (298 K), cal/gmole	9838
Catalyst Parameters	
particle diameter d_p, cm	0.1
void fraction ϵ	.38
density ρ_s, g/cm^3	1.2
heat capacity c_{ps}, cal/g K	.22
Reactor Parameters	
heat transfer coefficient h_w, cal/sec cm^2 K	.1e-3
axial thermal conductivity k_z, cal/sec cm K	.0005
radial thermal conductivity k_r, cal/sec cm K	.0005
effective axial diffusivity D_e, cm^2/sec	6.29

Table 2.3: Base Case Operating Conditions and Reference Values

Base Case Operating Conditions	
inlet pressure P, atm	1.5
mass flow rate per unit area G^*, g/sec cm^2	2.1045e-2
feed temperature T_f^*, K	643.15
wall temperature T_w^*, K	700
CO feed composition x_{CO}, mole %	7
H_2O feed composition x_{H_2O}, mole %	44
CO_2 feed composition x_{CO_2}, mole %	7
H_2 feed composition x_{H_2}, mole %	29
total feed concentration c_o, g mole/cm^3	2.588e-5
Reference Values	
reference heat capacity $c_{pg_{ref}}$, cal/gK	0.5428
reference mass flow rate per unit area G^*_{ref}, g/sec cm^2	2.1045e-2
reference average molecular weight M_{ref}, g/gmole	13.55
reference heat of reaction ΔH_{ref}, cal/gmole	9194
reference time t_{ref}, sec	1025.6
reference temperature T^*_{ref}, K	706.15
reference thermal velocity u_o, cm/sec	0.0585

Equations 2.52 and 2.53 with the temperature derivative set equal to zero.

As the literature review discussed, Bonvin's work [13] used a relatively small number of interior collocation points (12 points) based on an eigenvalue analysis of the state-variable model. Studies to determine the number of collocation points needed to have an accurate steady state simulation are given later in this section. Additional model validation in terms of having a sufficient number of interior collocation points is performed in the next section for the dynamic simulation. It is found that using 12 interior collocation points in the steady state simulation provides accurate results while the dynamic simulation requires 20 points. These validation studies also explain some "oscillatory" behavior that Bonvin observed [13].

The steady state axial temperature and conversion profiles and their change due to changes in the reactor input variables presented next were obtained using 12 interior collocation points. The Newton-Raphson algorithm was used with a tolerance of 10^{-6}. The tolerance is defined as the maximum absolute difference between the current solutions and previous solutions at all 12 collocation points. The parameters and operating conditions are given in Tables 2.2 and 2.3.

Steady state axial temperature and conversion profiles for the base case operating conditions are shown in Figure 2.6. The steady state temperature profile shows that a hot spot is located about half way through the reactor bed. The location of such a hot spot is a result of the exothermic reaction, thermodynamic equilibrium and the cooling system. It is a common phenomenon in nonadiabatic fixed bed reactors.

The steady state conversion profile shows that most of the reaction takes place in the front part of the reactor. Since the reaction is exothermic and governed by thermodynamic equilibrium, as gas passes through the catalyst bed, the reactor temperature

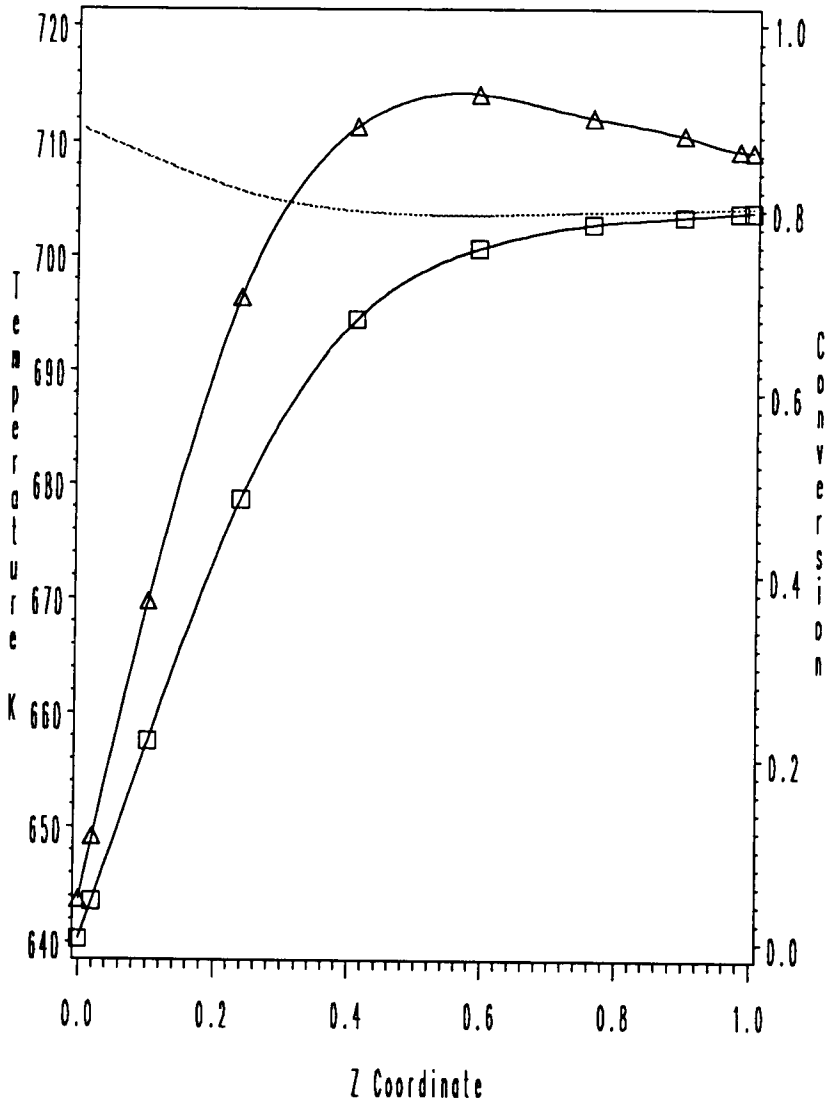

Figure 2.6: Base case steady state temperature and conversion profiles. Triangle: Temperature. Square: Conversion. Dot: Equilibrium conversion.

is raised by the heat of reaction and thus the equilibrium conversion becomes less favorable for the forward reaction. Also the cooling system is heating up the front part of the reactor and cooling down the end of the reactor due to heat transfer through the wall.

The equilibrium constant expressed in terms of feed mole fractions and equilibrium conversion is

$$K_p = \frac{(x_{CO_{2_o}} + x_{CO_o} x_{eq})(x_{H_{2_o}} + x_{CO_o} x_{eq})}{(x_{H_2O_o} - x_{CO_o} x_{eq}) x_{CO_o} (1 - x_{eq})} \tag{2.67}$$

Solving for x_{eq} and discarding the extraneous root yields

$$x_{eq} = \frac{-b - \sqrt{b - 4ac}}{2a} \tag{2.68}$$

where

$$\begin{aligned} a &= (1 - K_p) x_{CO_o}^2 \\ b &= (x_{CO_{2_o}} + x_{H_{2_o}} + K_p (x_{CO_o} + x_{H_2O_o})) x_{CO_o} \\ c &= x_{CO_{2_o}} x_{H_{2_o}} - K_p x_{CO_o} x_{H_2O_o} \end{aligned} \tag{2.69}$$

Using Equation 2.5 for the functional dependence of K_p on temperature along with Equation 2.68, Figure 2.7 is produced which shows the equilibrium conversion as a function of temperature for the base case feed mole fractions. This equation is also used to draw the line in Figure 2.6 which shows the equilibrium conversion for the reactor temperature at that location over the entire length of the reactor. For example at 714 K, the hot spot temperature in the steady state profile of Figure 2.6, the equilibrium conversion is .79. This equilibrium conversion line shows that the last half of the reactor is dominated by the thermodynamic equilibrium. From the hot spot to the reactor end, the temperature is very slowly decreasing while the conversion is slowly increasing. In

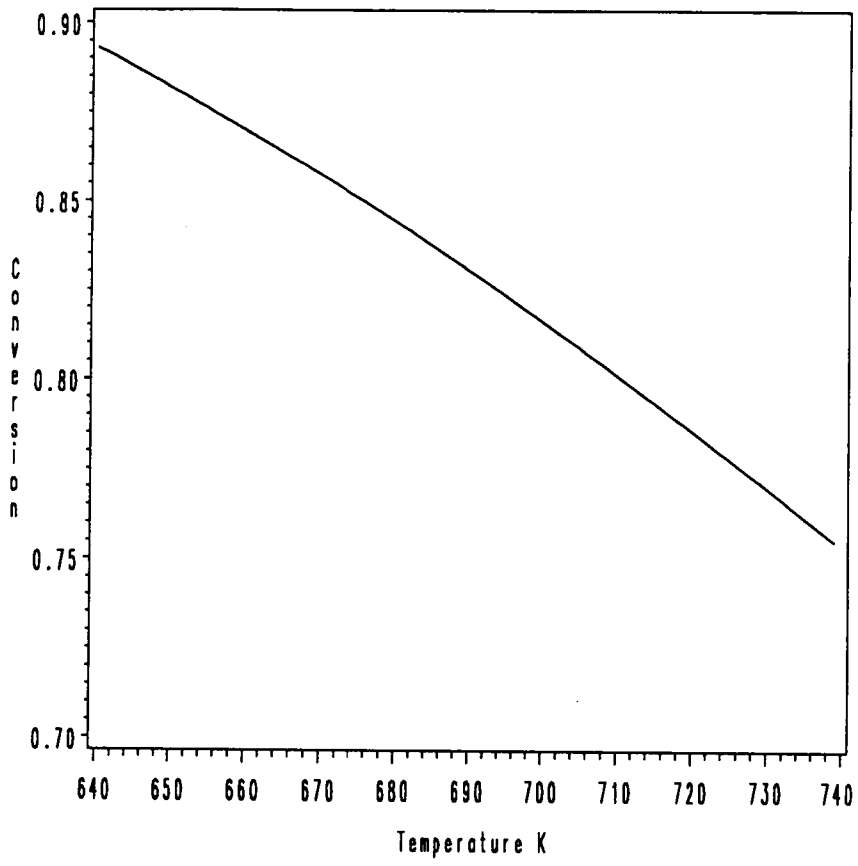

Figure 2.7: Temperature dependence of equilibrium conversion.

the last one-fourth of the reactor the conversion is very close to equilibrium. Recognizing this fact is very helpful in understanding several aspects of the reactor behavior throughout this work.

Figures 2.8 and 2.9 are included to show the effect of changes in feed temperature on the reactor temperature and conversion profiles. An increase in the feed temperature of 64.3 K causes an increase in the reactor temperature over the whole temperature profile. This leads to a higher conversion rate in the front part of the reactor. However, despite more reaction in the front part of the reactor the exit conversion is less than that resulting from the base case feed temperature. This is due to the higher temperature profile (see Figure 2.8) in the last part of the reactor which dictates a lower equilibrium conversion. On the other hand, a decrease in the feed temperature of 64.3 K results in a decrease in the reactor temperature over the whole profile which leads to a lower conversion rate over most of the reactor. But in this case the exit conversion nearly reaches that of the base case. This exit conversion is essentially the equilibrium conversion at the exit temperature. These relatively large temperature changes (+64 K to −64 K) lead to small conversion changes at the reactor exit. This results from the reactor being designed such that the exit conversion is near equilibrium along with the cooling through the reactor wall. The cooling due to the wall tends to fix the reactor exit temperature. Figure 2.8 shows an exit temperature difference of 13.5 K. Figure 2.9 shows this leads to an exit conversion difference of only 2 %.

The effect of changes in reactor wall temperature on the temperature and conversion profiles are shown in Figures 2.10 and 2.11. Again, the changes considered are 10 % of the base case wall temperature, a relatively large ±70 K. As expected the disturbance in the wall temperature has much more effect on the reactor temperature towards the end

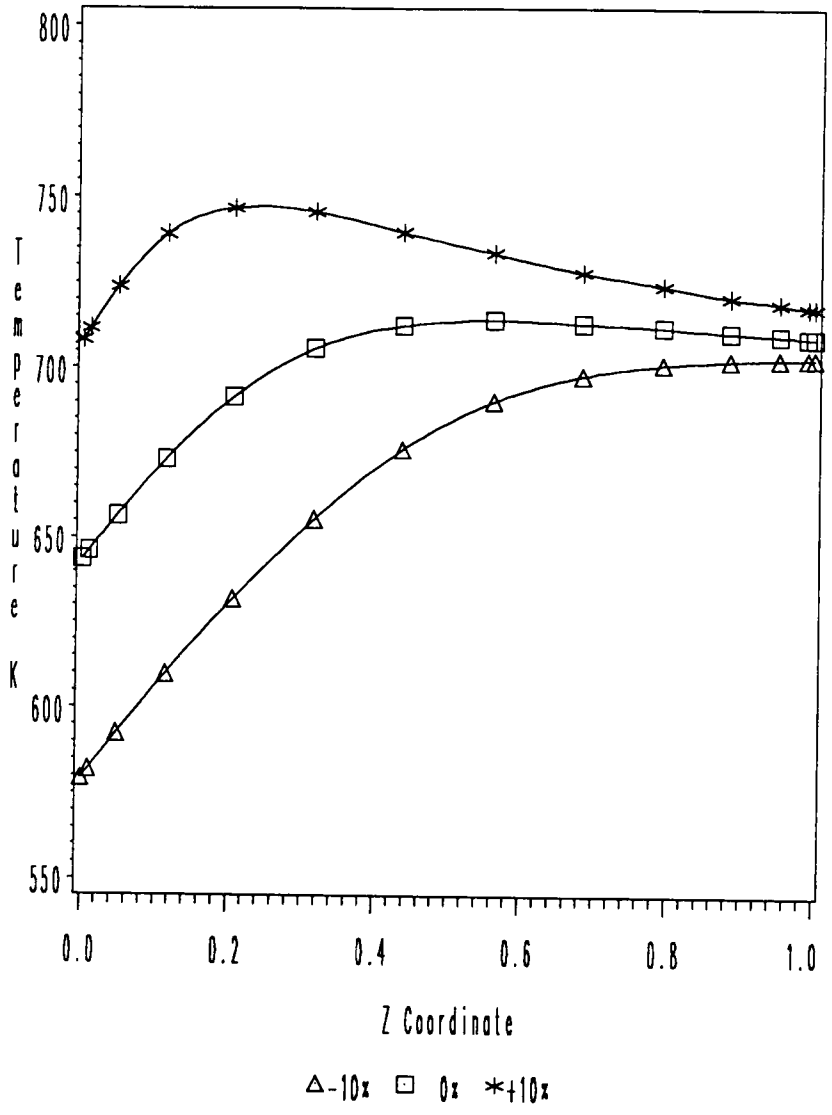

Figure 2.8: The effects of the feed temperature changes on the steady state temperature profile ($\pm 10\%$ changes in the feed temperature ($T_f^* = 643$K)).

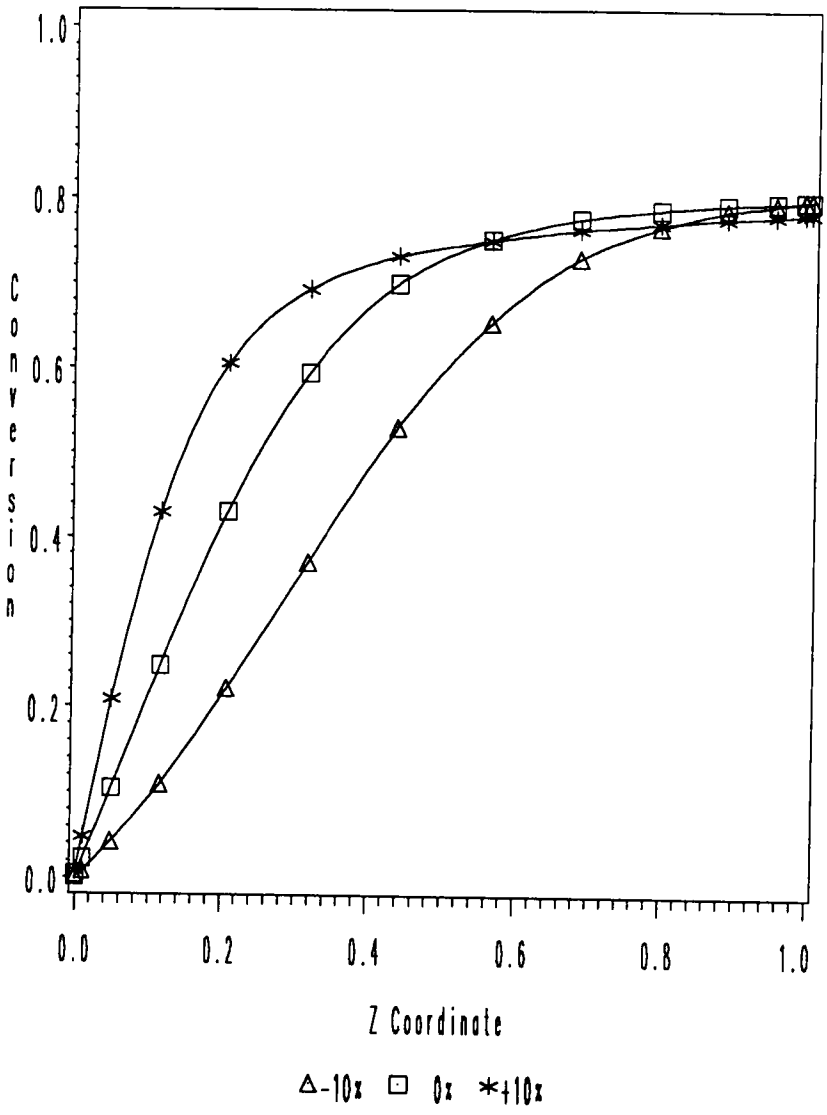

Figure 2.9: The effects of the feed temperature changes on the steady state conversion profile ($\pm 10\%$ changes in the feed temperature ($T_f^* = 643$K)).

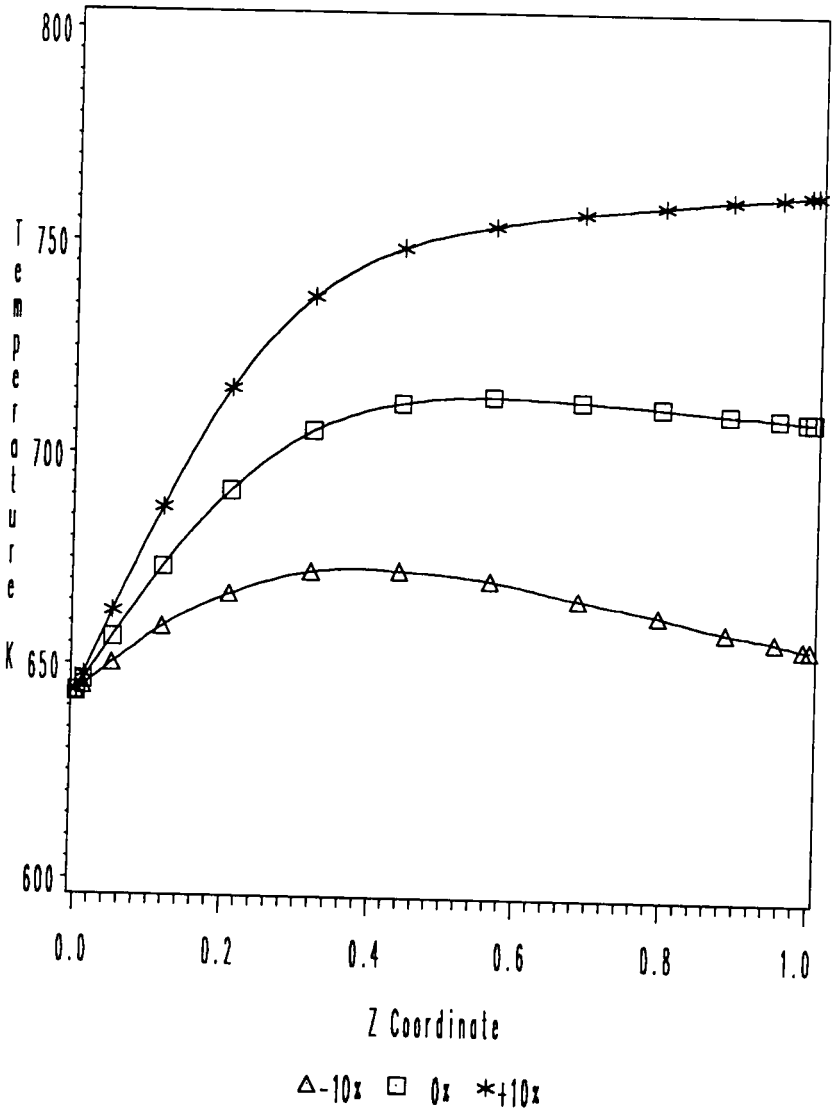

Figure 2.10: The effects of the wall temperature changes on the steady state temperature profile ($\pm 10\%$ changes in the wall temperature ($T_w^* = 700\text{K}$)).

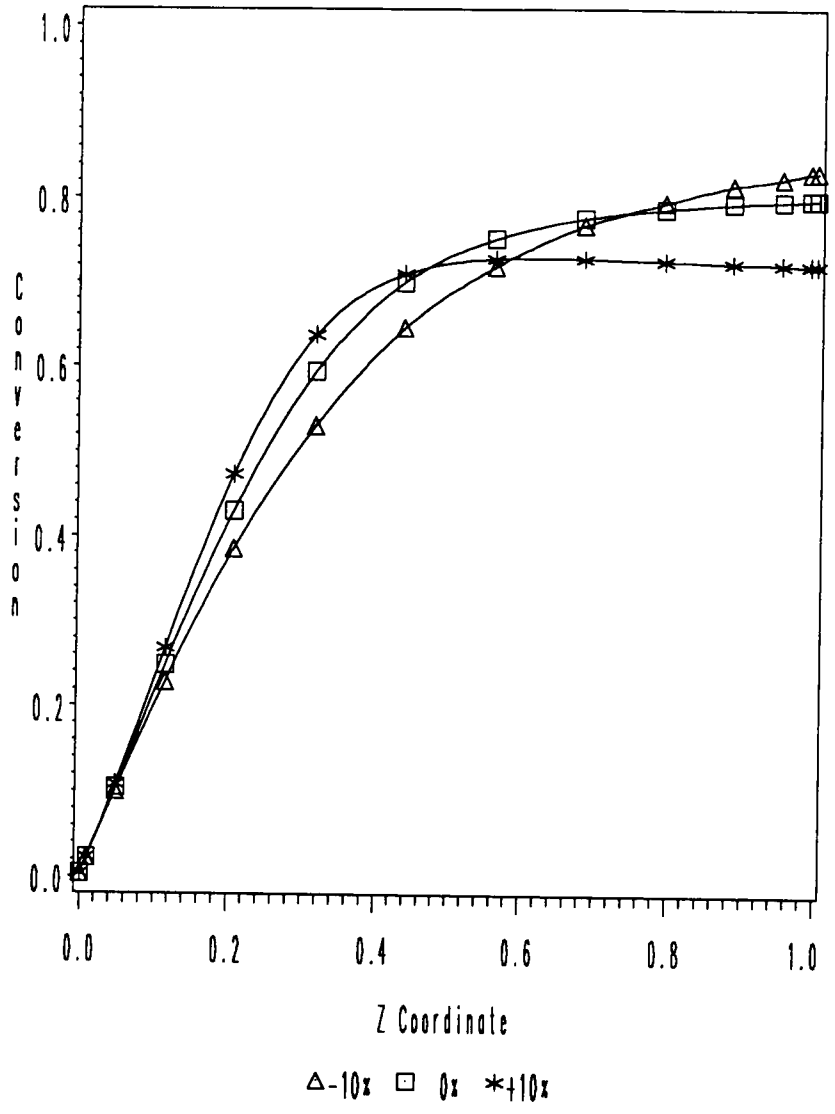

Figure 2.11: The effects of the wall temperature changes on the steady state conversion profile ($\pm 10\%$ changes in the wall temperature ($T_w^* = 700\text{K}$)).

of the reactor. This is in contrast to the response to changes in the feed temperature where the largest changes occur in the front part of the reactor. The increase in the wall temperature causes an increase in the reactor temperature which causes the equilibrium conversion to be less. At the reactor outlet the temperature is 53 K higher than the base case temperature. This causes the conversion at the exit to be .72 which is 8 % less than the base case. Figure 2.11 shows nearly a constant conversion from $z = .4$ to 1. The conversion actually drops slightly as the reactor temperature is being increased (see Figure 2.11) due to the high wall temperature. On the other hand, a decrease in wall temperature results in a decrease in the reactor temperature profile which causes the equilibrium conversion to be higher especially towards the end of the reactor. The equilibrium conversion at the reactor exit temperature is .885. In this case, the reaction is spread more uniformly across the reactor and actually leads to a higher conversion than the base case. However, operating with this wall temperature disturbances would have considerable more effect on the exit conversion, that is, the conversion profile is not flat at the end of the reactor.

Figures 2.12 and 2.13 show the effects of changes in the mass flow rate on the reactor temperature and conversion profiles. An increase in mass flow rate of 10 % from the base case cools down the front part of the reactor due to more heat convection from the higher mass flow rate. This moves the hot spot temperature towards the end of the reactor. The reactor temperature in the last half of the reactor is higher as more reactant is supplied by the higher mass flow rate. The conversion is decreased with an increase in mass velocity due to the equilibrium limitation in reaction rate. The behavior to a 10 % decrease in mass flow rate is just the opposite to the positive change. But compared to the reactor response to the feed temperature and the wall

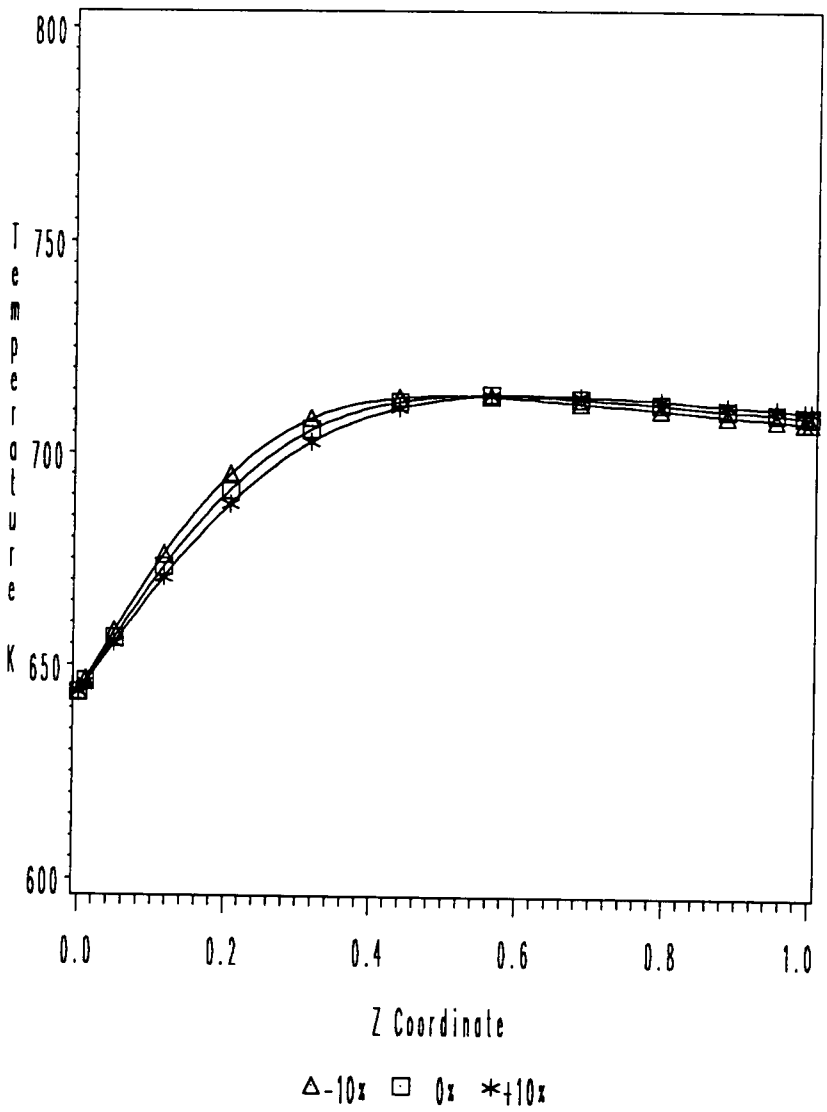

Figure 2.12: The effects of the mass velocity changes on the steady state temperature profile ($\pm 10\%$ changes in the mass flow rate ($G^*_{ref} = 2.1045$ g/sec cm^2)).

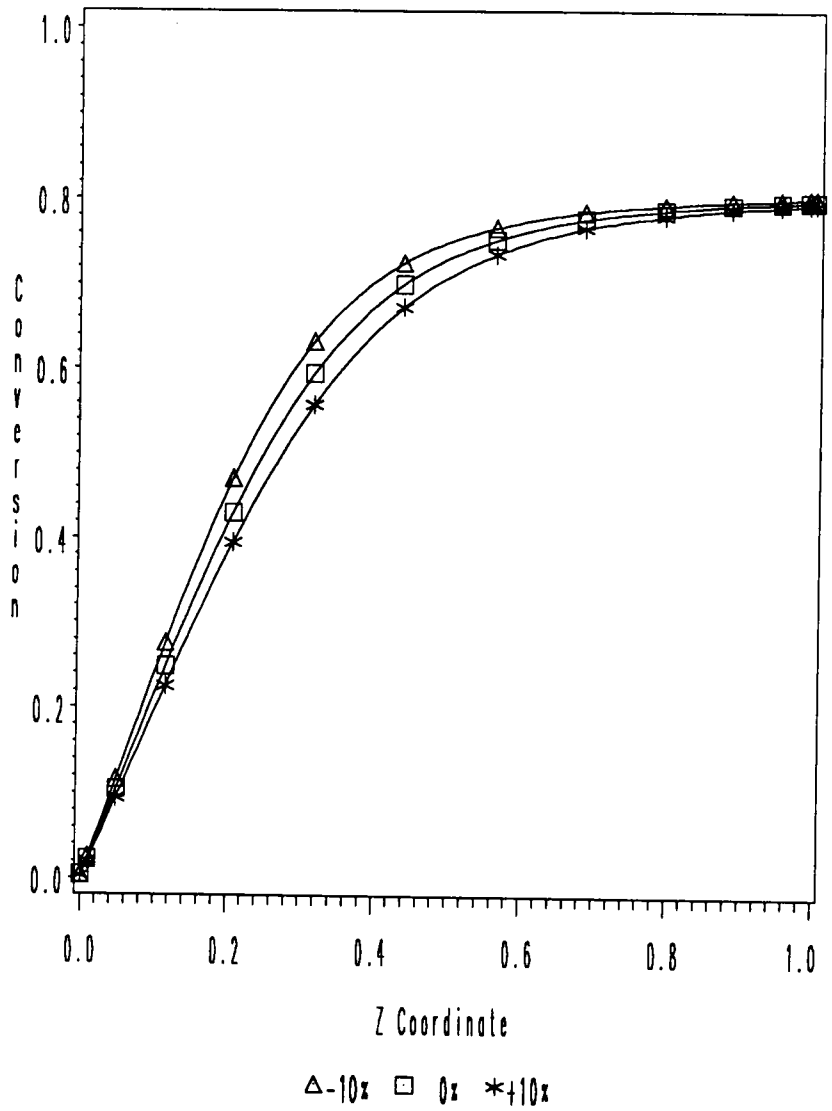

Figure 2.13: The effects of the mass velocity changes on the steady state conversion profile ($\pm 10\%$ changes in the mass flow rate ($G^*_{ref} = 2.1045$ g/sec cm^2)).

temperature changes, the overall effects on the reactor due to changes in mass flow rate are small.

Figures 2.14 and 2.15 show the effects of changes in CO feed mole fraction on the reactor temperature and conversion profiles. An increase in feed CO mole fraction causes a higher reaction rate in the front part of the reactor and thus a higher temperature. Figure 2.15 shows only a slightly higher conversion is achieved due to the equilibrium constraint. The largest change in the temperature profile occurs in the central part of the reactor. However, an increase in CO mole fraction does not change the exit conversion, because it is close to equilibrium conversion. The conversion profile is essentially the same as the base case from $z = 0.7$ to the reactor exit. A decrease in CO mole fraction causes a lower reaction rate throughout the reactor and the temperature drops throughout the reactor.

These types of simulations indicate the steady state changes caused by changes in manipulated variables. This information can be used to calculate steady state gains (linearized representation of the nonlinear system) which will be used later in the selection of sensor locations and manipulated variables for the reactor control in Chapter 4. There are five possible manipulated variables (reactor pressure, feed temperature, wall temperature, CO mole fraction, and mass flow rate) all except reactor pressure are considered in this study.

These variables were all increased or decreased from their base case values (see Figures 2.8 to 2.15). The steady state gains are calculated as the reactor temperature change at each sensor location divided by the size of the change in the manipulated variable. The size of the change in the manipulated variable is defined or scaled differently than is typically done. The dimensionless variables were not used due to scaling

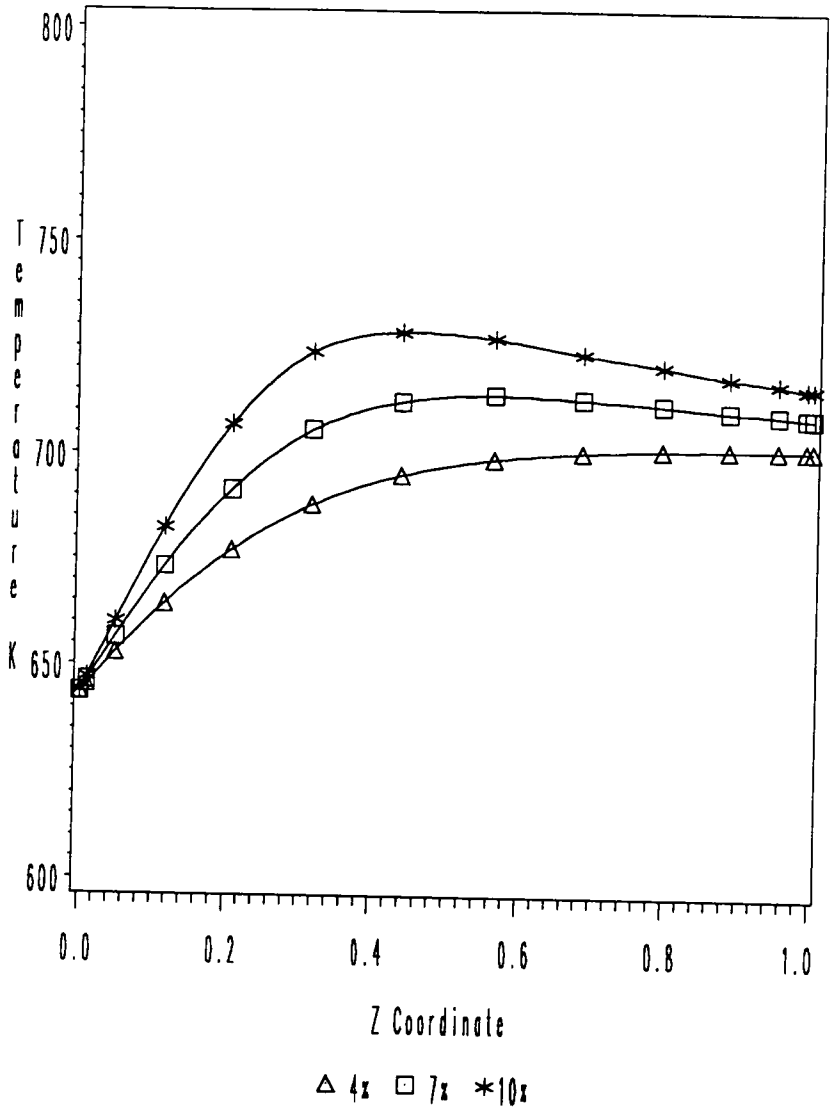

Figure 2.14: The effects of the CO mole fraction changes on the steady state temperature profile (x_{CO} = 4, 7 and 10 CO mole %).

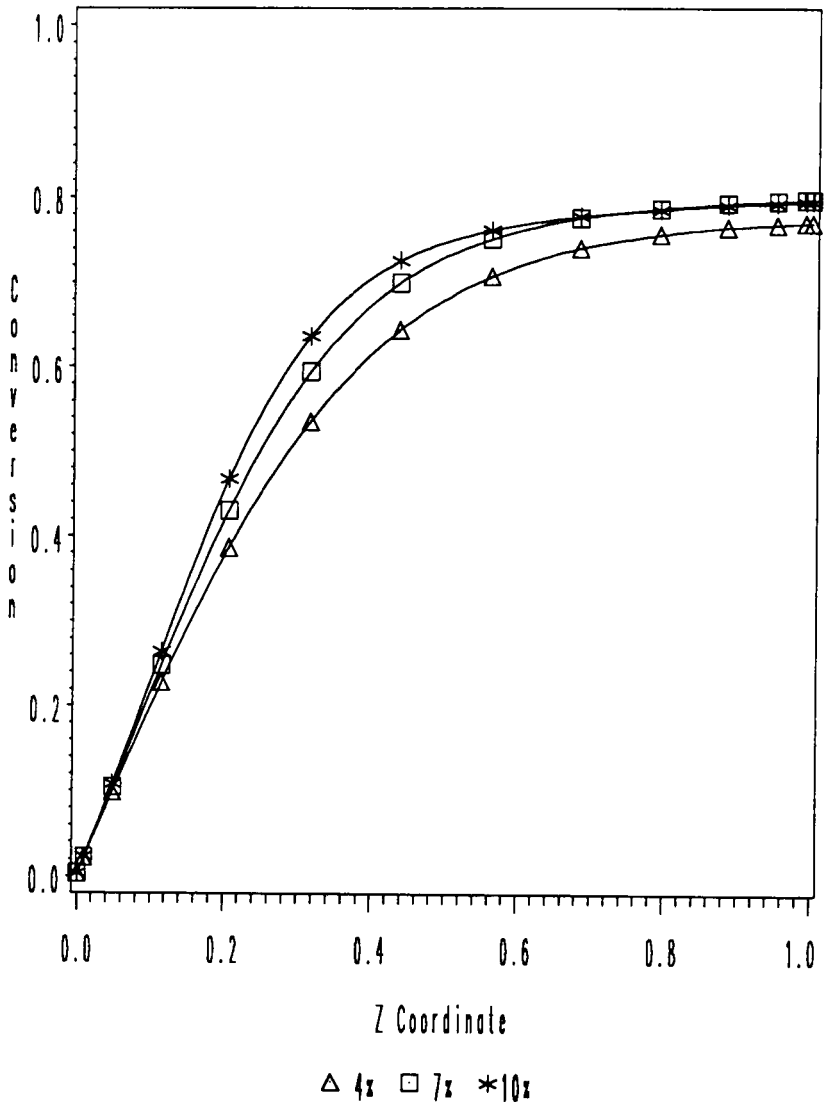

Figure 2.15: The effects of the CO mole fraction changes on the steady state conversion profile (x_{CO} = 4, 7 and 10 CO mole %).

problems [35,99] which can arise in the application of Singular Value Analysis presented in Chapter 4. The input variables have the units listed with their base case operating values in Table 2.3, thus, the gains have units. However, in an attempt to appropriately scale the gains they are calculated as follows:

1. The steady state gains from feed temperature and wall temperature to the reactor temperatures were calculated as the ratio between reactor temperature changes in K at the each sensor location and input variable temperature change in K. Thus, this gain has units of (K/K). This is the usual procedure in calculating a gain.

2. The gains from CO mole fraction to the reactor temperatures were calculated as the ratio between reactor temperature changes in K at each sensor location and the CO mole percent change rather than CO mole fraction. Thus, this gain has units of K/CO mole %.

3. The gains from mass flow rate to the reactor temperatures were calculated as the ratio between reactor temperature changes in K at each sensor location and percent change in mass flow rate from its base case operating condition value. Thus, this gain has units of K/G change %.

Tables 2.4 and 2.5 show the steady state temperature gains for both positive and negative changes in the four possible manipulated variables.

The strong nonlinearities of the model, depending on the temperature locations shows in the steady state gains as they are different for the positve and negative step changes in these manipulated variables. The nonlinearity shows in the steady state gains for all four inputs. The gains are most uniform for changes in the wall temperature. For the other three inputs differences of 20 to 25 % arise at various temperature positions.

Table 2.4: Steady State Temperature Gains to Changes in the Feed Temperature and the Wall Temperature (Units: K/K)

Sensor	*Feed Temp.* $(\Delta T/\Delta T_f)$		*Wall Temp.* $(\Delta T/\Delta T_w)$	
Location (z)	Neg. Step	Pos. Step	Neg. Step	Pos. Step
1 (0.0034)	0.9108	0.9173	0.0090	0.0089
2 (0.0180)	0.9104	0.9335	0.0344	0.0344
3 (0.0439)	0.9097	0.9528	0.0785	0.0785
4 (0.0804)	0.9053	0.9554	0.1426	0.1432
5 (0.1268)	0.8936	0.9210	0.2207	0.2215
6 (0.1820)	0.8632	0.8320	0.3092	0.3090
7 (0.2446)	0.8058	0.7056	0.3944	0.3866
8 (0.3131)	0.7142	0.5693	0.4699	0.4483
9 (0.3861)	0.5985	0.4520	0.5267	0.4900
10 (0.4617)	0.4758	0.3600	0.5720	0.5250
11 (0.5383)	0.3666	0.2940	0.6054	0.5570
12 (0.6139)	0.2796	0.2450	0.6367	0.5910
13 (0.6869)	0.2162	0.2110	0.6613	0.6230
14 (0.7554)	0.1706	0.1850	0.6851	0.6550
15 (0.8180)	0.1410	0.1660	0.7048	0.6800
16 (0.8732)	0.1199	0.1500	0.7233	0.7030
17 (0.9196)	0.1057	0.1400	0.7360	0.7200
18 (0.9561)	0.0960	0.1310	0.7478	0.7350
19 (0.9820)	0.0909	0.1260	0.7550	0.7430
20 (0.9966)	0.0874	0.1230	0.7592	0.7480

Table 2.5: Steady State Temperature Gains to Changes in CO Mole Fraction and Mass Flow Rate (Units:K/CO mole %, K/G change %)

Sensor	*CO Mole Fraction* ($\Delta T/\Delta x_{co}$)		*Mass Flow Rate*($\Delta T/\Delta G$)	
Location (z)	Neg. Step	Pos. Step	Neg. Step	Pos. Step
1 (0.0034)	0.0183	0.0170	-0.0032	-0.0025
2 (0.0180)	0.0690	0.0657	-0.0093	-0.0076
3 (0.0439)	0.1623	0.1603	-0.0195	-0.0160
4 (0.0804)	0.2917	0.2990	-0.0324	-0.0269
5 (0.1268)	0.4527	0.4807	-0.0446	-0.0379
6 (0.1820)	0.6157	0.6703	-0.0521	-0.0458
7 (0.2446)	0.7550	0.8153	-0.0503	-0.0473
8 (0.3131)	0.8320	0.8643	-0.0393	-0.0411
9 (0.3861)	0.8447	0.8300	-0.0250	-0.0290
10 (0.4617)	0.8030	0.7433	-0.0100	-0.0160
11 (0.5383)	0.7373	0.6533	0.0020	-0.0050
12 (0.6139)	0.6637	0.5667	0.0100	0.0030
13 (0.6869)	0.5947	0.5033	0.0140	0.0090
14 (0.7554)	0.5303	0.4533	0.0160	0.0130
15 (0.8180)	0.4830	0.4133	0.0180	0.0150
16 (0.8732)	0.4417	0.3767	0.0190	0.0160
17 (0.9196)	0.4100	0.3567	0.0190	0.0170
18 (0.9561)	0.3867	0.3367	0.0190	0.0170
19 (0.9820)	0.3737	0.3267	0.0190	0.0170
20 (0.9966)	0.3640	0.3200	0.0190	0.0170

The largest differences appear in the gains for the feed temperature, however it should be noted large ($\pm$ 70 K) changes were made in this temperature.

2.6.2 Dynamic Simulation Results and Discussions

The motivation for the model development in this study is oriented to control system design which cannot be fulfilled with only the steady state simulation. The model has been developed to simulate dynamically the effects of process disturbances and input changes. Starting from the steady state for the base case operating conditions and making a step or pulse change in feed temperature, feed composition, mass flow rate or wall temperature, the simulation can show the dynamic behavior of the process. Understanding of such dynamic behavior under these disturbances is critical in process design, optimization and control.

Two factors which are important to obtain accurate and reliable simulation results are the number of collocation points and the time step size used in integrating the ODEs. In general, the more collocation points used and the smaller the step size the more accurate the simulation. The validity of the model developed in this work is tested by varying the number of orthogonal collocation points in the axial direction (say 8, 12, 16 and 20 interior collocation points). When increasing the number of collocation points causes only a small change in the simulation results, this is an indication that enough points are being used for an accurate simulation.

The Gear integration subroutine from ODEPACK [54] with a variable step size is used in this study and the error criteria is varied from 10^{-4} to 10^{-8}. The term error criteria is used to denote both the absolute error and relative error used in the Gear subroutine. These two errors are always set equal in these simulations. When decreasing

the error criteria leads to little change in the simulation output, this is an indication that the error in the simulation is small. One must recognize that these two factors are interactive and do comparisons among simulations where both factors are varied as part of the validation study.

In all of the dynamic plots presented in this section, the initial conditions for the simulations were the steady state temperature and conversion profiles for the base case operating conditions. All of the reactor inputs are also set to the base case values (see Table 2.3), then a step change is made in one input to illustrate the dynamic behavior of the reactor to that input variable.

Figure 2.16 shows in a 3 dimensional plot the effect of a 10% increase in the feed temperature on the axial reactor temperature profiles obtained from a simulation with 12 interior collocation points and an error criteria of 10^{-6}. Due to the nature of the distributed system the response of the axial reactor temperature is different with its position and time. For example, positions further down the reactor show more dead time behavior. Due to the presence of the cooling system the outlet temperature shows less change in comparison to the temperature in the front part of the reactor. The hot spot shifts toward the front of the reactor. The surface clearly contains a trough where temperature drops before increasing. This is the wrong-way behavior exhibited by the reactor. The inverse response moves from the front of the reactor near time zero to the end of the reactor in a dimensionless time just short of 2.

Figure 2.17 shows the same dynamic simulation as Figure 2.16 but is based on 20 interior collocation points. The striking comparison between these two figures is that the oscillatory character exhibited in the first figure is greatly reduced in the second. This is especially evident on the flat surface at the start of the response. This flat

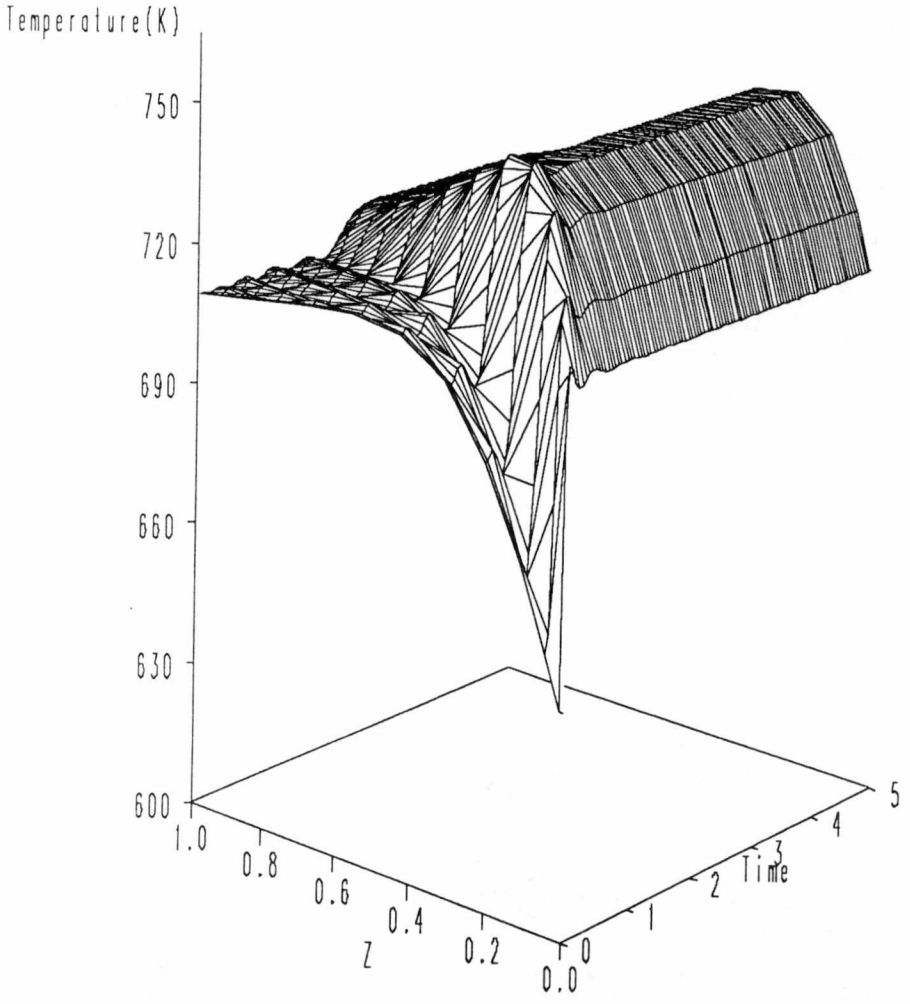

Figure 2.16: Dynamic simulation of the temperature profile response to a 10% increase in the feed temperature with 12 interior collocation points.

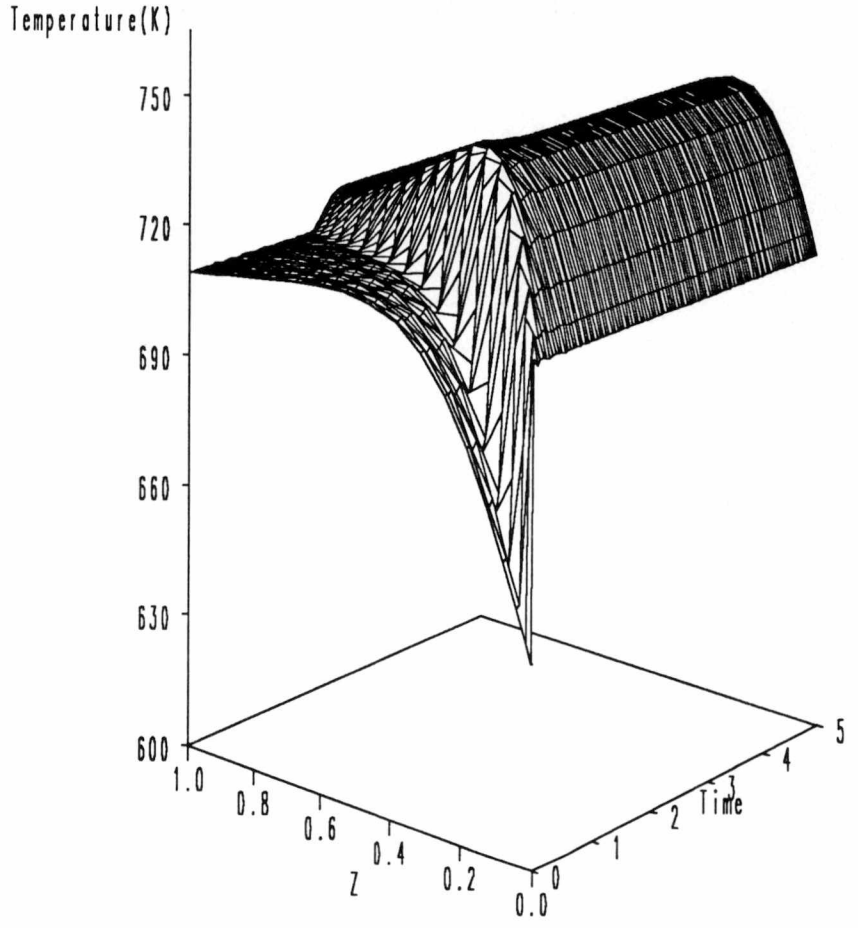

Figure 2.17: Dynamic simulation of the temperature profile response to a 10% increase in the feed temperature with 20 interior collocation points.

surface is due to the dead time in the response. This dead time is obviously longer for positions that are further from the reactor entrance. This is an illustration of the temperature wave caused by the step change in feed temperature. There should be relatively little temperature change on this dead time surface where Figure 2.16 has considerable oscillatory variation. This behavior is not real but is a numerical artifact.

There exists a trade-off between accuracy and the size (number of equations) of the nonlinear ODE model. One approach often used to resolve this dilemma is to use an eigenvalue analysis which investigates the convergence pattern of eigenvalues as the number of collocation points is increased. This convergence property is a guide to the selection of the number of collocation points necessary to obtain a good approximation of the PDE model. Previous studies [14,64] on two different types of reactors indicated that about 12 collocation points resulted in reliable simulation results.

In this research the appropriate number of collocation points is investigated by running the simulation based on a different number of points. Dynamic simulations show that the oscillatory behavior is most dominant for step change in feed temperature. Thus, this study mainly uses step changes in feed temperature.

The discrete location of the axial temperatures depend on the number of collocation points used and on the roots of the Jacobi polynomial. Thus, the axial position, at which temperature values are obtained, varies as the number of points is changed. Therefore, in order to compare the results of the dynamic simulations with 12, 16, and 20 points their temperature values are interpolated to the axial positions of the simulation with 12 points.

Figure 2.18 shows the effects of different number of collocation points on the temperature simulation to step changes in feed temperature at z = .038 and z = .98 (error

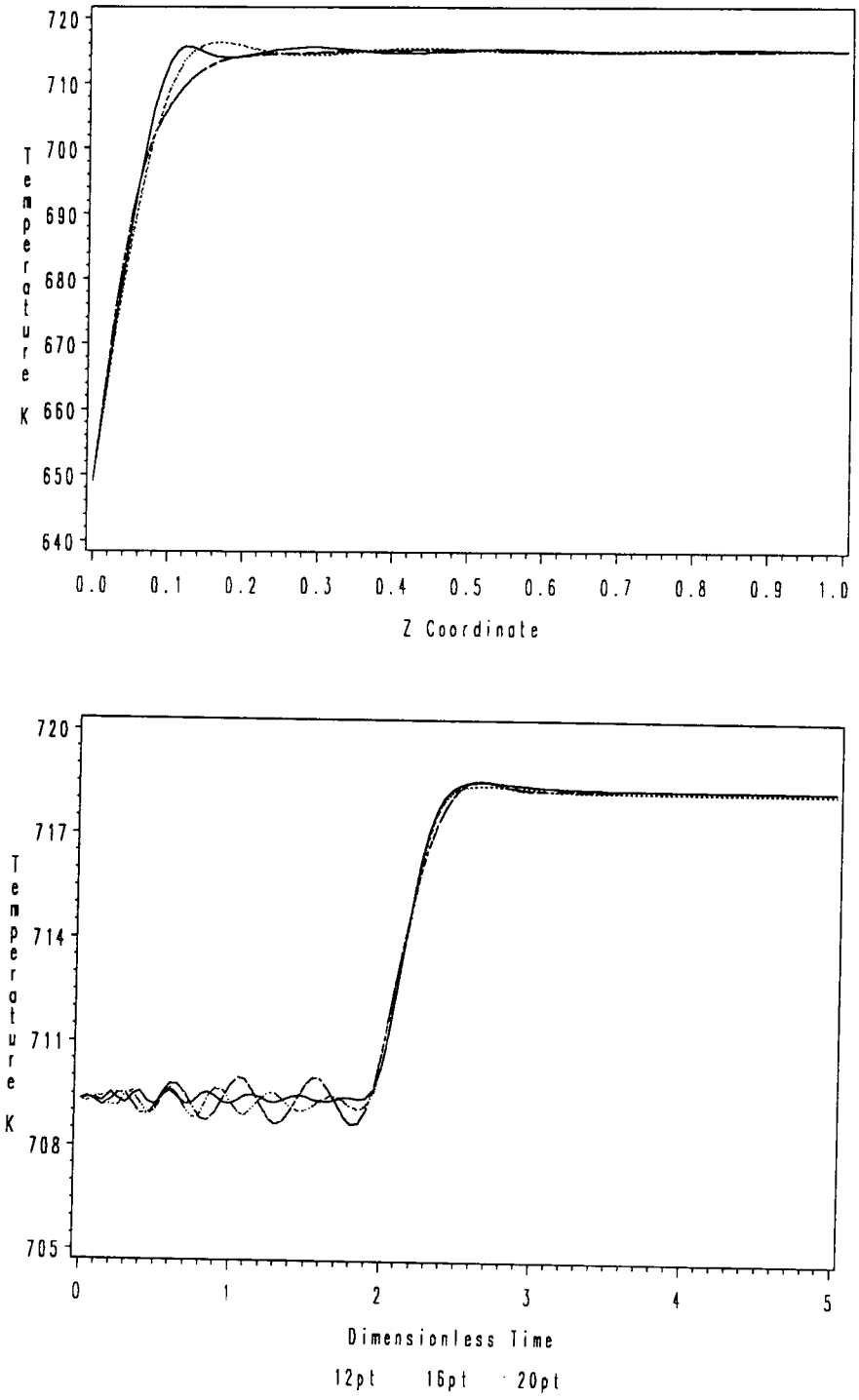

Figure 2.18: The effect of different number of interior collocation points on the dynamic simulation of reactor temperature to a 10% step change in the feed temperature (error criteria = 10^{-6}). Top: T at z= .038. Bottom: T at z= .98.

criteria = 10^{-6}). As the number of collocation points decreases, the simulation shows more and more oscillatory behavior in the first period of time, which relate to numerical error. The front part of the reactor simulation at z = .038 in Figure 2.18 shows differences at the temperature peaks. But the front part of the reactor simulation shows relatively small differences compared to the end of the reactor. These simulation results indicate that more than 12 interior collocation points are necessary in this study to get an accurate nonlinear simulation in spite of the results of previous eigenvalue analysis studies [14,64]. In fact, Bonvin observed this oscillatory behavior in his studies, but did not address the problem.

The dynamic simulations in this research will use 20 collocation points. By using this number of points the oscillation amplitude in Figure 2.18 is kept under 1/2 K.

It is also important to note the confirmation of the fact that 12 collocation points provide an accurate steady state simulation as discussed in the last section. Figure 2.18 shows essentially no difference at steady state between the simulations based on 12, 16, or 20 points.

Figure 2.19 shows a comparison of simulations with different error criteria to step changes in feed temperature at the front (T1 at z = 0.00344) and the end of the reactor (T20 at z = 0.9966). The temperature response simulations for T1 are almost identical to each other. But at the end of the reactor the temperature simulations show considerable difference when the error criteria is 10^{-4}. The same type of analysis has been done for changes in the mass flow rate. Figure 2.20 shows the simulation results with different error criteria to changes in molar flow rate at the front of the reactor and the end of reactor. Figure 2.20 shows that the front part of the reactor is cooled down due to more heat convection down stream from the higher flow rate. These simulation results are

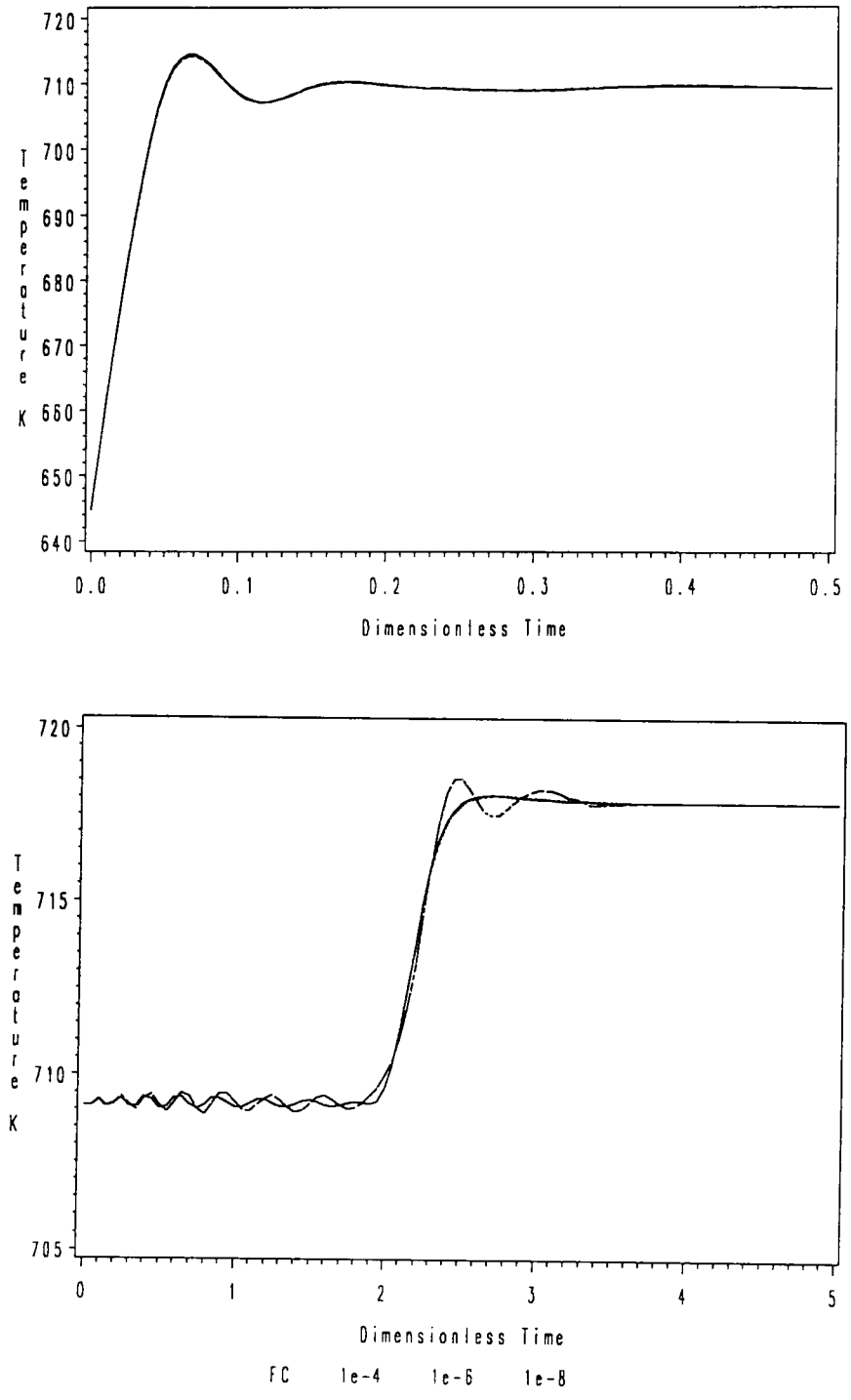

Figure 2.19: The effect of different error criteria on the dynamic simulation of reactor temperature to a 10% step change in the feed temperature. Top: T1 at z = $.34357e-2$. Bottom: T20 at z = .99656.

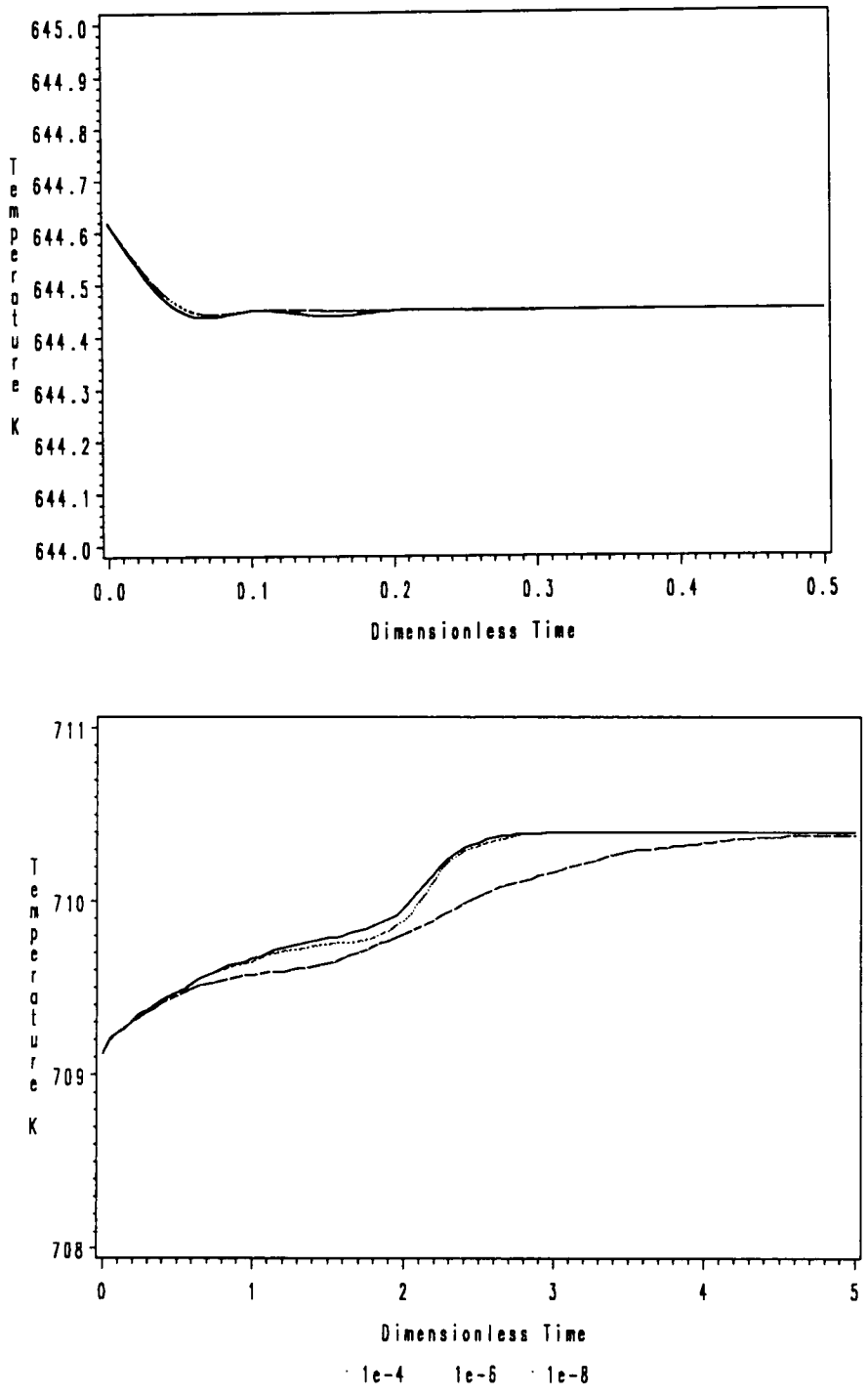

Figure 2.20: The effect of different error criteria on the dynamic simulation of reactor temperature to a 10% step change in the mass flow rate. Top: T1 at z = $.34357e-2$. Bottom: T20 at z = .99656.

almost identical. Towards the end of reactor, there are minor deviations between the simulations using the error criteria of 10^{-6} and 10^{-8}. The simulation running with an error criteria of 10^{-4} shows up to 1/2 K variation from the other simulations. Thus, an error criteria of 10^{-8} will be used in all dynamic simulations in the control studies found in Chapter 5.

Figure 2.20 shows interesting dynamic behavior at the end of the reactor. It seems that two types of responses arising from the step input in mass flow rate are added together. This can be explained in that the increase in mass flow rate brings more reactant into the reactor, and thus more reaction takes place which causes the reactor temperature to rise. Later the thermal wave from the front part of the reactor also caused by additional reaction causes the reactor temperature to rise again.

Analysis based on various dynamic simulations indicate that for an accurate simulation in this study more than 12 interior collocation points are required and while the effect of the error criteria is relatively minor, it should be kept below 10^{-6}. From now on, throughout the remaining control study, 20 interior collocation points and a 10^{-8} error criteria will be used for dynamic simulations.

2.7 Conclusion

A two dimensional dynamic model of a fixed bed reactor carrying out the water-gas shift reaction has been developed and evaluated. This partial differential equation model is discretized in the radial and axial directions by the orthogonal collocation procedure. The order of the resulting nonlinear ordinary differential equation is kept relatively low by using one interior collocation point in radial direction.

Rigorous dynamic and steady state simulations provide a comprehensive analysis of the reactor behavior under different operating conditions. In most cases, steady state conversion profiles show that most of the reaction takes place in the front half part of the reactor. Since the reaction is exothermic and governed by thermodynamic equilibrium, as the gas passes through the catalyst bed, the reactor temperature is raised by the heat of reaction and thus the equilibrium conversion becomes less favorable. Steady state simulations are able to show the steady state changes to changes in process input variables with a small number of collocation points (12 pt).

Dynamic simulations illustrate the transient behavior of the reactor under changes in process input variables. Analysis based on various dynamic simulations indicate that for an accurate simulation more than 12 interior collocation points are required and while the effect of the error criterior is minor, it should be kept below 10^{-6}. Therefore in this research 20 interior collocation points will be used with the error criteria set at 10^{-8}.

2.8 Nomenclature

A_o	outside heat transfer area, cm^2
$A_{i,j}$	collocation matrix
$B_{i,j}$	collocation matrix
Bi	Biot number, $h_w\ R_i\ /k_r$
c_{CO}	CO feed concentration, g $mole/cm^3$
c_o	total feed concentration, g $mole/cm^3$
c_p	heat capacity, cal/gK
c^*_{pg}	gas heat capacity, cal/gK
c_{pg}	dimensionless gas heat capacity, $c^*_{pg}/c_{pg_{ref}}$
d_p	particle diameter, cm
D_e	effective axial diffusivity, cm^2/sec
E	activation energy, $cal/$ g mole
G	dimensionless mass flow rate per unit area, G^*/G_{ref}
G^*	mass flow rate per unit area, g/cm^2 sec
G_{ref}	reference mass flow rate per unit area, g/cm^2 sec
h_w	heat transfer coefficient, inner wall-bed, $cal\ /sec\ cm^2$
ΔH	dimensionless heat of reaction, $\Delta H^*/\Delta H^*_{ref}$
ΔH^*	heat of reaction, cal/g mole
K_{eq}	equilibrium constant
$K_{i,j}$	controller gain
k_o	pre-exponential factor, g $moles\ /atm^{1/2}\ cm^3$ sec
k_r	radial thermal conductivity, $cal\ /sec$ cm K
k_z	axial thermal conductivity, $cal\ /sec$ cm K

L	reactor length
M	average molecular weight of the feed, g/g mole
N	number of interior collocation points
P	reactor pressure, atm
r	dimensionless radial coordinate, r^*/R_i
r^*	radial coordinate, cm
R_g	ideal gas constant
R_i	inside radius of tube, cm
t	dimensionless time, t/t_{ref}
t^*	time, sec
t_{ref}	reference time used in dimensionless variables, L/u_o
T	dimensionless temperature, T/T_{ref}
T^*	temperature, K
T_f	dimensionless feed temperature, T_f^*/T_{ref}
T_f^*	feed temperature, K
T_{HS}	a constant used in Equation 2.4, K
T_w	dimensionless wall temperature, T_w^*/T_{ref}
T_w^*	wall temperature, K
u^*	feed velocity, cm/sec
u_o	reference thermal velocity, cm/sec
x	CO conversion, $(c_{CO_o} - c_{CO})\ /c_{CO_o}$
x_{CO}	CO mole fraction
x_{CO_2}	CO_2 mole fraction

x_{H_2} H_2 mole fraction

x_{H_2O} H_2O mole fraction

z dimension axial coordinate, z^*/L

z^* axial coordinate, cm

Greek Symbols

β_a dimensionless reaction rate constant

$P^{1/2}\ L\ k_o\ /\ \rho_s\ c_{ps}(1-\epsilon)\ u_o\ T^*_{ref}$

β_b dimensionless reaction rate constant

$P^{1/2}\ L\ k_o\ /\ \epsilon\ G^*_{ref}$

ϵ void fraction

γ dimensionless activation energy, $E\ /\ R_g\ T^*_{ref}$

υ_a dimensionless axial thermal dispersion coefficient

$k_z\ /\ \rho_s\ c_{ps}\ (1-\epsilon)\ u_o\ L$

υ_m dimensionless axial mass dispersion coefficient

$G^*_{ref}\ L\ /\ M_{ref}\ c_o\ D_e$

υ_r dimensionless radial thermal dispersion coefficient

$k_r\ L\ /\ \rho_s\ c_{ps}\ (1-\epsilon)\ u_o\ R_i^2$

υ_w dimensionless axial thermal conduction coefficient

$G^*_{ref}\ c^*_{pg_{ref}}\ \epsilon\ L\ /\ k_r$

ψ dimensionless lumped heat transfer coefficient

$8\ \upsilon_r\ B_i\ /\ (4+B_i)$

ρ density, g/cm^3

ξ dimensionless flow rate

$G^*_{ref}\ c^*_{pg_{ref}}\ \epsilon\ /\ \rho_s\ c_{ps}\ (1-\epsilon)\ u_o$

Subscripts

f	feed
g	gas
o	inlet conditions
ref	reference value
s	catalyst
w	wall

Superscripts

*	dimensional variable

CHAPTER 3

Fixed Bed Reactor Control

3.1 Introduction

Control of fixed bed reactors in the chemical industry is characterized by several problems. These systems are distributed in nature or often described as having large dead times, highly nonlinear and multivariable processes. The response times of the outlet process variables to inlet condition changes vary widely. Generally the outlet concentration changes orders of magnitude faster than outlet temperature. Thus the system is termed to be stiff to denote the associated numerical solution problems. Furthermore, interaction between reactor temperature and reaction rate can cause wrong-way behavior or inverse response in the case of exothermic reactions. These reactors are often sensitive to changes in the operating conditions and exhibit stability problems. Several examples [13,71] are known to exhibit multiple steady state profiles. Each of these characteristics contributes to making such reactor control complex.

In most process plants, the reactor is at the front end of the process train, thus the overall plant production rate is governed by its production rate and disturbances at the reactor can be propagated throughout the rest of the plant. Often, such disturbances can ruin down stream products, destroy reactor catalyst and damage process equipment. This is why care is taken to not subject the reactor to rapid or unpredictable load changes and considerable effort is put into control strategies to compensate for such incidents. The effective design of a reactor control strategy depends on a sound knowledge of the

reactor system. This research intends to develop a dynamic reactor model and use numerical solution techniques to understand the reactor's behavior and to assess its sensitivity to process disturbances and to predict its future behavior. Such a model and analysis will guide the effective design of control structures.

The common aspects of a fixed bed reactor control problem, which have to be considered in model development and the design of reactor control system, are

- distributed parameter
- multivariable and interaction
- nonlinearity
- large time delays
- sensitivity
- stiffness
- inverse response
- sensor locations
- stability
- robustness
- tuning

Operation of this type of reactor is a regulator control problem. The control strategy may manipulate inputs as concentration, temperature and flow rate on a high frequency (or continuous) basis to maintain a given production rate, or temperature profile.

3.2 Review of Reactor Control

The early stages of reactor control and applied mathematical analysis centered on the continuous stirred tank reactor (CSTR) extensively. Aris and Amundson [5,6] investigated multiple steady states and stability of a CSTR. The model was that for a lumped parameter system carrying out an irreversible first-order exothermic reaction. Control at or near an unstable steady state was often necessary due to compromised optimum operating conditions, for example, in terms of conversion or selectivity and catalyst longevity. The unstable steady state was made stable by using a negative feedback P, PI, or PID controller. This pioneering set of papers led to a tremendous amount of literature directed at the single-input single-output lumped parameter system control problem. Bruns and Bailey [21,22] used a nonlinear feedback controller for operating a nonisothermal CSTR near an unstable steady state. The nonlinear relay with hysteresis switch, which was analyzed by describing function analysis and Tsypkin's method, stabilized the reactor around the unstable steady state. A similar experimental implementation was used by Wandarey and Renken [115] to control the first order catalytic oxidation of a hydrocarbon in an autothermal CSTR. The reactor was stabilized near an unstable region by periodic ignition and extinction of the reaction. Chang and Schmitz [24,25] used a conventional feedback PI controller to control a nonadiabatic CSTR around an unstable steady state. In these examples the CSTR was operated near or around the steady state in that small amplitude limit cycle behavior was sustained.

Large numbers of papers based on numerical studies have been presented on the feedback control of tubular reactors. This problem differs in character due to the dis-

tributed nature of the tubular reactor. Paradis and Perlmutter [84] studied, which is one of the early publications to treat this problem, the feedback control of a nonadiabatic tubular reactor. A finite difference method was used to discretize the partial differential equations in space. Different kinds of control strategies, single variable and multivariable control with and without input constraint, were used. Strangeland and Foss [106] applied a feedforward control scheme to a fixed bed reactor which used a secondary reactant injection at the middle of the reactor, with temperature measurements from the front part of the reactor, to reject slowly varying disturbances. A fixed bed reactor was controlled by exploiting the interaction between the response of temperature and concentration profiles in the bed. The outlet state of the reactor was controlled through reactor temperature measurement and manipulation of flow rate of a secondary feed stream.

Georgakis, Aris and Amundson [43,44,45] studied numerically the control of a jacketed nonadiabatic tubular reactor. The distributed parameter model was discretized by the method of orthogonal collocation and linearized near an unstable steady state. The system was stabilized around the unstable steady state profile by modal control and the concentration profile was estimated by the Luenberger observer utilizing temperature measurements. Later, it was shown [13] that for the parameters used in the simulation, the system model had an unrealistically low Peclet number. Joffe and Sargent [57] developed an on-line optimal control scheme for an adiabatic tubular reactor. The reaction was the consecutive type, $A \rightarrow B \rightarrow C$, with B the desired product. The initial catalyst activity and the decay rate were required in the control scheme and were estimated from the measurements. Vakil, Michelson, and Foss [108] investigated a feedforward scheme of a fixed bed reactor subject to random feed disturbances and afflicted with random

temperature measurement noise. A Kalman filter and an optimal controller were used. The reactor model was converted to state space form through orthogonal collocation in space.

A multivariable linear quadratic feedback controller for a butane hydrogenolysis reactor has been developed by Jutan and coworkers [58,59,60,61]. The partial differential equations of a nonadiabatic packed bed reactor model were converted to a low order state space model by using orthogonal collocation and linearized around a steady state. The model parameters were estimated by a Kalman filter from the reactor operating conditions. Then, the estimated model was used to develop a multivariable stochastic controller which regulated the exit concentrations through temperature measurements and adjustments in the feed flow rate. The process disturbances were characterized by adding white noise vectors to the state space model variables. The variance-covariance matrices of the white noise vectors were diagonal and two variance parameters were estimated from data. The controller was found to perform well in the presence of significant changes in catalyst activity. Later, two different assumed model structures for the stochastic disturbances combined with the state space model were investigated [62]. In the first structure, arbitrary white noise was added to the process state equations and known measurement noise was used for the measurement equation. In the second structure, an identified disturbance was associated with process noise and measurement noise was considered negligible. Controllers based on these two structures performed well on a laboratory reactor. Use of the previously determined measurement noise and separately identifying the process state noise were suggested. Wright et al. [116] investigated an inferential control scheme for the same system. Two methods were used to infer and control the product composition. The first method used orthogonal colloca-

tion techniques and the quasi steady state approximation for the product composition to reduce the model equations. The model parameters were obtained from pilot plant transient data. The second method used empirically fitted functions of the reactor bed temperatures and inlet flow rate to infer product composition. Coefficients of the estimator were updated on-line. Harris et al. [52] applied self-tuning regulators to control the same packed bed reactor. A number of self-tuning and adaptive algorithms were implemented to control the reactor hot spot temperature. Constraints on the manipulated variable were handled by Clarke's modification of the basic self-tuning regulator algorithm. Optimal sensor location for a packed bed tubular reactor was investigated by Harris et al. [53]. The optimal sensor locations were found to be those surrounding the hot spot location. They found that for good state estimation and good linear quadratic control of the reactor, only one or two well located temperature measurements were necessary rather than the entire temperature profile.

Sorensen [100,101] developed an optimal controller using a Kalman filter to control a nonadiabatic fixed bed reactor carrying out hydrogen oxidation. The reactor model was converted to the state space form by orthogonal collocation in the space coordinate and was linearized around a steady state. The method was applied to the on-line control of a pilot plant reactor. The state of the reactor was estimated by a Kalman filter from temperature, concentration and flow rate observations and the reactor was controlled by manipulation of the inlet temperature, the inlet concentration, and the flow rate. Later, Sorensen and coworkers [102,103] compared the discrete and continuous forms of Kalman filtering and optimal control for the same system. It was shown that the computational effort of the two implementations differed slightly, although the discrete version provided more realistic results at low sampling rates. When the discrete time

variance was evaluated with time intervals (varying from 0.167 to 5 minute) equal to the control intervals, oscillatory behavior of the axial temperature variance profile arose and was due to the time discretization of the control action. However, when the variance was evaluated with much shorter time intervals than the one used for control, the oscillations disappeared.

A nonlinear control strategy was proposed by Giger and coworker [47] to control the temperature peaks in the adiabatic fixed bed reactors for hydrodeaklylation. The temperature peaks were controlled by a secondary feed stream into the reactor at an intermediate point. A proportional controller was used to control feed flow rate as a function of inlet gas temperature and an intermediate bed temperature.

Foss and coworkers [113,114] investigated the control of product concentration in a two-bed reactor. The exothermic reaction between hydrogen and oxygen on a platinum catalyst was considered. Algorithms for control and estimation of product concentration were based on Linear Quadratic Gaussian control theory. Control action was done by manipulation of the temperature and hydrogen flow rate of a quench stream injected between the beds. Instead of recursive parameter estimation, nonlinear least-square fitting of steady state profiles was used to focus on the concentration reconstruction and control configuration analysis. A multivariable proportional integral controller, which manipulated the flow rate and temperature of an injected quench stream, was tested on a two-bed laboratory reactor. The control system was shown to perform well against a step-like 20% disturbance in feed concentration and in maintaining the hot spot temperature. Later [40], by the use of the characteristic locus method, a cascade of dynamic compensators, which suppressed the interactions between the variables, was developed for the same type of reactor. Three inputs, the flow rate and temperature of a quench

stream injected between the bed and the feed temperature, regulated the product concentration and temperature. Lappinga and Foss [66] investigated dual mode control with PI controller for the preheat exchanger of an autothermal reactor system. Regulation of the preheat temperature was achieved by the Smith-predictor configuration of internal model control. It was shown to be useful in a situation where a fast response was required from a system characterized by large time constants and dead times.

Bonvin and coworkers investigated the control of an autothermal reactor at an unstable state numerically [13] and experimentally [14,15,16,17]. The exothermic water-gas shift reaction was carried out by an iron-oxide catalyst at atmospheric pressure. The distributed parameter system equations were discretized in space through orthogonal collocation and linearized around a steady state. Modal control with state feedback was used to stabilize the system and also different model reduction techniques were compared. Convergence of the eigenvalues of the linearized model was found to be difficult to achieve in the unstable region. Thus, in that region a high order model (27 nonlinear ODEs) was needed to accurately describe the reactor behavior. A controller with state feedback showed good control action against an inlet heat pulse perturbation around the unstable region. Later, a pole placement self-tuning controller was developed by McDermott [73,74,75] and used to control the same system. The control objective was to regulate two temperatures in the catalyst bed with one just before the hot spot and the other at the exit of the bed. The manipulated variables were heat input at the feed entrance and feed flow rate. A 36th-order nonlinear reactor ODE model was used to simulate the operation at an upper steady state and intermediate unstable steady state.

Variable measurement structures within the framework of tubular reactor control were investigated by Alvarez and coworkers [1]. A fast and time-adaptive selection of

the best measurements was used in a low order and simple control scheme. The approach was based on a recursive computation of the state estimate errors. The adaptive nature of the measurement structure allowed changes in the sensitive area of the reactor to be followed. The estimates of the states were mostly affected by the projection of the previous errors into the state estimates which was defined by the structure of the system.

Mandler and et. al. [71] investigated the control strategies of a laboratory fixed bed reactor with feed-effluent heat exchange. Steady state relationships were presented to give an insight into the control problems. Later, they [72] developed an Internal Model Controller (IMC) for a fixed bed methanation reactor. The controller performance in terms of model uncertainty was tested by means of the Structured Singular Value (μ) analysis. Model uncertainty was described in terms of norm bounds. The control system was a single-input/single-output (SISO) design. The inlet feed temperature was used as the manipulated variable with the control objective being the regulation of the outlet gas temperature around a set point value where the conversion was mild. The sensitivity of the reactor was very high and the danger of a reactor runaway clearly existed.

Lee and Lee [68] developed a discrete-time multivariable adaptive control scheme for a nonadiabatic fixed bed reactor carrying out the partial oxidation of n-butane to maleic anhydride. The temperature measurement location in the reactor was determined by analysis of the steady state and dynamic reactor behavior. Later, an on-line optimization scheme [69] was applied to the system. The scheme consisted of identifying a dynamic model to use with the optimization procedure and using an adaptive controller to reach the new optimal point.

3.3 Control Problem and Objective

In general, the primary control objective of a fixed bed reactor is to operate within product quality specifications. For a fixed bed reactor, the specifications are typically placed on the exit stream composition. Therefore, it is necessary that the reactor is operated near the design concentration profile. When the reactor is subjected to process disturbances, such as changes in heat input, feed temperature, feed composition and flow rate, a control scheme is required to maintain the profile. Since reliable on-line concentration sensors are not available, the control strategy is directed at sustaining the reactor's temperature profile. By controlling the temperature profile, it is hoped that the concentration profile and exit composition are indirectly maintained.

Often, secondary control objectives also have to be met. In the case of tubular reactors carrying out exothermic reactions, controlling the hot spot temperature can be a major concern. Additional complicating factors which must be dealt with in the control of these types of reactors are the inverse response (often referred to as wrong-way behavior) and large dead times. The temperature and concentration changes in the reactor interact through the chemical reaction. They also propagate through the bed at distinctively different velocities. This can cause the wrong-way or inverse response behavior, one of the characteristic features of a packed bed reactor with exothermic reaction. Wrong-way behavior is used to describe the phenomenon such as a sudden decrease in feed temperature resulting in higher transient temperatures in the reactor bed, before the reactor bed temperature decreases to a new steady state temperature lower than original steady state temperature. To see how this might physically happen consider a sudden drop in the feed temperature, this will cause the front of the reactor

to cool down. With the reactor entrance at a lower temperature less conversion will take place, so the conversion will increase in sections down stream from the entrance leading temporarily to more reaction and thus higher temperatures downstream. Once the temperature wave propagates downstream and reduces the downstream temperature, the reaction rate will decrease causing the temperature to drop further.

The reactor with economizer (heat exchanger) system has an interesting aspect due to interactions between the two different units (the reactor and the economizer). A disturbance in the reactor can act as positive feedback through the economizer and thus affect total system stability. In such a case, keeping the reactor stable may become the main control objective and control of the feed temperature to the reactor becomes quite important.

The choice of controlled and manipulated variables plays an important role in this control problem and the development of effective control strategies. Thus, another objective of this research is to investigate the best sensor locations for measurement and the most effective inputs to be used for the design of control system structures. This study is presented in Chapter 4.

The control studies in this research apply two different types of control algorithms (Classical PI and DMC or QDMC) to this complicated nonlinear distributed reactor system. Chapter 5 contains these studies which represent only initial studies.

For single-input single-output control, two different cases will be tried and compared with PI controller performance: in the first case, DMC uses the feed temperature to control the reactor temperature close to the entrance, and in the second case, QDMC uses the feed temperature to control the reactor temperature right after the hot spot.

For multi-input multi-output control, two different cases with the QDMC algorithm

will be tried: the first case uses the feed temperature and the wall temperature to control the reactor temperature close to the entrance and close to the exit, and the second case uses the feed temperature and the wall temperature to control the reactor temperature close to the entrance and that right after the hot spot.

In all four cases, the control algorithms are tested for their ability to reject disturbances and maintain operation near the steady state concentration profile. The control strategy is directed at maintaining the reactor temperature at the selected sensor locations. By controlling the reactor temperature it is intended that the conversion profile and the exit conversion will be maintained indirectly.

Beside comparing the effectiveness of the four cases at achieving the main objective of maintaining the exit conversion, evaluation will be made on their success at meeting secondary control objectives. The secondary objectives addressed are keeping the temperature (or temperatures) under control at its set point (their set points) and reducing the excursions in the hot spot temperature.

CHAPTER 4

Sensor Location and Control Loop Pairing

4.1 Introduction

The choice of controlled and manipulated variables plays a very important role in this control problem and the development of effective control strategies. The objective of this chapter is to investigate the state variables to measure and the most effective inputs for the design of control system structure. Since fixed bed reactors are distributed chemical processes, the selection of manipulated variables and the sensor locations, along with control loop pairing are complicated problems associated with sensor sensitivity, conditioning, and sensor interaction to achive the desired control objectives. The control objective of maintaining a specific temperature profile to get the outlet concentration at an optimum level within a safe operating range is common. Since the measurement of concentration usually requires costly equipment and involves time lag, often it is estimated from the temperature profile along the reactor. Thus the selection of sensor locations has a large impact on the controller performance.

It is desirable in a control system that the sensor locations are sensitive to changes caused by the manipulated variables and provide good process conditioning for the control system structure. In the case of SISO design it is also desirable to minimize interactions so that changes in a manipulated variable mainly affects only one of controlled variables. Moore et. al. [77] showed that Singular Value Decomposition (SVD)

can be a useful tool in the selection of sensor locations and manipulated variables. The main idea to be developed in this section is the following: analyze a strategy based on the SVD analysis that will select the two best sensor locations for temperature measurements along the reactor and the two best manipulated variables from four potential manipulated variables (feed temperature, wall temperature, CO mole percent, and mass flow rate).

4.2 Singular Value Decomposition and Physical Interpretation

Singular Value Decomposition (SVD) has received a great deal of attention in the multivariable control area [35,36,46,63,98,99]. One application is to use the decomposition information from the steady state gain matrix to establish loop pairings similar to the RGA approach. Another development is the Singular Value Analysis Controller (SVAC) [99] that uses measurements of all controlled outputs to adjust all inputs. With the SVAC, the inputs and outputs are not paired. Thus, it is as a true multivariable controller. Also the number of inputs and outputs do not have to be equal. The design of this controller uses the steady state gain matrix so it does not incorporate dynamic information.

The decomposition can be applied to nonsquare or rectangular matrices. SVD is a decomposition of a matrix into two orthonormal matrices that are bases for both the range (output) space and the domain (input) space of a matrix and the diagonal matrix.

$$KG_{m\times n} = U_{m\times m}\Sigma_{m\times n}V^T_{n\times n} \tag{4.1}$$

where U is a $m \times m$ orthonormal matrix. The column vectors of U are called left singular (output) vectors. It can be interpreted that each column vector represents a direction

in the output space defined by a linear combination of sensor values. The first column vector points in the most sensitive sensor combination direction. The second column vector represent the next most sensitive direction and so on.

V is a $n \times n$ orthonormal matrix. The column vectors of V are called right singular (input) vectors. It can be interpreted that each column vector represent a direction in the input space defined by a linear combination of manipulated variables. The first column vector points in the direction of the most effective control actions which gives the largest response on the sensors. The second column vector represent the next most effective control actions of the manipulated variables on the sensors and so on.

Σ is a diagonal matrix and its nonzero elements (σ_1, σ_2, ...,σ_n, in descending order) are called singular values which determine the rank as the number of nonzero diagonal elements in the matrix. The condition number (K), a ratio between the maximum and minimum singular value, indicates the difficulty of implementing multivariable control in terms of system conditioning. A large condition number indicates a difficult system to control due to weak responses to control actions in the secondary directions.

The U and V matrices contain information about sensor interaction. The first column of V (Input Direction) is connected to the first column of U (Output Direction) by σ_1. The larger an element is in a column the more that input or output direction is defined by the associated physical variable.

For example, when the SVD of the steady state gain matrix is

$$\begin{bmatrix} 1 & 0 \\ 0 & -1 \end{bmatrix} \begin{bmatrix} \sigma_1 & 0 \\ 0 & \sigma_2 \end{bmatrix} \begin{bmatrix} 0 & -1 \\ 1 & 0 \end{bmatrix} \tag{4.2}$$

input 2 effects only output 1 and input 1 effects only output 2. Thus, there is no interaction in this example.

On the other hand, when the SVD of the steady state gain matrix is

$$\begin{bmatrix} \frac{1}{\sqrt{2}} & -\frac{1}{\sqrt{2}} \\ -\frac{1}{\sqrt{2}} & \frac{1}{\sqrt{2}} \end{bmatrix} \begin{bmatrix} \sigma_1 & 0 \\ 0 & \sigma_2 \end{bmatrix} \begin{bmatrix} -\frac{1}{\sqrt{2}} & \frac{1}{\sqrt{2}} \\ \frac{1}{\sqrt{2}} & -\frac{1}{\sqrt{2}} \end{bmatrix} \tag{4.3}$$

input direction 1 and 2 are both equally weighted by the two inputs. Likewise, the two output directions are equally weighted by both outputs.

Condition number (K) contains sensitivity and process conditioning information. The term, process conditioning, describes the ability of the inputs to change the outputs. The condition number (K) is used to quantify this characteristic, in the sense, the lower the condition number the better the process is conditioned. $K = 1$ is the best conditioning possible. When K gets larger, the process conditioning gets worse as the process is harder to move in the second direction indicated by corresponding second column vectors of U and V.

The term, sensitivity, refers to the ratio of the magnitude of change in an output to the magnitude of change in an input. The larger the ratio the more sensitive the relationship. A process steady state gain gives the sensitivity between a specific input and a specific output. The condition number (K) gives an indication of the relative sensitivity between the most sensitive input/output direction and the least sensitive input/output direction. These relationships are identified by using the SVD on the steady state gain matrix. They are expressed in terms of an input direction (a linear combination of all inputs with magnitude 1) to an output direction (a linear combination of all outputs with magnitude 1). The condition number is

$$\begin{aligned} K &= \frac{\text{Most Sensitive Input/Output Direction}}{\text{Least Sensitive Input/Output Direction}} \\ &= \frac{\sigma_1}{\sigma_n} \end{aligned}$$

For example, when σ_1 is 0.001 and σ_2 is 0.0005, the process is well conditioned ($K = 2$).

But the smallest singular value ($\sigma_2 = 0.0005$) indicates poor sensitivity. In consequence, it will lead to poor control. On the other hand, when σ_1 is 4 and σ_2 is 2, the process is well conditioned ($K = 2$). Also the smallest singular value ($\sigma_2 = 2$) indicates good sensitivity. In consequence, it will lead to good control.

Moore et. al. [77] called the reciprocal of the condition number, $1/K$, an index for "sensor interaction". But from the above discussion, it would be more proper to call that term an index for "process conditioning". Thus, from now on the term, $1/K$, will be called "process conditioning" in this dissertation.

There are four possible manipulated variables considered in this reactor control system:

F: Feed temperature

W: Wall temperature

C: CO mole percent

M: Mass flow rate

The gain matrix in Table 4.1 was created by averaging the steady state gain values obtained from both positive and negative changes in the possible manipulated variables (see Tables 2.4 and 2.5). Recall from Chapter 2 that the unit used for all ΔT was K and for Δx_{CO} was mole %. The units used for ΔG were G change % where these units are defined as the percent change in G from its base case value (G change % = $\frac{G^* - G^*_{ref}}{G^*_{ref}} \times 100$).

For a two-input and two-output control system configuration, there are six possible combinations of manipulated variables (FW, FC, FM, WC, WM, and CM). Each combination has a 20×2 gain matrix which describes the temperature gain at each sensor location with respect to each manipulated variable.

But the smallest singular value ($\sigma_2 = 0.0005$) indicates poor sensitivity. In consequence, it will lead to poor control. On the other hand, when σ_1 is 4 and σ_2 is 2, the process is well conditioned ($K = 2$). Also the smallest singular value ($\sigma_2 = 2$) indicates good sensitivity. In consequence, it will lead to good control.

Moore et. al. [77] called the reciprocal of the condition number, $1/K$, an index for "sensor interaction". But from the above discussion, it would be more proper to call that term an index for "process conditioning". Thus, from now on the term, $1/K$, will be called "process conditioning" in this dissertation.

There are four possible manipulated variables considered in this reactor control system:

F: Feed temperature

W: Wall temperature

C: CO mole percent

M: Mass flow rate

The gain matrix in Table 4.1 was created by averaging the steady state gain values obtained from both positive and negative changes in the possible manipulated variables (see Tables 2.4 and 2.5). Recall from Chapter 2 that the unit used for all ΔT was K and for Δx_{CO} was mole %. The units used for ΔG were G change % where these units are defined as the percent change in G from its base case value (G change % = $\frac{G^* - G^*_{ref}}{G^*_{ref}} \times 100$).

For a two-input and two-output control system configuration, there are six possible combinations of manipulated variables (FW, FC, FM, WC, WM, and CM). Each combination has a 20×2 gain matrix which describes the temperature gain at each sensor location with respect to each manipulated variable.

Table 4.1: Average Steady State Gain for Feed Temperature, Wall Temperature, CO Mole Percent, and Mass Flow Rate

Sensor Location (z)	Feed Temp. $(\Delta T/\Delta T_f)$	Wall Temp. $(\Delta T/\Delta T_w)$	CO Mole %. $(\Delta T/\Delta x_{co})$	Mass Flow Rate $(\Delta T/\Delta G\%)$
1 (0.0034)	0.91405	0.00895	0.01767	-0.00285
2 (0.0180)	0.92195	0.03440	0.06733	-0.00845
3 (0.0439)	0.93125	0.07850	0.16133	-0.01775
4 (0.0804)	0.93035	0.14290	0.29533	-0.02965
5 (0.1268)	0.90730	0.22110	0.46667	-0.04125
6 (0.1820)	0.84760	0.30910	0.64300	-0.04895
7 (0.2446)	0.75570	0.39050	0.78517	-0.04880
8 (0.3131)	0.64175	0.45910	0.84817	-0.04020
9 (0.3861)	0.52525	0.50835	0.83733	-0.02700
10 (0.4617)	0.41790	0.54850	0.77317	-0.01300
11 (0.5383)	0.33030	0.58120	0.69533	-0.00150
12 (0.6139)	0.26230	0.61385	0.61517	0.00650
13 (0.6869)	0.21360	0.64215	0.54900	0.01150
14 (0.7554)	0.17780	0.67005	0.49183	0.01450
15 (0.8180)	0.15350	0.69240	0.44817	0.01650
16 (0.8732)	0.13495	0.71315	0.40917	0.01750
17 (0.9196)	0.12285	0.72800	0.38333	0.01800
18 (0.9561)	0.11350	0.74140	0.36167	0.01800
19 (0.9820)	0.10845	0.74900	0.35017	0.01800
20 (0.9966)	0.10520	0.75360	0.34200	0.01800

The decomposition of this 20×2 gain matrix is a 20×2 U matrix (the first two column vectors of U), a 2×2 V matrix, and two singular values. For example, in the case of feed temperature and wall temperature (FW) as manipulated variables, the decomposition results are presented in Table 4.2. PRO-MATLAB [88] is used for numerical analysis of SVD of the gain matrices throughout this study.

4.3 Selection of Sensor Locations

The SVD analysis of a steady state gain matrix not only provides insight into the control of multivariable processes, but also provides tools to evaluate possible sensor locations in terms of the sensor sensitivity to control inputs and process conditioning. The analysis which follows is based on the concept of sensor selection by SVD analysis developed by Moore et. al. [77]. There are three methods of selection of sensor location selection: principle component analysis, modified principle component method, and partial SVD analysis.

4.3.1 Principal Component Analysis

The principle component analysis (PCA) bases the selection of sensor location on the principle components in the left singular (output) vectors, U. Each column of U represents a direction in the output space. These directions are orthonormal and are defined as a linear combination of the process outputs. In the case of SVD analysis of FW control, there are two vectors in U, each has 20 elements. In each vector the elements represent the weighting in the output direction for each of the 20 potential sensor locations in the reactor. The first column vector points in the most sensitive output

Table 4.2: Feed Temperature and Wall Temperature (FW) SVD Analysis

$$U = \begin{bmatrix} 0.2292 & -0.3233 \\ 0.2366 & -0.3156 \\ 0.2484 & -0.3006 \\ 0.2620 & -0.2736 \\ 0.2730 & -0.2329 \\ 0.2770 & -0.1750 \\ 0.2716 & -0.1084 \\ 0.2580 & -0.0391 \\ 0.2396 & 0.0230 \\ 0.2215 & 0.0780 \\ 0.2067 & 0.1230 \\ 0.1968 & 0.1608 \\ 0.1908 & 0.1900 \\ 0.1879 & 0.2144 \\ 0.1866 & 0.2324 \\ 0.1865 & 0.2476 \\ 0.1866 & 0.2581 \\ 0.1872 & 0.2670 \\ 0.1876 & 0.2720 \\ 0.1877 & 0.2750 \end{bmatrix}$$

$$V = \begin{bmatrix} 0.7563 & -0.6531 \\ 0.6531 & 0.7573 \end{bmatrix}$$

$$\Sigma = \begin{bmatrix} 3.4058 & 0 \\ 0 & 1.8252 \end{bmatrix}$$

direction and the second column vector points in the next most sensitive direction.

The procedure for PCA sensor location selection is simpl. Perform the SVD analysis on the gain matrix and then select the locations which correspond to the most sensitive element in each left singular vectors. For the FW example (see Table 4.2), the element with the lagest absolute value (0.2770) in the first column vector of U is the sixth element which corresponds to sensor 6 (T6). The largest absolute value of an element (0.3233) in the second column vector of U is the first element or sensor 1 (T1).

The PCA results for all six of the possible sets of manipulated variables taken two at a time are presented in Section 4.3.4. These results These results are compare with two other sensor selection procedures.

4.3.2 Modified Principal Component Analysis

Modified principle component analysis (MPCA) is a modification the of the principal component analysis. It adjusts the sensor selection to consider both between sensor sensitivity and interaction. There are some cases where sensor sensitivity requirements must be traded off for sensor interaction reduction. This method takes the difference between the absolute value of the corresponding elements of the two left singular (output) vectors, that is,

$$\ell_i = |U_{1i}| - |U_{2i}| \quad i = 1, .., 20 \tag{4.4}$$

where ℓ_i is the MPCA index, U_{1i} is the ith element in the first left singular vector of U, and U_{2i} is the ith element in the second left singular vector of U. The position of the positive peak and negative peak in this index is taken as the position of the primary sensor location and the secondary sensor location, respectively. For example, Figure 4.1 plots the this index for the manipulated variables FW. The modified procedure in this

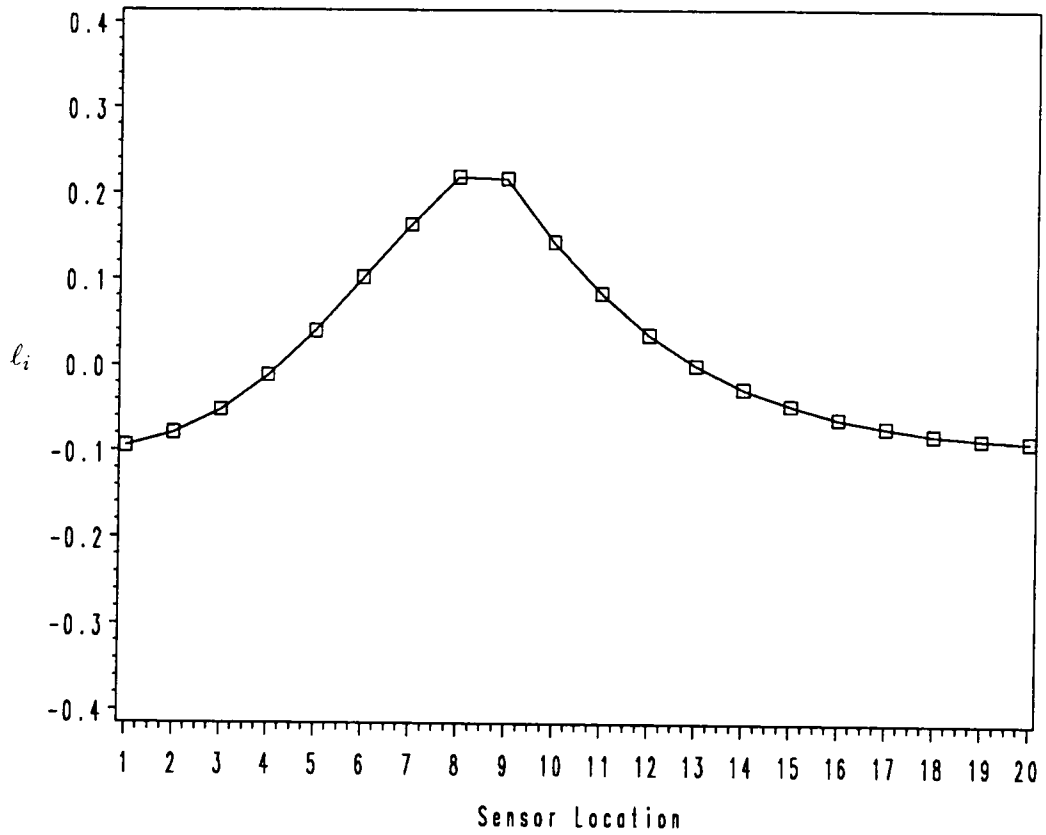

Figure 4.1: Modified Principal Component Analysis: $|U_{1i}| - |U_{2i}|$ vs. sensor location

example suggests that sensor locations 1 and 8 are good choices (positive and negative peaks).

Again, the MPCA results for five other manipulated variable sets are collected in Section 4.3.4 for comparison to results from other sensor placement methods.

4.3.3 Partial Singular Value Analysis

Partial singular value analysis (PSVA) investigates the best two sensor locations by analyzing the SVD of all possible two-input and two-output systems. For the reactor with 20 sensor locations for each two input combination there are 190 possible two-input and two-output systems or 2×2 steady state gain matrices. The selection of the best sensors and best manipulated variables by the PSA method is based on minimizing the condition number and maximizing the sensitivity.

The process conditioning is the reciprocal of the condition number. The largest value for process conditioning is therefore 1. The larger the reciprocal of the condition number implies the better the multivariable control structure from the aspect of process conditioning.

The sensor sensitivity is largely concerned with the sensitive measurement. This is indicated by the second singular value of each two input and two sensor combination. This term is associated with the weaker direction in terms of process response to control system action which requires greater response than the noise level of the sensor for practical control system consideration.

When the selection of the sensor location considers both process conditioning and sensitivity a compromise is often required. A term called "intersivity", which is the product of these two terms (the second singular value / the condition number), is used.

It is desired to have both the process conditioning and sensor sensitivity large. Thus, the idea is look for the largest intersivity.

The procedure for this method is first to perform 2-input and 2-output partial SVD analysis for the 190 possible sensor combinations of two temperature sensor locations for each manipulated variable set. One way to evaluate this information is to use 3 dimensional plots. They are a processs conditioning (sensor location 1 vs. sensor location 2 vs. $1/K$), a sensor sensitivity (sensor location 1 vs. sensor location 2 vs. $1/\sigma_2$), and an intersivity (sensor location 1 vs. sensor location 2 vs. σ_2/K) plots.

Figure 4.2 shows with a 3-D plot the process conditioning for all possible combinations of two temperature measurements with the feed temperature and the wall temperature as manipulated variables (FW control). This plot addresses the process conditioning for all combinations of sensors taken two at a time for the inputs, the feed temperature and wall temperature. The peak occurs for temperature sensors placed at collocation points 1 and 20 to measure temperatures, T1 and T20. The process conditioning has a high value of 0.79 as the highest value possible is 1.

Figure 4.3 is formatted in the same manner as Figure 4.2 only σ_2, the second (smaller) singular value, is plotted. This plot addresses the sensitivity of the least sensitive (the second) sensor for all combinations of sensors taken two at a time for the inputs, the feed temperature and wall temperature. Again the peak occurs for temperature sensors placed at collocation points 1 and 20 to measure temperatures, T1 and T20.

Figure 4.4 is also formatted in the same manner as Figure 4.2 only $\sigma 2/K$ is plotted. This analysis addresses the compromise in the selection of sensor location between process conditioning and sensor sensitivity. Figures 4.2 and 4.3 show there is no com-

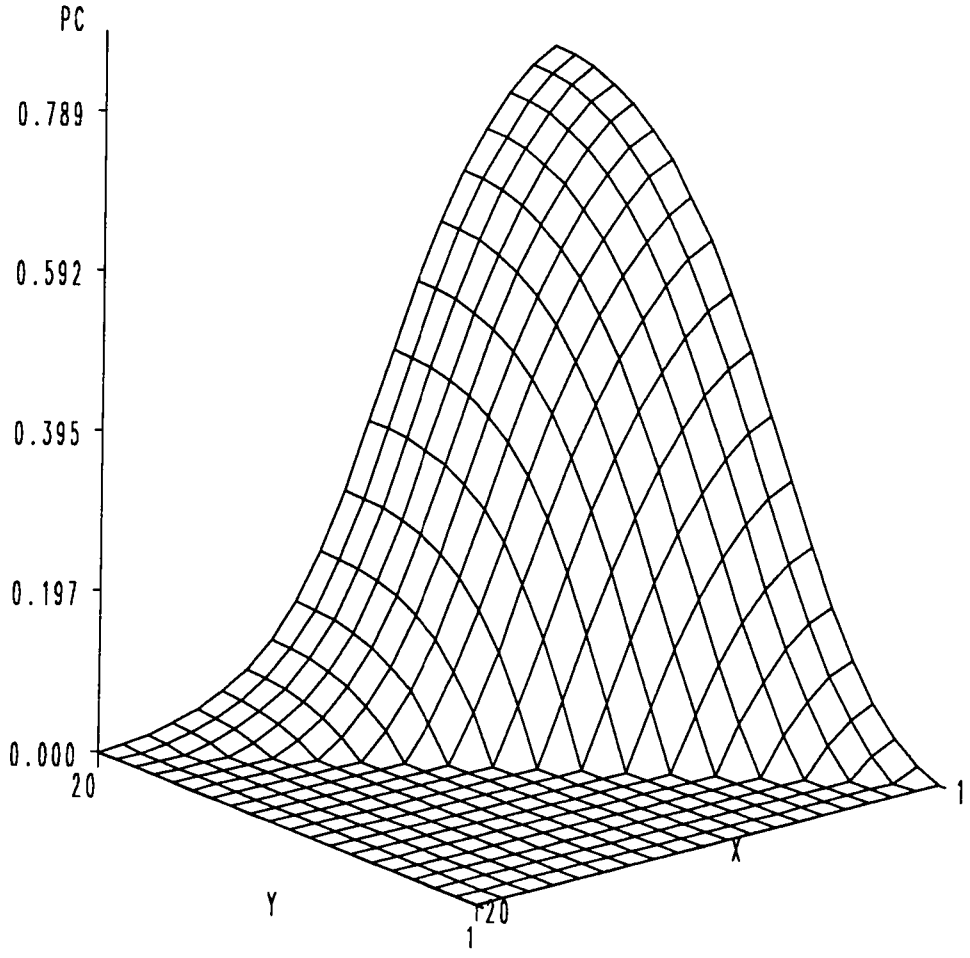

Figure 4.2: Process conditioning (1/condition number) vs. sensor location for the feed temperature and the wall temperature as manipulated variables.

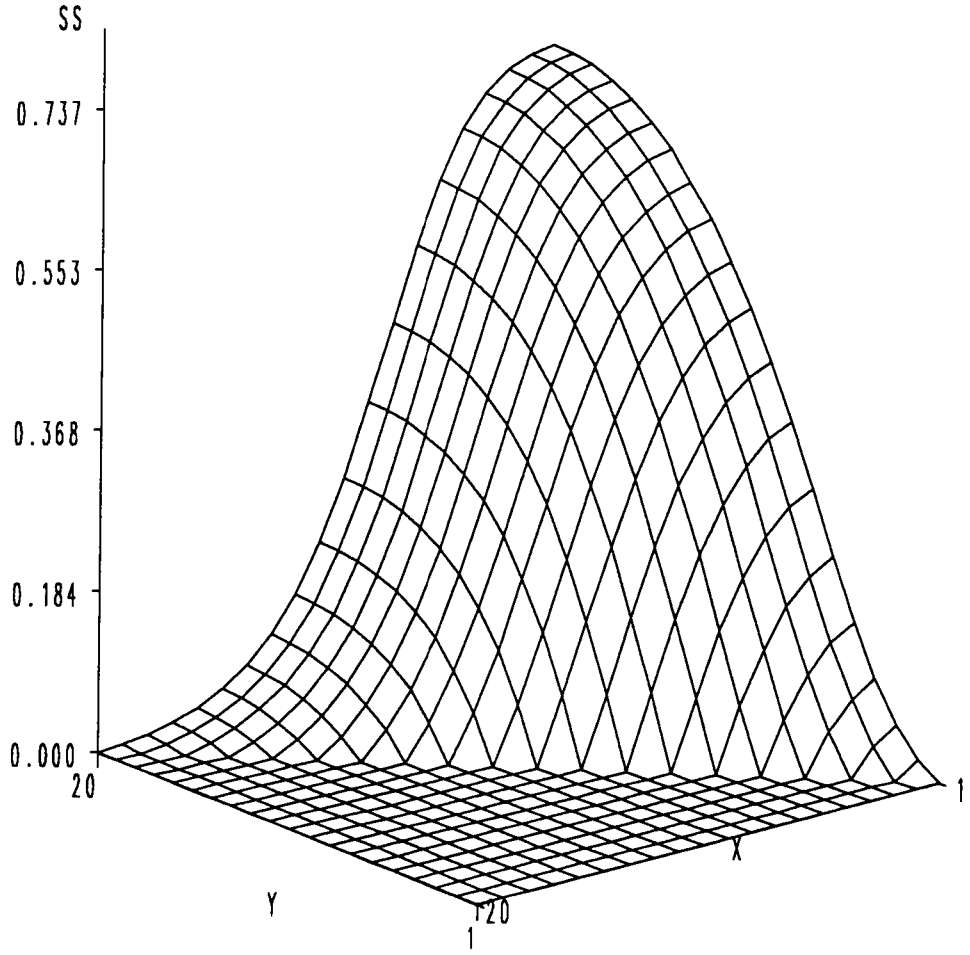

Figure 4.3: Sensor sensitivity (the second singular value) vs. sensor location for the feed temperature and the wall temperature as manipulated variables.

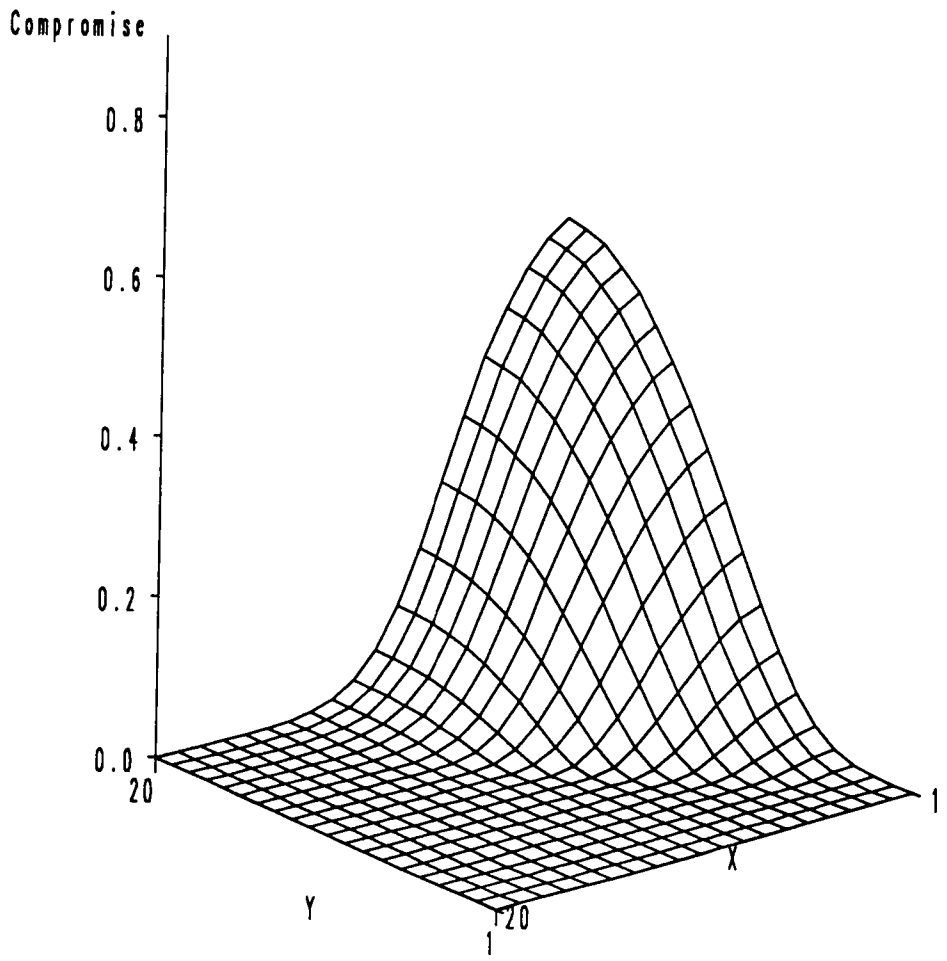

Figure 4.4: Sensor intersivity (the second singular value/condition number) vs. sensor location for the feed temperature and the wall temperature as manipulated variables.

promise as both process conditioning and sensor sensitivity are optimized at the same axial positions at 1 and 20. Figure 4.4 confirms this with the enhanced peak at sensor locations.

The overall analysis based on PSVA indicates that temperature sensors placed at collocation points on 1 and 20 are the best structure for the multivariable problem. When feed temperature and wall temperature are the manipulated variables. This physically makes sense, as observed in the steady state simulations in Chapter 2 and the steady state gains in Table 4.1. The feed temperature has its largest effect on the front of the reactor while the wall temperature has its largest effect on the end of the reactor.

For the case of feed temperature and CO mole percent as manipulated variables (FC control), Figure 4.5 shows the process conditioning peak is at sensor locations 1 and 11 where conditining is 0.6. In Figure 4.6 the sensor sensitivity surface shape is observed to be very similar to process conditioning. The peak is located at sensor locations 1 and 10 where $\sigma_2 = 0.7$. Once again Figure 4.7 shows there is no compromise to bemade as the conditioning and sensor sensitivity are both best using essentially the same two sensors. This analysis indicates that for the FC control structure utilizing temperature sensors 1 and 11 is the best choice for the multivariable system. The results seems resonable, since the feed temperature is expected to be most effective in the front part of the reactor and the CO mole percent is expected to be most effective at the center. This is different than the case of feed temperature and wall temperature as manipulated variables as one sensor locationed near the center of the reactor bed.

Figures 4.8 and 4.9 show the process conditioning and sensor sensitivity when the feed temperature and mass flow rate are used as manipulated variables (FM control).

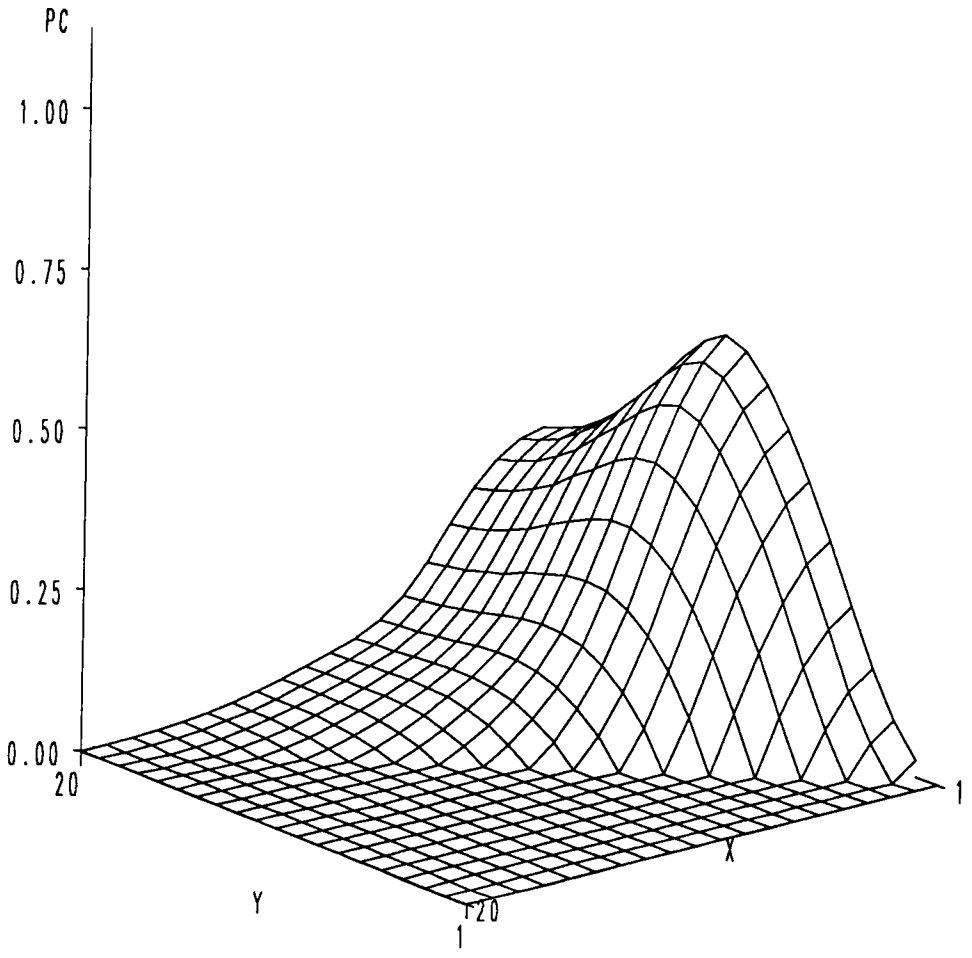

Figure 4.5: Process conditioning (1/condition number) vs. sensor location for the feed temperature and CO mole percent as manipulated variables.

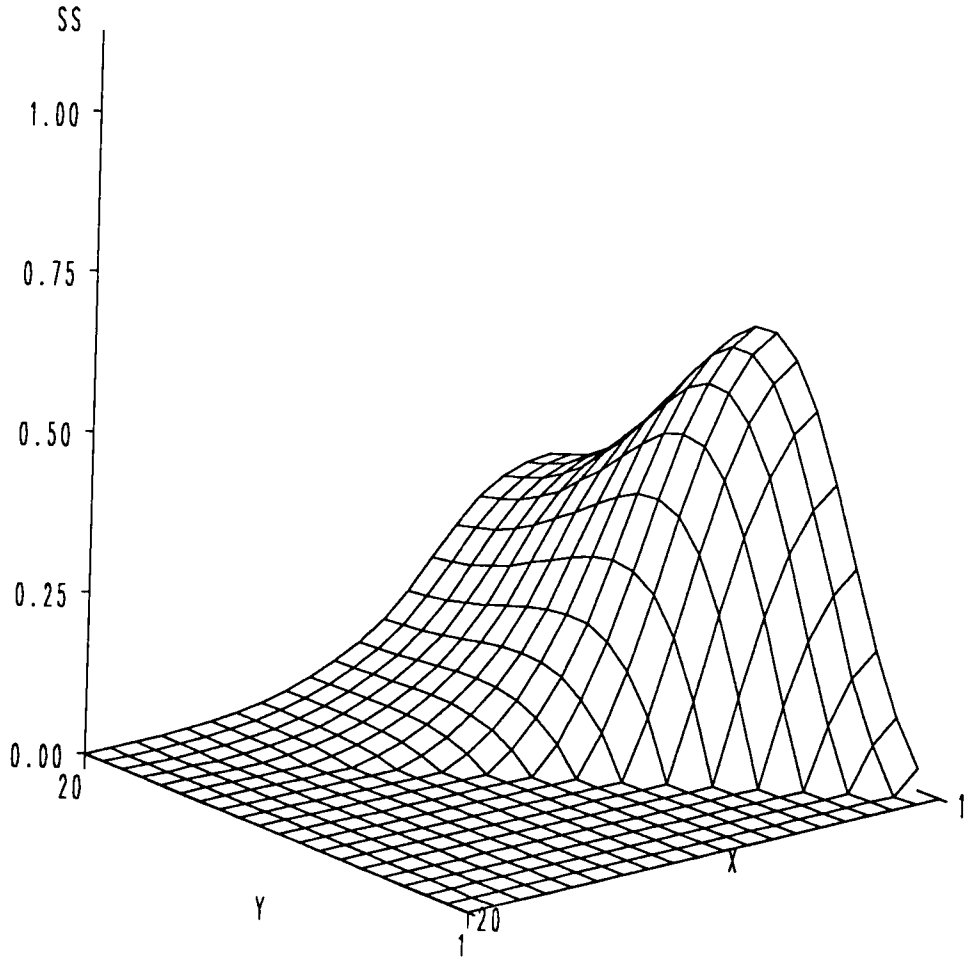

Figure 4.6: Sensor sensitivity (the second singular value) vs. sensor location for the feed temperature and CO mole percent as manipulated variables.

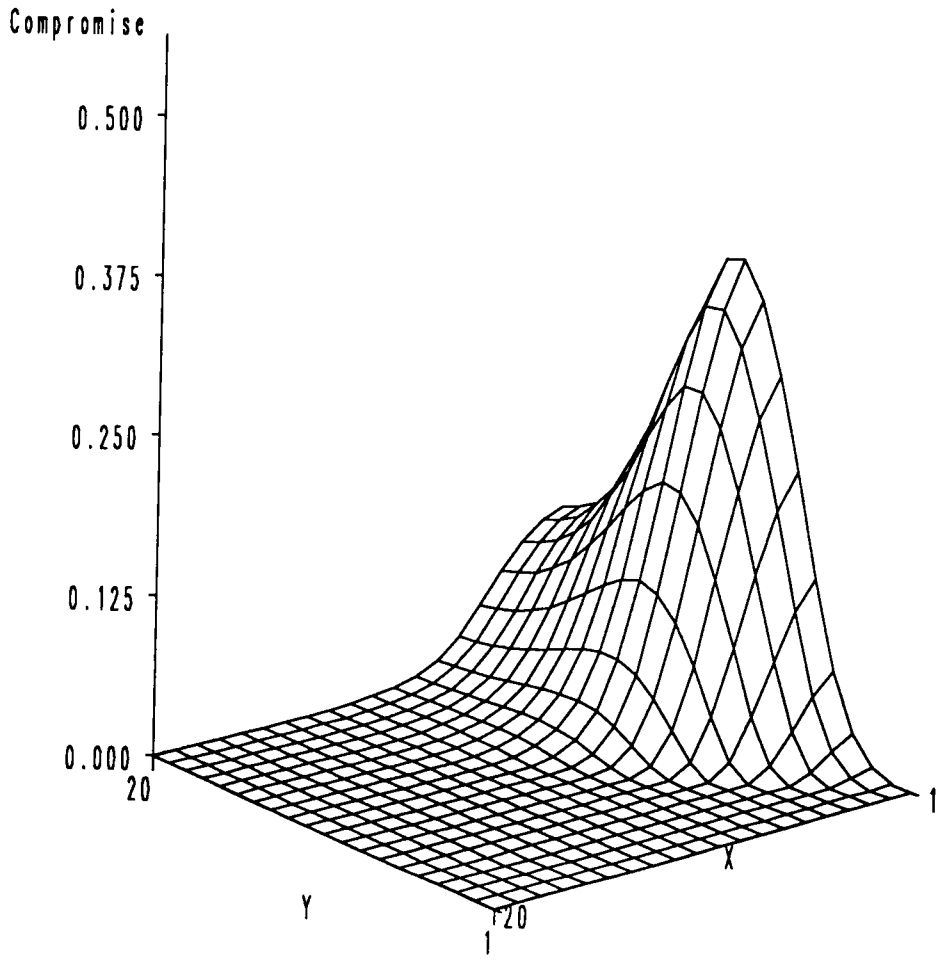

Figure 4.7: Sensor intersivity (the second singular value/condition number) vs. sensor location for the feed temperature and CO mole percent as manipulated variables.

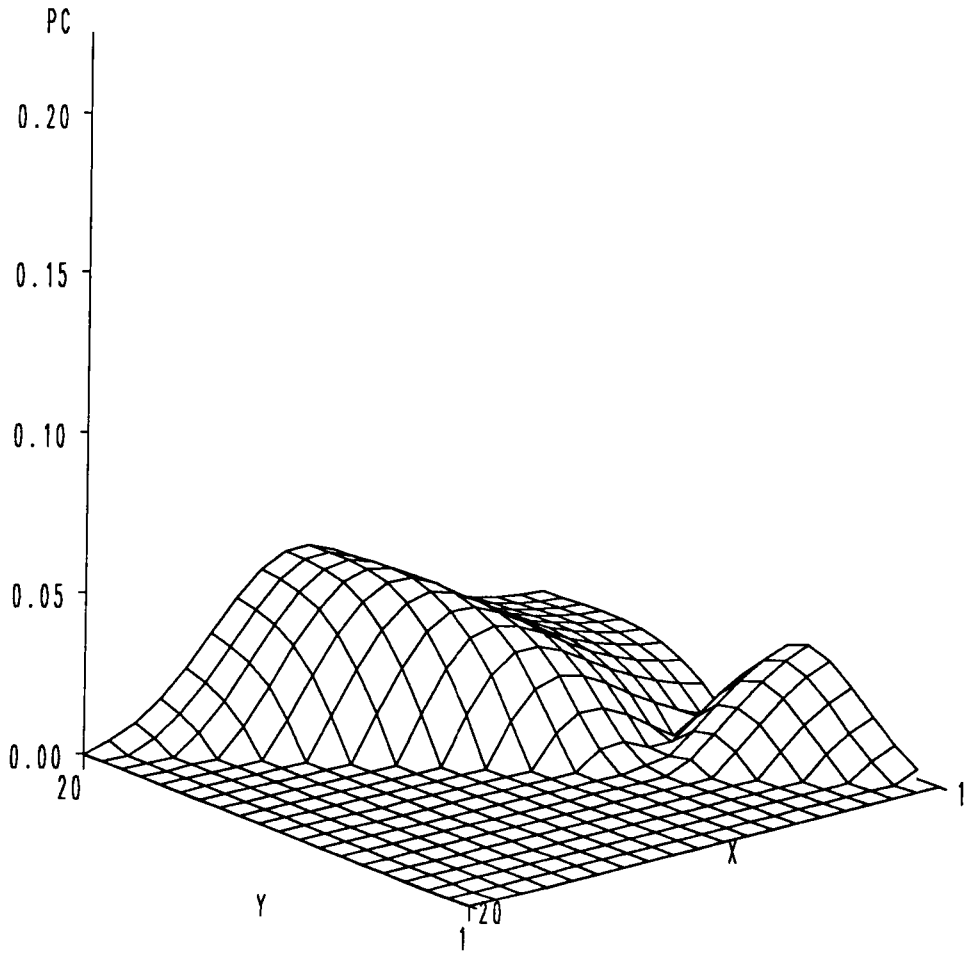

Figure 4.8: Process conditioning (1/condition number) vs. sensor location for the feed temperature and mass flow rate as manipulated variables.

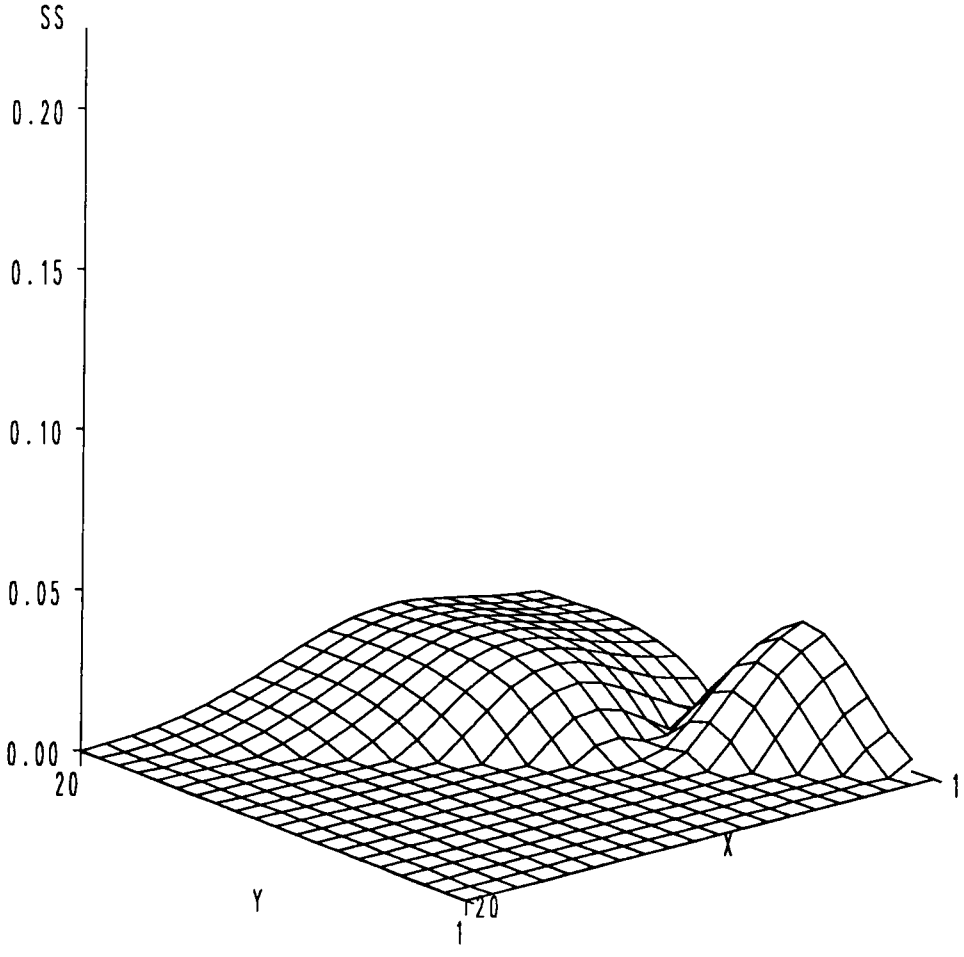

Figure 4.9: Sensor sensitivity (the second singular value) vs. sensor location for the feed temperature and mass flow rate as manipulated variables.

Figure 4.8 shows that process is the poorly conditioned with a maximum conditioning of .03. The best sensor locations are spread into two major peaks in terms of process conditioning. Considering only the maximum value on the surface choice for process conditioning is sensor locations 11 and 20. The sensor sensitivity surface in Figure 4.9 indicates the front part of reactor (sensor location 1 and 7) is a better choice than the end of the reactor for such multivariable system, but σ_2 is very small (σ_2=.04). Again, the process conditioning surface is similar to the sensitivity surface. Overall both the terms of process conditioning and sensitivity are low so this would be a poor control structure selection. The conditioning and sensitivity surfaces both show two peaks. The global optimum on the two surfaces ends up on different peaks so there is perhaps some compromise in the FM control case. Figure 4.10 identifies sensor locations 1 and 7 to be slightly better by the compromise guide.

Figures 4.11 and 4.12 show the surfaces for process conditioning and sensor sensitivity of the wall temperature and mass flow rate as manipulated variables (WM control). Figure 4.11 shows that the process is poorly conditioned. The process conditioning is peak at sensor locations 6 and from 13 to 20. The sensor sensitivity plot in Figure 4.12 also indicates the same sensor locations are the best. But σ_2 is relatively small. Again, Figure 4.13 shows there is no compromise to be made.

Figures 4.14 through 4.16 for the manipulated variables of the wall temperature and CO mole percent (WC control) show the surface for process conditioning, sensor sensitivity and intersivity. This case is very similar to the wall temperature and mass flow rate as manipulated variables (WC), again the best sensor locations are at 6 to 7 and 20. In this case the process conditioning and sensor sensitivity terms are considerably larger. The results seem physically reasonable in that the mass flow rate and CO mole

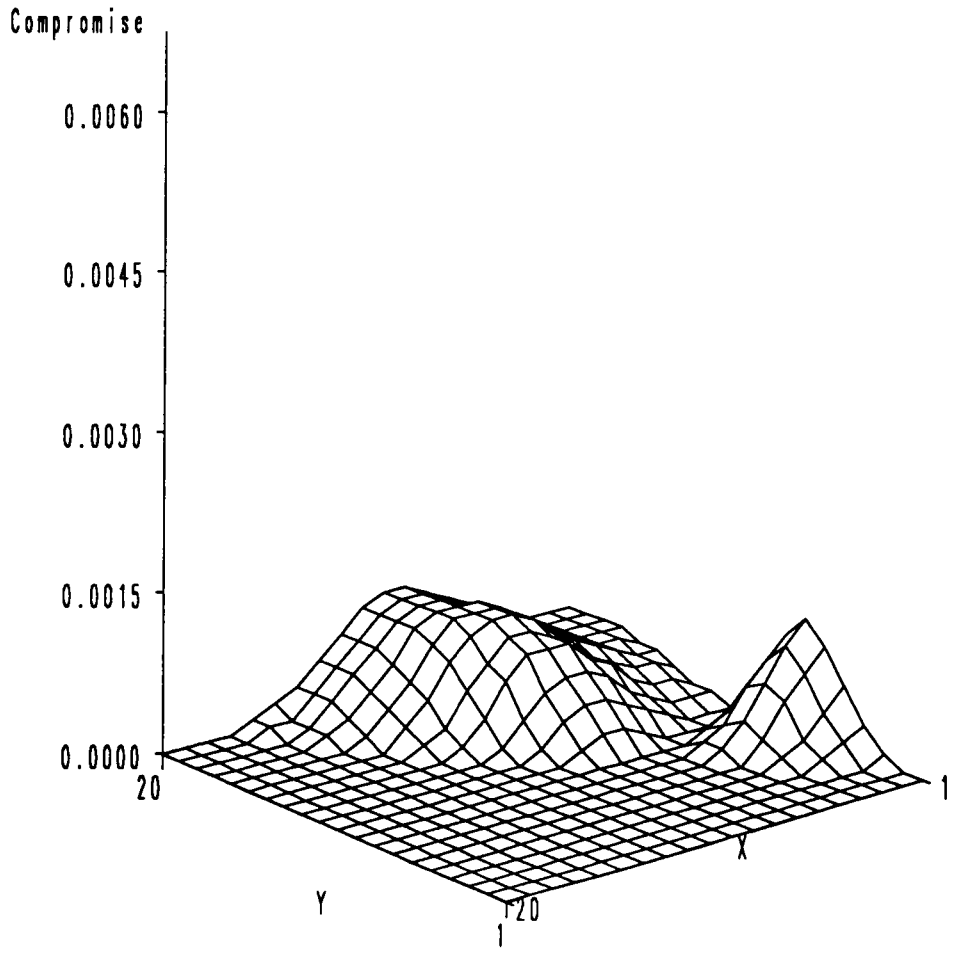

Figure 4.10: Sensor intersivity (the second singular value/condition number) vs. sensor location for the feed temperature and mass flow rate as manipulated variables.

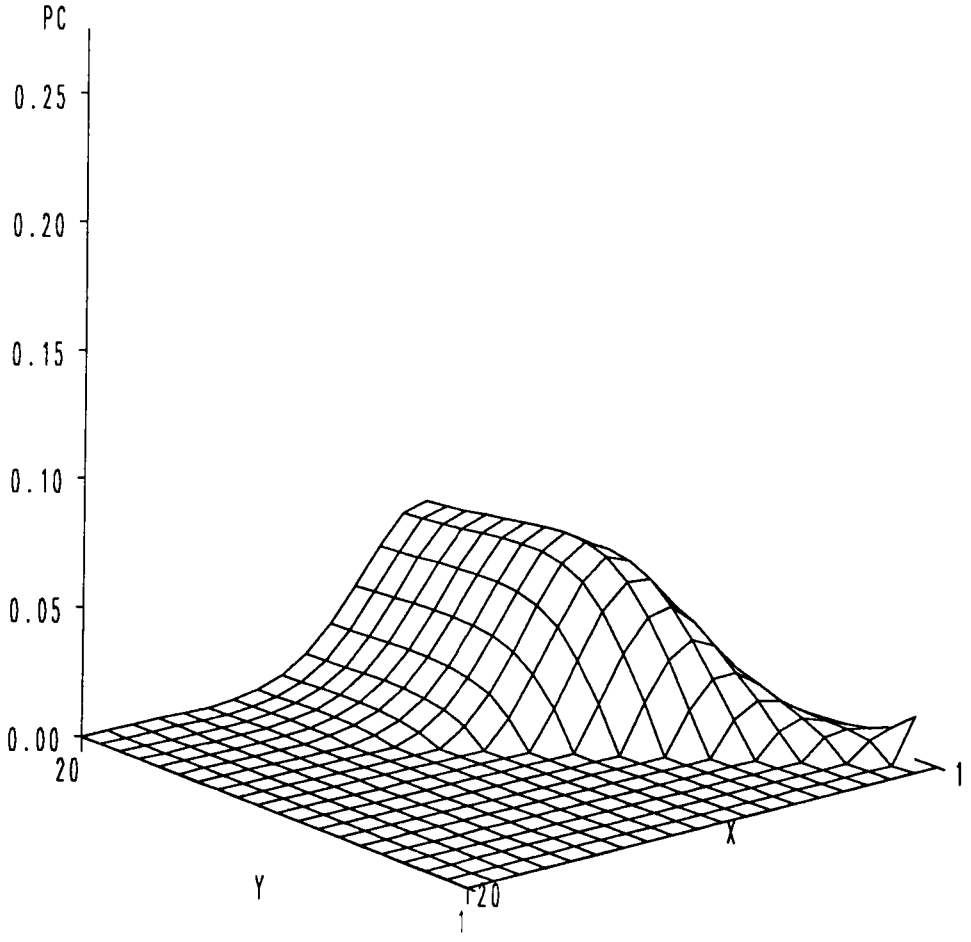

Figure 4.11: Process conditioning (1/condition number) vs. sensor location for the wall temperature and mass flow rate as manipulated variables.

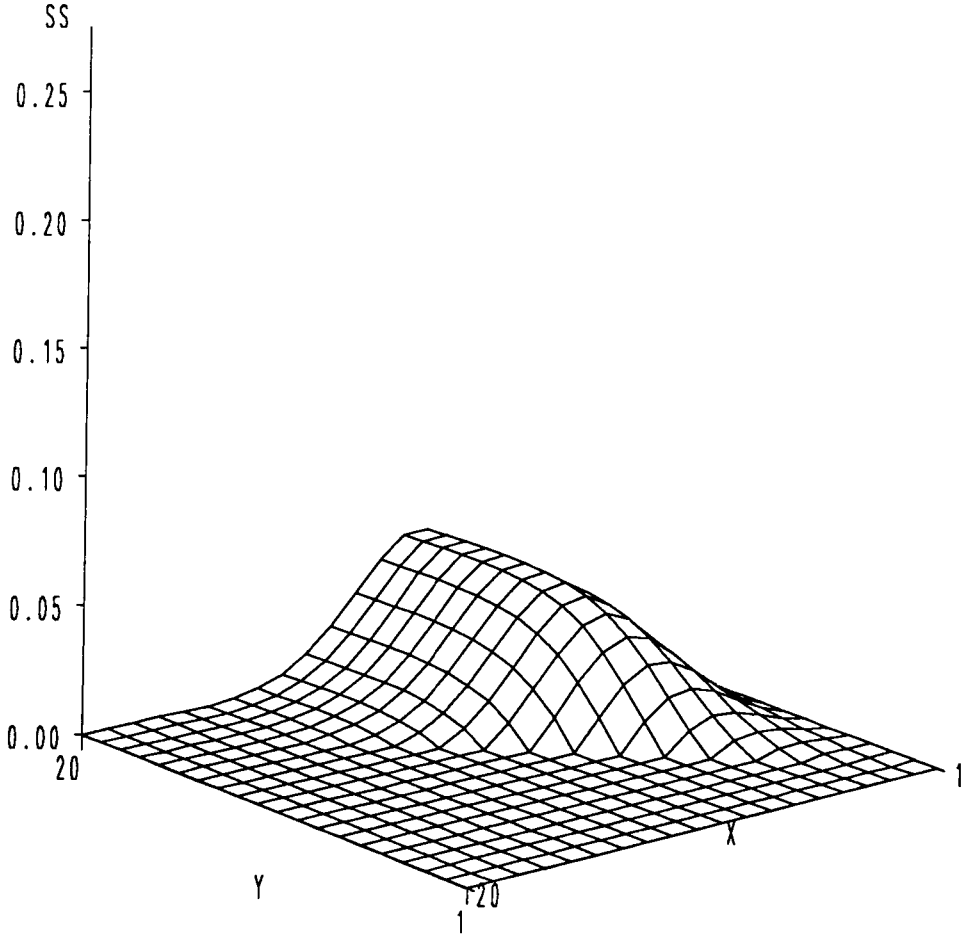

Figure 4.12: Sensor sensitivity (the second singular value) vs. sensor location for the wall temperature and mass flow rate as manipulated variables.

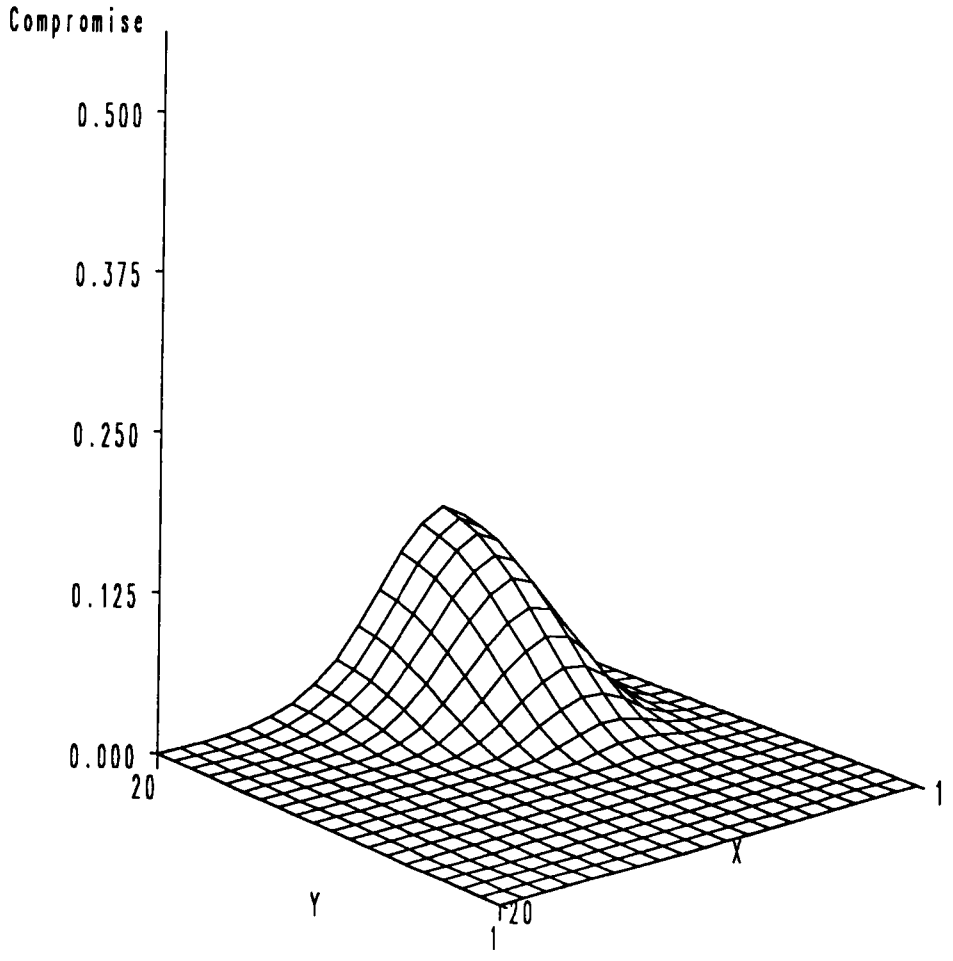

Figure 4.13: Sensor intersivity (the second singular value/condition number) vs. sensor location for the wall temperature and mass flow rate as manipulated variables.

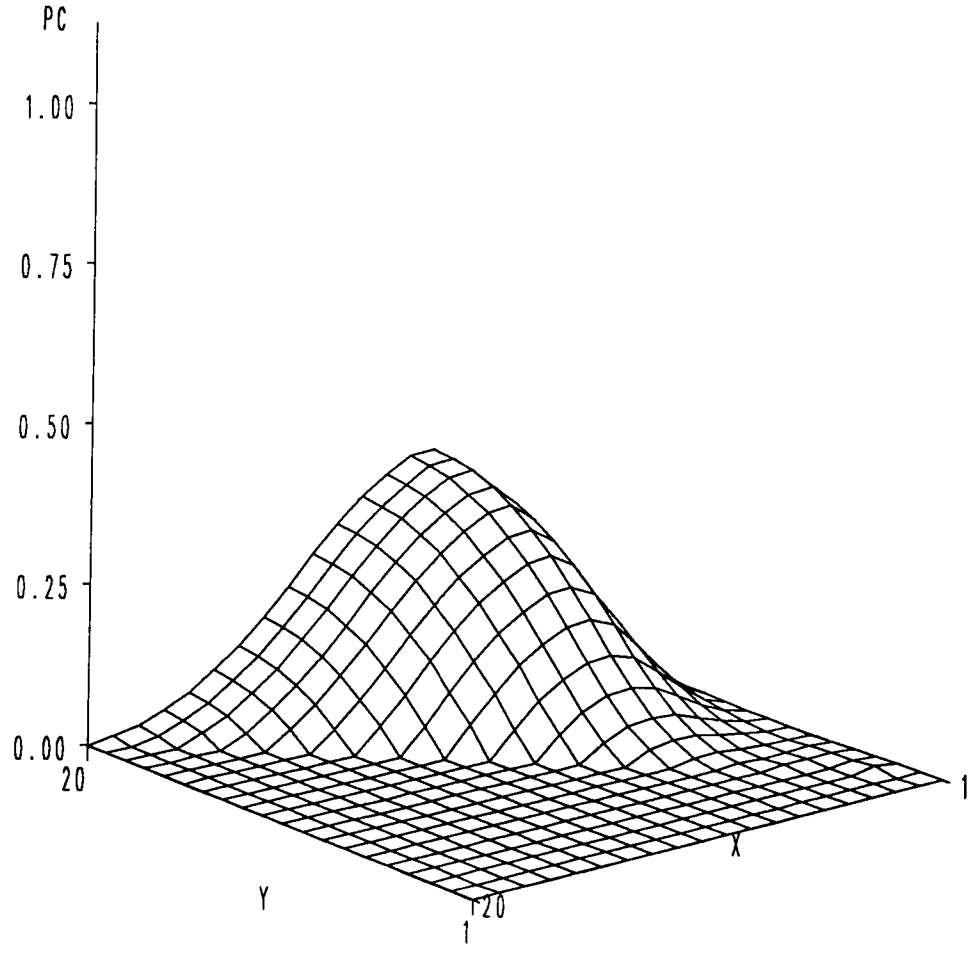

Figure 4.14: Process conditioning (1/condition number) vs. sensor location for the wall temperature and CO mole percent as manipulated variables.

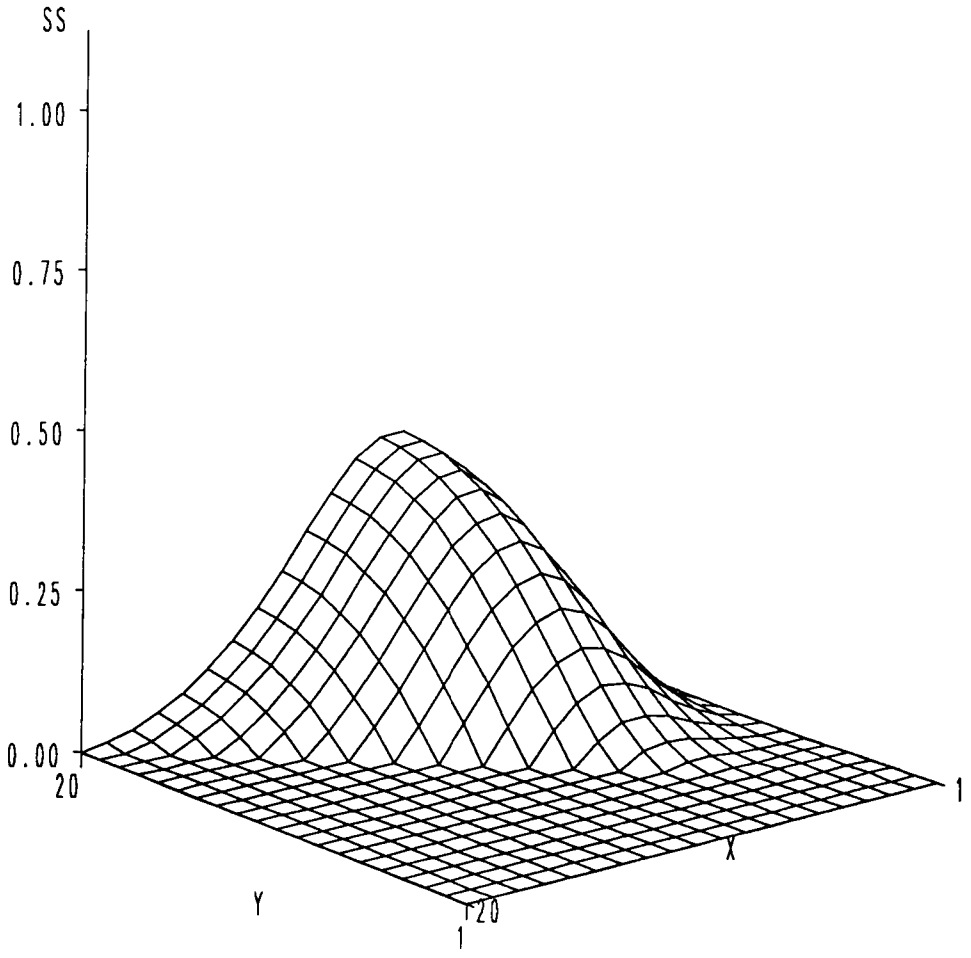

Figure 4.15: Sensor sensitivity (the second singular value) vs. sensor location for the wall temperature and CO mole percent as manipulated variables.

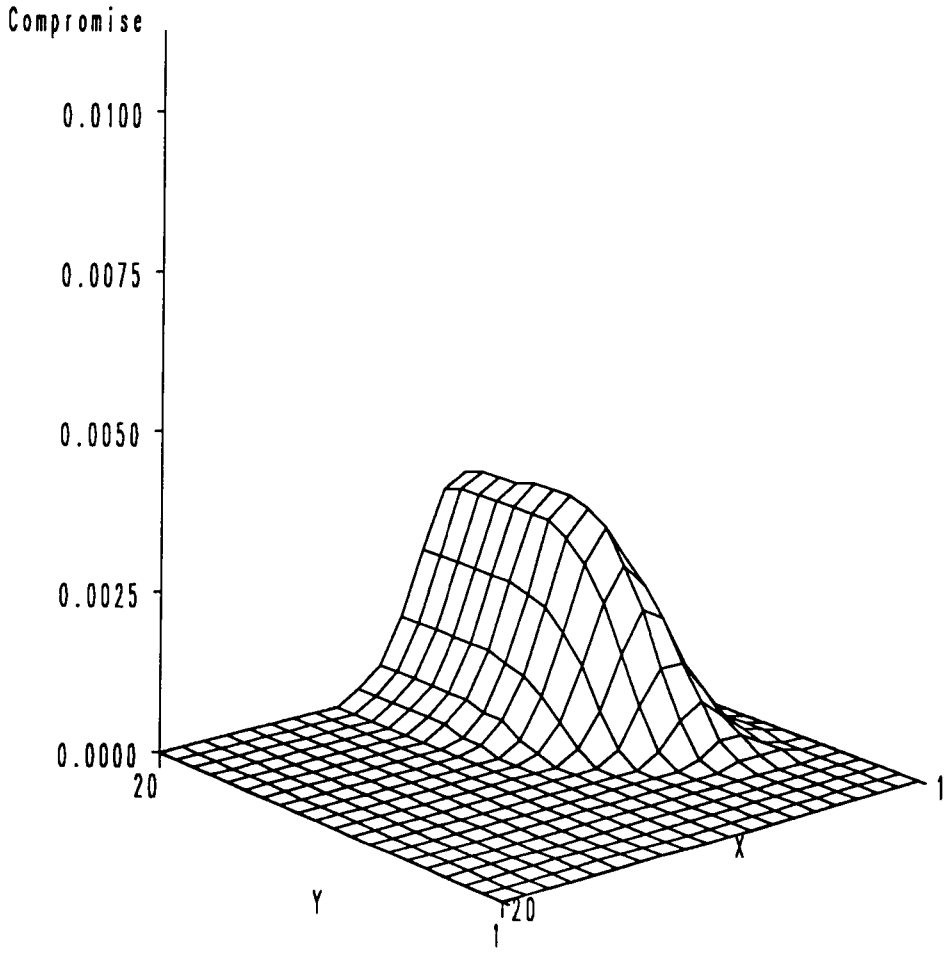

Figure 4.16: Sensor intersivity (the second singular value/condition number) vs. sensor location for the wall temperature and CO mole percent as manipulated variables.

percent have a similar effects on the reactor, since both variables increase the amount of CO to react. The analysis indicates that the temperature sensors 6 and 20 is the best choice for this multivariable system.

Finally, the aspects of sensor sensitivity and conditioning with CO mole percent and mass flow rate as manipulated variables are illustrated in Figure 4.17 and Figure 4.19. These figures indicate that the sensor locations 4 and 20 are the choice for this multivariable system. Note that both inputs will have a similar effect on the reactor, thus poor process conditioning is expected. The sensor sensitivity is generally small which would be expected from the steady state gains at locations 4 and 20 for CO mole percent and mass flow rate to the temperature shown in Table 4.1.

4.3.4 Results and Discussions

Table 4.3 collects the selection of temperature sensor locations based on three different methods (PCA, MPCA, PSVA). The first two methods (PCA, MPCA) include all 20 potential temperature sensors in the SVD analysis, in this case a 20×2 steady state gain matrix, while the third method (PSVA) uses all possible 2×2 gain matix in the so called partial SVD analysis which is based on sensors which will be actually used in the 2×2 control strategy.

In general, the singular values of the PSVA are less than the singular values from the PCA. The selection of sensor location by partial singular value analysis has a tendency to spread out the sensor locations compared to the principal component analysis in this study. PCA usually chooses the sensor locations in the most sensitive region while PSVA chooses the sensor locations where the sensor sensitivity is sacrificed to achieve better process conditioning [77].

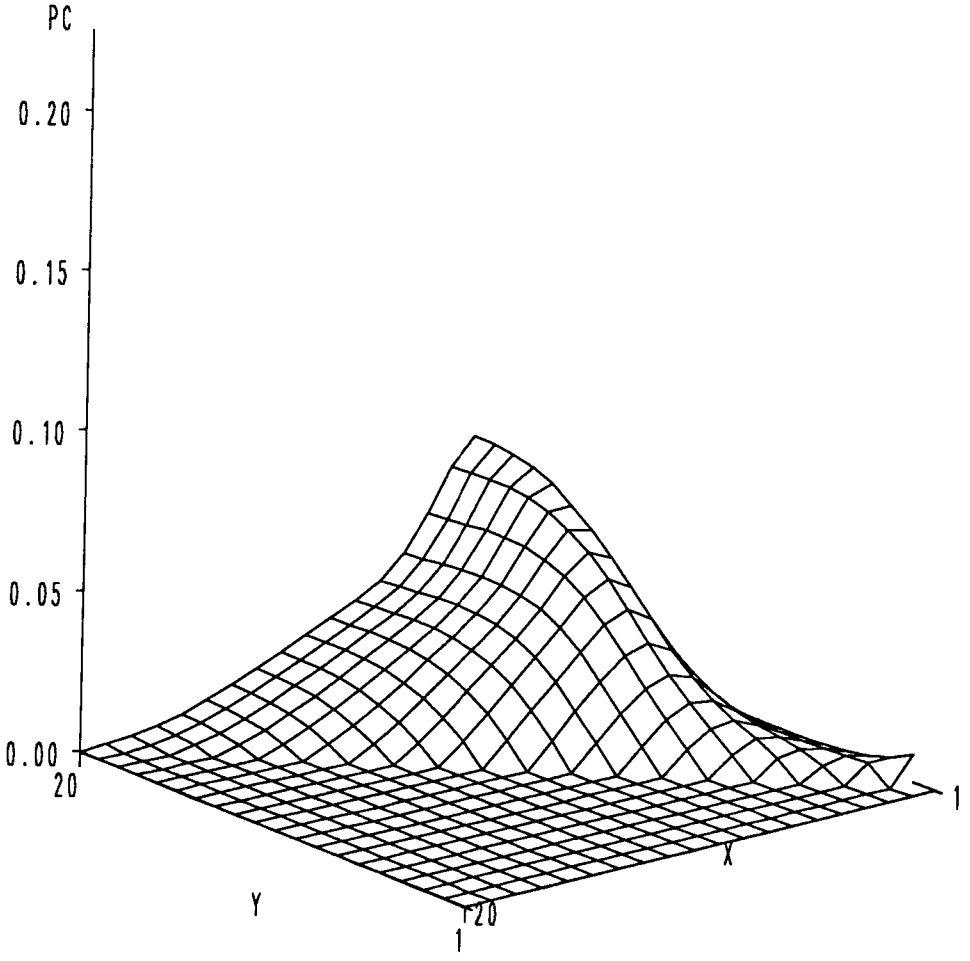

Figure 4.17: Process conditioning (1/condition number) vs. sensor location for CO mole percent and mass flow rate as manipulated variables.

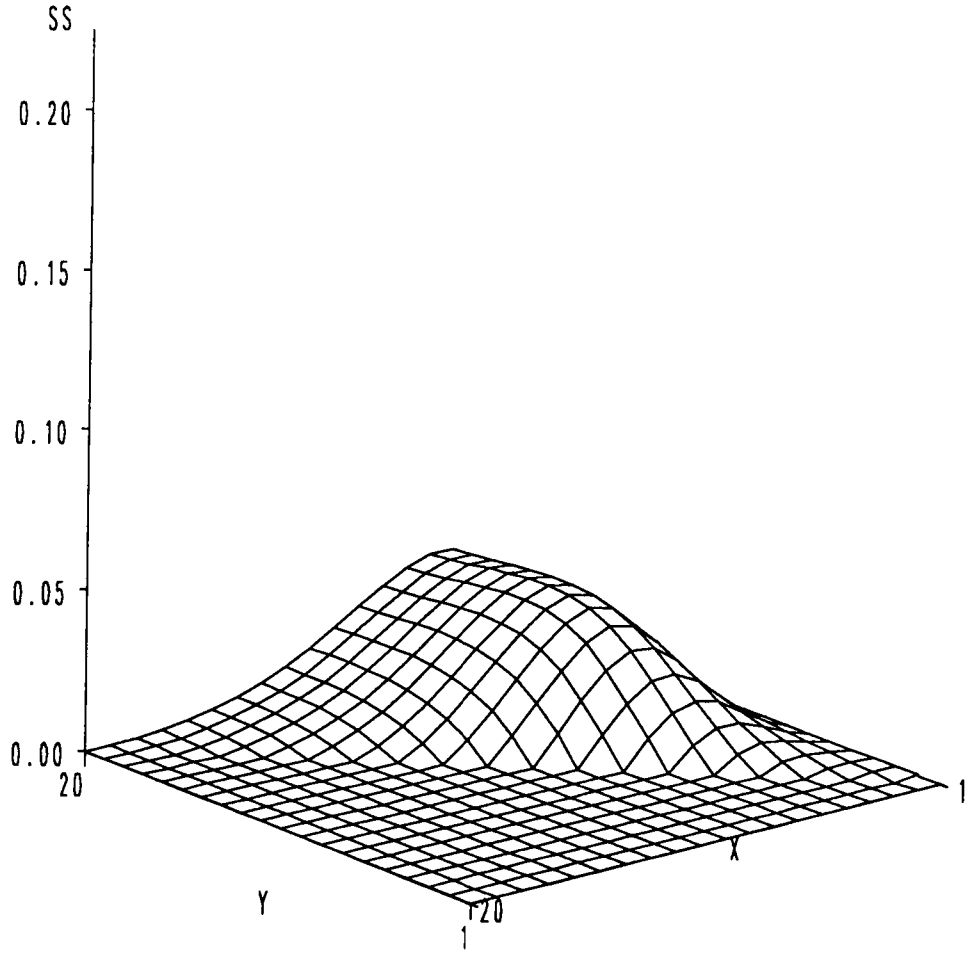

Figure 4.18: Sensor sensitivity (the second singular value) vs. sensor location for CO mole percent and mass flow rate as manipulated variables.

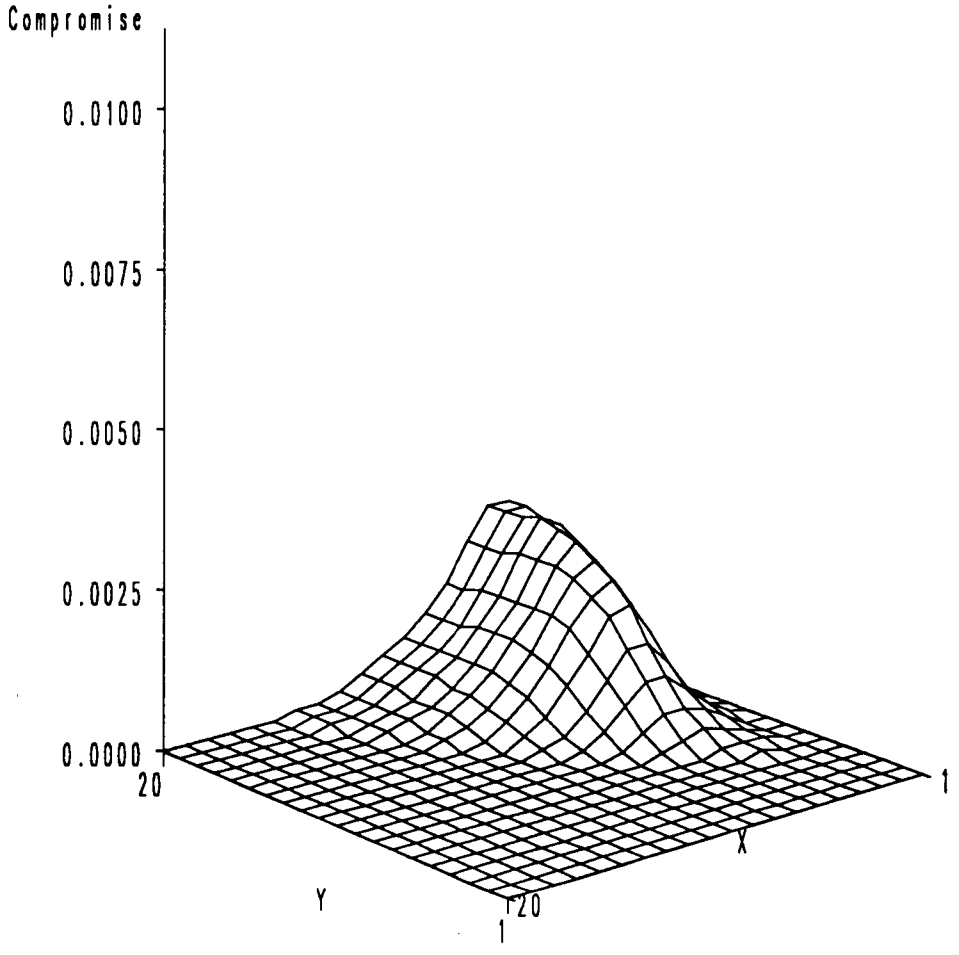

Figure 4.19: Sensor intersivity (the second singular value/condition number) vs. sensor location for CO mole percent and mass flow rate as manipulated variables.

Table 4.3: The Selection of Sensor Locations and Condition Number by PCA, MPCA, PSVA

Manipulated Variables	*PCA* (σ_1,σ_2,K)	*MPCA*	*PSVA* (σ_1,σ_2,K)
F W	1,6(3.05,1.83,1.67)	1,8	1,20(0.93,0.74,1.27)
F C	1,6(3.24,1.39,2.34)	1,7	1,11(1.03,0.61,1.67)
F M	3,7(2.60,0.08,31.51)	4,20	1,7(1.19,0.04,33.16)
W C	7,9(3.29,0.86,3.84)	12,20	6,20(1.03,0.37,2.80)
W M	6,20(2.42,0.11,21.65)	6,11	6,20(0.81,0.05,15.63)
C M	6,8(2.38,0.10,23.43)	3,5	4,20(0.45,0.03,13.21)

Since the results of PSVA are more consistent with the results of the steady state simulations in Chapter 2, it seems more proper to use PSVA for selecting sensor locations. A conclusion from these studies is that the best control system configuration is to use the feed temperature and wall temperature as the manipulated variables with sensor locations at 1 and 20, since it has the best process conditioning (0.79) and the strong sensor sensitivity in the weaker direction in terms of precess response to control action. The control schemes involving mass flow rate as one of the manipulated variables shows poor process conditioning and weak sensor sensitivity.

4.4 Control Loop Pairing

The SVD analysis can give helpful insight to this type of controller design problem. From the Section 4.2 (see Examples 4.2 and 4.3), the orthonormal matrices U and

V contain information about manipulated variable and sensor interaction. The first column of V (Input Direction) is connected to the first column of U (Output Direction) by σ_1. For both the input and output direction the larger the element in the respective column, the more that direction is defined by the physical variable associated with that element.

The input-output pairing procedure for a control loop from SVD analysis is that the sensor associated with the largest element of the first left singular (output) vector, which is the first column of U, is paired with the manipulated variable associated with the largest element of the first right singular (input) vector, which is the first column of V. This establishes the first feed back control loop. For the second loop the sensor associated with the largest element of the second left singular (output) vector is paired with the manipulated variable associated with the largest element of the second right singular (input) vector and so on for the next loop, until all manipulated variables and sensors are paired for the desired number of loops. The more dominant the largest elements in both the input and output direction the better the pairing. As the elements became less dominant the more interaction, there is between the process inputs and outputs.

For example, consider the PSVA results for the case of feed temperature and wall temperature (FW) as manipulated variables with sensor locations 1 and 20 (see Scheme 1 in Table 4.4). The largest elements in the first left column singular vector and the first right singular column vector indicate that T1 should be paired with F, the feed temperature. The largest elements in the second left column singular vector and the second right column singular vector indicate that T20 should be paried with W, the wall temperature.

The PSVA analysis of all six possible control schemes are presented in Table 4.4 with the suggested pairing. Pairing results for schemes 3 and 6 will have some interaction because the magnitude of all elements in their respective V matrices are of similar size. Even more interaction is expected in scheme 4, because the elements in both the U and V matrix are of similar magnitude.

4.4.1 Relative Gain Array (RGA)

Another approach to single loop design pairing for multivariable control is the Relative Gain Array method [20] which pairs the manipulated and controlled variables to minimize interaction and to indicate the amount of interaction. This method requires an equal number of input (manipulated) variables and output (controlled) variables.

The Relative Gain Array has been widely used for a measure of loop interaction and the pairing of controlled and manipulated variables as presented in numerous papers, some of them covering industrial practice [93]. It uses only steady state gain information for a measure of loop interaction. Niederlinski [81] has extended the technique to provide a stability test for the system with selected pairings.

The relative gain matrix was developed by Bristol [20] based on the steady state gain matrix. The elements in the matrix are defined as follows:

$$\lambda_{ij} = \frac{\frac{\partial c_i}{\partial m_j}|_m}{\frac{\partial c_i}{\partial m_j}|_c} \tag{4.5}$$

where c is a control variable and m is a manipulated variable. The numerator is the steady state gain. The denominator is the steady state gain when all the other loops (except the jth loop) are closed and contain integral control actions so that all the other control variables are returned to their set point values. The relative gain matrix has a property that the relative gains in each column and row add up to unity. For low order

Table 4.4: Partial Singular Value Analysis for control schemes 1 through 6

U Matrix			V Matrix			Pairing
T1	0.9610	-0.2767	F	0.9434	-0.3316	T1 with T20
T20	0.2767	0.9610	W	0.3316	0.9434	T20 with W
Scheme 1	FW					
U Matrix			V Matrix			Pairing
T1	0.9176	-0.3976	F	0.8249	-0.5653	T1 with F
T11	0.3976	0.9176	C	0.5653	0.8249	T11 with C
Scheme 2	FC					
U Matrix			V Matrix			Pairing
T1	0.9996	0.0281	F	0.7702	-0.6378	T1 with F
T7	-0.0281	0.9996	M	0.6378	0.7702	T7 with M
Scheme 3	FM					
U Matrix			V Matrix			Pairing
T6	0.6541	-0.7664	C	0.6361	-0.7716	T6 with C
T20	0.7564	0.6541	W	0.7716	0.6461	T20 with W
Scheme 4	WC					
U Matrix			V Matrix			Pairing
T6	-0.0024	1.0000	M	0.3796	-0.9251	T6 with M
T20	1.0000	0.0024	W	0.9251	0.3796	T20 with W
Scheme 5	WM					
U Matrix			V Matrix			Pairing
T4	-0.0128	0.9999	M	0.6543	-0.7562	T4 with M
T20	0.9999	0.0128	C	0.7562	0.6543	T20 with C
Scheme 6	CM					

systems this reduces the number of elements in the matrix which has to calculated. For higher-order systems the relative gain matrix calculations can be simplified by using matrix inversion. The relative gain matrix, Λ, can be expressed as follows:

$$\Lambda = \mathrm{KG}\ H^T \tag{4.6}$$

where KG is the steady state gain matrix and $H = KG^{-1}$. The pairing rule is basically to pair on positive RGA elements that are closest to 1 and maintain closed loop stability. Detailed discussions on pairing rules and interpretation of RGA can be found in many references [95,96,105].

After the pairings are selected, Niederlinski's theorem is used to check the stability of the proposed pairings. The theorem uses the steady state gain matrix which has been arranged so that the control loop pairings are on the diagonal elements in the matrix. The theorem states that the closed-loop system using the RGA pairings is unstable if

$$\frac{det|KG|}{\prod_{i=1,n}^{n} KG_{ii}} < 0 \tag{4.7}$$

where $det|KG|$ is the determinant of KG matrix and KG_{ii} are the diagonal elements in the matrix.

Another interaction index has been presented by Nisenfeld and Schultz [82]. They define an interaction index for a multivariable control loop as follows:

$$I_{ij} = \left| \frac{1 - \lambda_{ij}}{\lambda_{ij}} \right| \tag{4.8}$$

If the interaction index is greater than unity, this pairing should be rejected to avoid instability due to loop interaction.

The results of the RGA analysis, Niderlinski Index, and condition number are presented in Table 4.5. The condition numbers from PSVA are added to the table to

Table 4.5: Relative Gain Array, Niderlinski Index and condition number for control scheme 1-6

	F	W		F	C
T1	1.0014	-0.0014	T1	1.0093	-0.0093
T20	-0.0014	1.0014	T11	-0.0093	1.0093
Niderlinski	Index =	0.9986	Niderlinski	Index =	0.9908
Condition	Number =	1.2673	Condition	Number =	1.6691
Scheme 1			Scheme 2		
	F	M		C	W
T1	1.0507	-0.0507	T6	1.2790	-0.2790
T7	-0.0507	1.0507	T20	-0.2790	1.2790
Niderlinski	Index =	0.9517	Niderlinski	Index =	0.7818
Condition	Number =	33.1594	Condition	Number =	2.7933
Scheme 3			Scheme 4		
	M	W		M	C
T6	0.8689	0.1311	T4	0.6561	0.3439
T20	0.1311	0.8689	T20	0.3439	0.6561
Niderlinski	Index =	1.1508	Niderlinski	Index =	1.5242
Condition	Number =	15.6283	Condition	Number =	13.2126
Scheme 5			Scheme 6		

provide conditioning information. The closer element are to 1 the less interaction, but no information is given by the RGA on process conditioning. For example, Scheme 1, 2, and 3 have excellent RGAs (pairing elements are very close to 1). However, Scheme 1 and 2 are well conditioned while Scheme 3 is not. Note the inputs and outputs are ordered so the pairing is on the diagonal for each control loop, these the steady state gain matrix is arranged appropriately to calculate the Niderlinski index. The results from RGA are discussed in the next section.

4.5 Results and Discussion

For this reactor control study, PSVA is used for the selection of sensor locations which considers process conditioning and sensor sensitivity. Analysis for two single loop designs for the multivariable system is done using PSVA and RGA analysis with condition number and Niderlinski index. Table 4.5 lists the Relative Gain Array, Niderlinski index and condition number for each set of temperature sensor locations and manipulated variables. Since the pairing results of PSVA are identical to those of RGA pairing, only condition number of each pairing is listed. The RGA and condition number suggest that controlling the temperature T1 by feed temperature and controlling the temperature T20 by wall temperature are the best SISO design control loop pairings. The Niderlinski index for the control scheme, 0.9986, is positive indicating local stablility and the condition number, 1.6687, indicates good process conditioning. Table 4.5 shows that all control schemes related to mass flow rate as a manipulated variable (Scheme 3, 5, and 6) have the worst process conditioning problems. Control scheme 6 shows the largest interaction, as is expected, since both inputs have a similar effect on the reactor.

PSVA, RGA, dynamic and steady state analysis all indicate that control schemes which include mass flow rate as a manipulated variables are not good control candidates due to the lack of sensor (output) sensitivity.

In general the SVD pairing procedure gives results consistent with RGA analysis. But there are cases in the literature [35,93] where the results of the SVD pairing and RGA pairing are quite different. In such cases it is best to consider both the RGA and SVD analysis, along with simulation if possible before a final decision is made on the pairing. As pointed out the SVD analysis is based on the open loop characteristics of the system in terms of input-output interaction, sensor sensitivity, and process conditioning. Thus, it has no stability information as the Niderlinski index in the RGA. On the other hand, the RGA analysis has no information on the high condition number.

4.6 Conclusion

A strategy based on singular value analysis of the steady state gain matrix was used to determine the selection of sensor locations. The selection of sensor locations by Partial Singular Value Analysis shows tendency to spread out the sensor locations compare to Principal Component Analysis in this study. This analysis was also used to select control loop pairings for SISO design on the MIMO system. The potential manipulated variables investigated for this reactor control system were

- F: Feed temperature
- W: Wall temperature
- C: CO mole percent

- M: Mass flow rate

The SVA results are also compared with analysis by RGA and Neiderlinski Index.

For the SISO control loop pairing, SVA, RGA, Niderlinski Index, and condition numbers are used. The results of SVA are consistent with RGA analysis. The best control configuration is to control sensor location 1 (T1), the temperature at $z = .34357e - 2$, using the feed temperature, and to control sensor location 20 (T20), the temperature at $z = .99656$, using the wall temperature.

4.7 Nomenclature

c	control variables
C	CO mole percent
F	feed temperature
KG	steady state gain matrix
I_{ij}	interaction index
K	codition number
m	manipulated variables
M	mass flow rate
U	range (output) space of a matrix
V	domain (input) space of a matrix
Λ	realtive gain matrix λ_{ij}
Σ	diagonal matrix of singular values σ_i
ℓ_i	MPCA index

CHAPTER 5

Dynamic Matrix Control (DMC/QDMC)

5.1 Introduction

Recently Dynamic Matrix Controller (DMC) has been used in many industrial applications [28,29,30,42,51]. DMC represents an important class of model predictive controllers; they are easy to implement and applicable to processes with difficult dynamic characteristics among which are nonlinear behavior, large dead time, and inverse response. This class of controllers has often proven superior to the conventional proportional-integral-derivative (PID) controller in dealing with such complex processes [30]. A fixed bed reactor has very challenging characteristics: highly nonlinear, distributed, and large time delays. Implementation of the DMC algorithm to a highly nonlinear distributed fixed bed reactor with large time delays is very interesting and the author has not found any reference to this application in the DMC literature.

DMC is a linear model predictive control technique which continuously predicts future outputs based on the response due to past inputs within the prediction time horizon required to reach a steady state. The optimal scheme of the controller is to find the set of input changes for the current control action and future control actions for the time horizon, which minimizes the sum of the square of the difference (error) between the set point and the predicted outputs over the time horizon. The general development of the DMC algorithm incorporated both feedforward characteristics and

the multivariable structure of a process. The DMC algorithm is derived from a technique of representing the dynamics of a process with a set of numerical coefficients, which are based on the step response of the process to the manipulated input. Then a least squares formulation is applied to the process representation to minimize the sum of the squares of the predicted error over a prediction time horizon.

The solution of the DMC problem has been extended to handle process constraints. The formulation with constraints is called QDMC (Quadratic Dynamic Matrix Control) [42]. The solution is found by running a quadratic program which minimizes the sum of squared differences of the controlled variable projections from set points subject to maintaining projections of the constrained variables within bounds.

5.2 DMC

The DMC algorithm uses an approximation of the system dynamic responses in terms of linear ordinary differential equations. As such the equations obey the superposition principle, a proportionality exits between the size of change in the input and the size of change in the output. A step response of a single-input single-output system is illustrated in Figure 5.1. Thus the step response can be represented as a set of discrete numbers, a_i which are the proportionality factors at each time interval, i, from the time of the single step change in the input.

$$\Delta y_i = a_i \Delta u \tag{5.1}$$

When there is a set of inputs (Δu_1, Δu_2, $\cdots$, Δu_n), the response can be written as

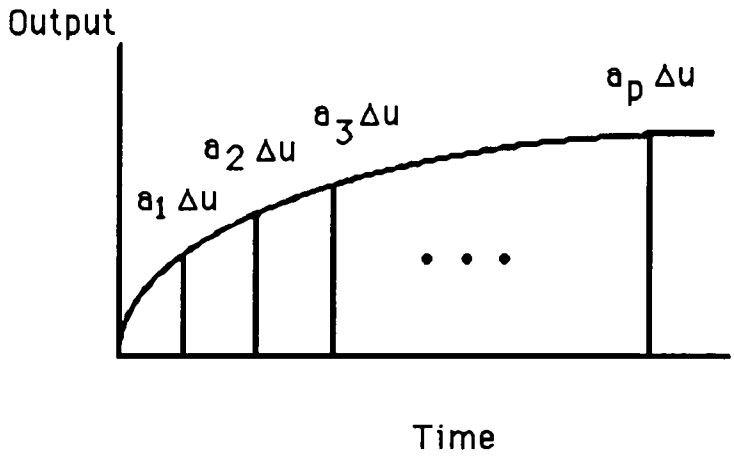

Figure 5.1: Output response to a step input of magnitude Δu at time, t=0

following

$$\begin{aligned}
\Delta y_1 &= a_1 \Delta u_1 \\
\Delta y_2 &= a_2 \Delta u_1 + a_1 \Delta u_2 \\
&\vdots \\
\Delta y_n &= a_n \Delta u_1 + \cdots + a_1 \Delta u_n \\
&\vdots \\
\Delta y_p &= a_p \Delta u_1 + \cdots + a_{p-n+1} \Delta u_n
\end{aligned} \tag{5.2}$$

In short form

$$\Delta y = A \Delta u \tag{5.3}$$

where

$$A = \begin{bmatrix} a_1 & 0 & \cdots & 0 \\ a_2 & a_1 & \cdots & 0 \\ \vdots & \vdots & \ddots & \vdots \\ a_n & a_{n-1} & \cdots & a_1 \\ \vdots & \vdots & & \vdots \\ a_p & a_{p-1} & \cdots & a_{p-n+1} \end{bmatrix} \tag{5.4}$$

The prediction of future outputs, P_i, from all the past inputs can be put into the following general form:

$$P_i = P_o + \sum_{j=1}^{p} a_j \Delta u_{i-j+1} + d_i \tag{5.5}$$

where i is discrete time; P_o is the output initial condition; Δu_{i-j+1} is a change in input at different time intervals i; d_i is a predicted disturbance which takes into account unmodeled effects on the output, such as unmeasured disturbances and modeling errors. Thus, the next predicted output is obtained by adding changes due to the new input to the old predicted outputs. When there is an unmeasured disturbance or a steady state offset between the process measurement and the predicted value of the output, the DMC algorithm adjusts the output prediction based on the assumption that the value of the difference (d_i) remains constant for all future time intervals of the prediction.

When the output is controlled using the prediction vector, an error can be presented as follows:

$$e_i = y_{s_i} - P_i \quad i = 1, p \tag{5.6}$$

where y_{s_i} is the set point and P_i is the predicted output at the time interval i. The control action of DMC from these errors can be represented as follows:

$$e = Ax \tag{5.7}$$

where

$$x = \begin{bmatrix} \Delta u_1 & \Delta u_2 & \dots & \Delta u_n \end{bmatrix}^T \tag{5.8}$$

is the vector of future moves. A least squares method is applied to solve the above equation. The squared error which is based on the difference between the set point and the predicted output is minimized. The optimized control action is

$$x = (A^T A)^{-1} A^T e = A^+ e \tag{5.9}$$

where A^+ is the pseudoinverse of A. Since matrix A is overdetermined in most cases, its pseudoinverse can be calculated from the singular value decomposition.

$$A^+ = V \Sigma^+ U^T \tag{5.10}$$

The first row of A^+ is used to calculate the necessary input over the next time interval. It is the only one that is actually implemented. The whole process is repeated again for the next time interval. For the case of a time invariant system, A^+ is fixed so it can be stored in the computer memory to be used again and they save computing time.

Since DMC has a tendency to produce tight control at the expense of large control action moves, it is necessary to suppress these large changes. This is addressed through move suppression which is added to the matrix A formulation. Move suppression is represented by a diagonal matrix (Λ) with positive elements. In general, such input penalties improve the stability of the control system in the case of model inaccuracy and reduce the amplitude of the change in the manipulated variables without affecting the absolute value of the error.

In the case of multivariable control, when some particular controlled variables require tighter control than others, then the corresponding relative weights of the diagonal

matrix (Γ) are increased. Putting all of these weighting matrices together, the DMC control action becomes

$$x = (A^T\Gamma^T\Gamma A + \Lambda^T\Lambda)^{-1}A^T\Lambda^T\Lambda e \tag{5.11}$$

Stability is related to the selection of the number of projections into the future (p) in such a way that dynamic and steady state effects from future control moves show in the prediction. Stability and its relation to the selection of the number of projections for the output into the future ($p \gg n$) is stated in detail by Garcia and Morari [41].

5.2.1 DMC for a Multivariable System

In the case of a multivariable system, the dynamic matrix A consists of blocks of dimensions $p \times n$ of step response coefficient matrices that models the response between the i^{th} output and the j^{th} input as follows;

$$A = \begin{bmatrix} A_{11} & A_{12} & \cdots & A_{1j} \\ A_{21} & A_{22} & \cdots & A_{2j} \\ \vdots & \vdots & \ddots & \vdots \\ A_{i1} & A_{i2} & \cdots & A_{ij} \end{bmatrix} \tag{5.12}$$

and the corresponding vector of control moves is

$$x = \begin{bmatrix} x_1^T & x_2^T & \ldots & x_j^T \end{bmatrix}^T \tag{5.13}$$

and the output projection error vector becomes

$$e = \begin{bmatrix} e_1^T & e_2^T & \ldots & e_i^T \end{bmatrix}^T \tag{5.14}$$

Thus, Equation 5.11 is valid also for a multivariable system which is defined by Equations 5.12 to 5.14.

5.3 Quadratic Dynamic Matrix Control (QDMC)

In practice, some of the manipulated variable moves are not applicable due to physical limitations. Quadratic Dynamic Matrix Control was developed to handle such constraint problems. The use of quadratic programming provides process constraint handling capability. The process constraints are formulated as linear inequalities. The following development is based on Garcia and Morshedi's work [42,51].

There are three usual types of process constraints in the formulation of QDMC. They are:

- manipulated variables constraints
- controlled variables constraints
- associated variables constraint

The controller should be able to predict future violations of these constraints and keep these variables within bounds. Constraints on these variables can be expressed as a system of linear inequalities.

For the manipulated variable,

$$\begin{bmatrix} -1 & 0 & \cdots & 0 \\ -1 & -1 & \cdots & 0 \\ \vdots & \vdots & \ddots & \vdots \\ -1 & -1 & \cdots & -1 \\ 1 & 0 & \cdots & 0 \\ 1 & 1 & \cdots & 0 \\ \vdots & \vdots & \ddots & \vdots \\ 1 & 1 & \cdots & 1 \end{bmatrix} x \geq \begin{bmatrix} u_1 - u_{max} \\ u_2 - u_{max} \\ \vdots \\ u_p - u_{max} \\ u_{min} - u_1 \\ u_{min} - u_2 \\ \vdots \\ u_{min} - u_p \end{bmatrix} \tag{5.15}$$

where u_{max} and u_{min} are the upper and lower limits of the manipulated variable.

For the controlled variable,

$$\begin{bmatrix} -A \\ A \end{bmatrix} x \geq \begin{bmatrix} y_s - y_{max} - e_1 \\ y_s - y_{max} - e_2 \\ \vdots \\ y_s - y_{max} - e_p \\ y_{min} - y_s + e_1 \\ y_{min} - y_s + e_2 \\ \vdots \\ y_{min} - y_s + e_p \end{bmatrix} \tag{5.16}$$

where y_{max} and y_{min} are the upper and lower limits of controlled variable.

The associated variables, which are not directly controlled but which must be kept

within bounds, use another projection vector similar to Equation 5.16.

$$\begin{bmatrix} -B \\ B \end{bmatrix} x \geq \begin{bmatrix} a_{c1} - a_{max} \\ a_{c2} - a_{max} \\ \vdots \\ a_{cp} - a_{max} \\ a_{min} - a_{c1} \\ a_{min} - a_{c2} \\ \vdots \\ a_{min} - a_{cp} \end{bmatrix} \tag{5.17}$$

where

$$a_c \geq \begin{bmatrix} a_1^* - (a_m - a^*) \\ a_2^* - (a_m - a^*) \\ \vdots \\ a_p^* - (a_m - a^*) \end{bmatrix} \tag{5.18}$$

is the associated variable projection vector. B is the dynamic matrix of the associated variables, a_m is the measured feedback, a^* is the effect of the past inputs on the projection of a, and a_{min} and a_{max} are the constraint limits.

All the constraints (Equations 5.15 to 5.18) can be put into a single inequality constraint matrix.

$$\begin{bmatrix} -1_L \\ 1_L \\ -A \\ A \\ -B \\ B \end{bmatrix} x \geq \begin{bmatrix} (u - u_{max}) \\ (u_{min} - u) \\ (y_s - y_{max} - e) \\ (y_{min} - y_s + e) \\ (a_c - a_{max}) \\ (a_{min} - a_c) \end{bmatrix} \tag{5.19}$$

or in short form

$$Cx \geq c \tag{5.20}$$

where 1_L is a lower triangular matrix of 1's.

From a given DMC Equation 5.11 and the inequality constraint Equation 5.20 one can define the following quadratic minimization problem.

$$\min_x S = \frac{1}{2}(Ax - e)^T \Gamma^T \Gamma (Ax - e) + \frac{1}{2} x^T \Lambda^T \Lambda x \tag{5.21}$$

$$s.t. \;\; Cx \geq c \tag{5.22}$$

The problem can then be rearranged into the following quadratic program.

$$\min_x F = \frac{1}{2} x^T H x - g^T x \tag{5.23}$$

$$s.t. \;\; Cx \geq c \tag{5.24}$$

where

$$H = A^T \Gamma^T \Gamma A + \Lambda^T \Lambda \tag{5.25}$$

$$g = A^T \Gamma^T \Gamma e \tag{5.26}$$

Solution of a quadratic program at each time interval provides an optimal set of moves which satisfies the constraints. Software for a quadratic programming algorithm can

be used to solve the problem. DQPROG from IMSL [56] subroutine is used in this study. The algorithm is based on M.J.D. Powell's implementation [90] of the Goldfarb and Idnani [50] dual quadratic programming (QP) algorithm for convex QP problems subject to general linear equality and inequality constraints.

5.4 Implementation

An implementation of the DMC and QDMC algorithm on a fixed bed reactor is described. Since the present study focuses on the QDMC application, only selected examples of DMC controller performances are presented.

A dynamic vector is created based on an average value of positive and negative step responses to the manipulated variables (feed temperature and wall temperature). The reactor temperature responses at three different locations, which are T3, T12, and T20 (at z = .04388, z = .61389, and z = .99656, respectively), for positive step changes in the input variables (T_f and T_w) are given in Figures 5.2 and 5.3. Most of the effect due to the feed temperature changes on reactor temperature takes place at the front of the reactor and most of the effect due to the wall temperature changes on reactor temperature takes place at the end of the reactor. For the reactor temperature response to the change in feed temperature shown in Figure 5.2, each sensor location has a different time response to reach steady state, and thus each location will have a different dynamic vector. As the sensor position considered is moved further toward the reactor end, more and more dead time behavior is exhibited. The ratio between dead time and time constant is about seven at the reactor exit. These reactor temperature responses to a step change in the feed temperature are the basis for the dynamic vector

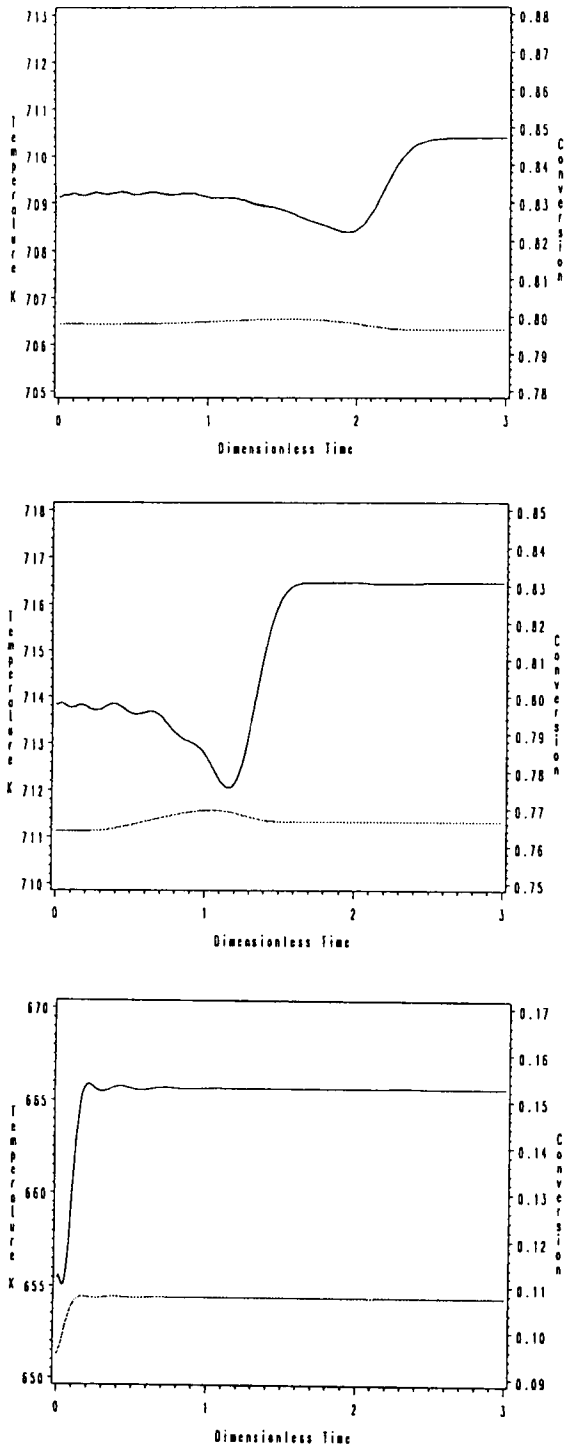

Figure 5.2: The response of reactor temperature to 10 K step change in feed gas temperature (solid line: temperature, dotted line: conversion). Top: T20 at z = .99656. Middle: T12 at z = .61389. Bottom: T3 at z = .04388.

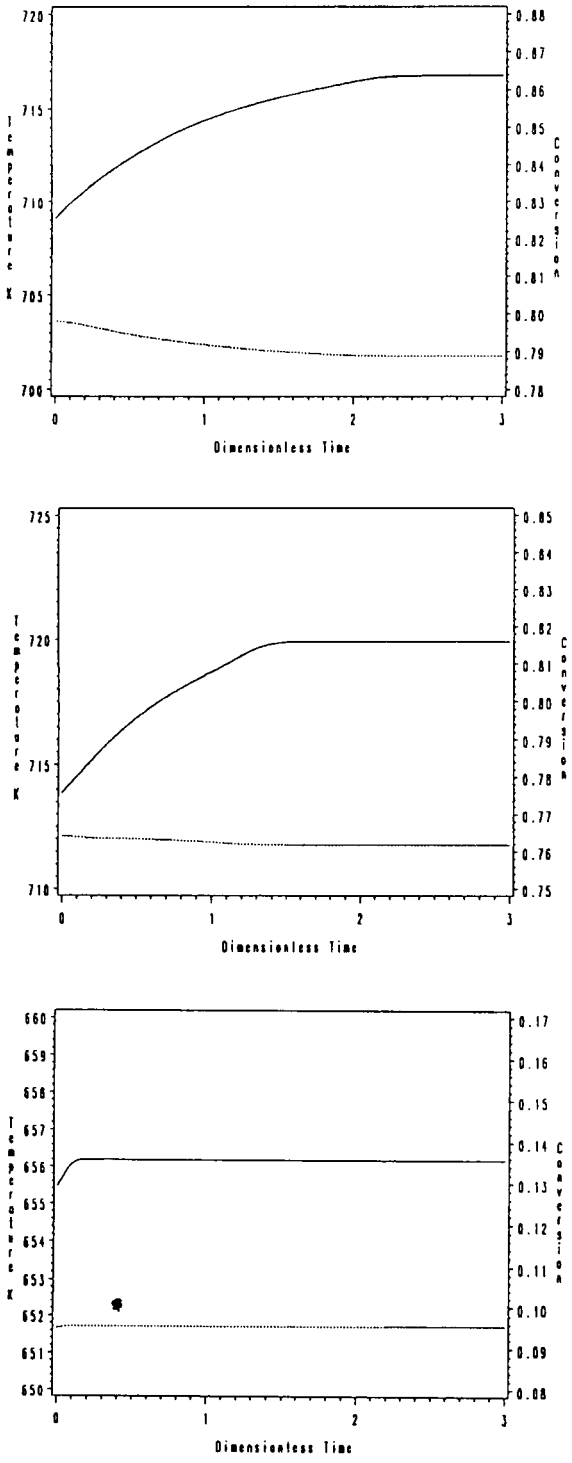

Figure 5.3: The response of reactor temperature to 10 K step change in wall temperature (solid line: temperature, dotted line: conversion). Top: T20 at z = .99656. Middle: T12 at z = .61389. Bottom: T3 at z = .04388.

needed for the prediction in DMC. Each dynamic vector is generated by taking the average value of the output response for both positive and negative step changes in the input variable. Additional step responses related to process disturbances (mass flow rate and CO mole fraction) are given in Figures 5.4 and 5.5. The CO mole fraction change has the most effect on the reactor temperature in the middle of the reactor while the effect of the mass flow rate change on reactor temperature is minimal throughout the reactor. The time constants of reactor temperature responses for positive step changes in the feed temperature at three different locations, which are T3, T12, and T20, are 0.12, 0.3, and 0.32, respectively, and large dead times at T12 and T20 are approximately 1.1 and 2.0, respectively. In consideration of the dynamic vector and DMC matrix size, the time interval between control movements used throughout this study with the DMC is selected as 0.03 dimensionless time (approximately 30.2 sec, 1 time unit = t_{ref} = 1025.6 sec) which is nominally 10 samples per time constant at T12.

For the application of single-input single-output (SISO) case, two control loops are selected. For the first case DMC and PI are implemented while for the second case QDMC and PI are employed. In both cases, the results are compared to the classical PI. In both cases, the feed temperature is used as the manipulated variable. In the first case, the DMC algorithm is used to control the temperature at T3 (z = 0.04388) by manipulating the feed gas temperature and the results are compared with those of the PI controller. In the second case, the QDMC algorithm is used to control temperature at T12 (z = 0.61389) by manipulating the feed gas temperature and, again, the results are compared to those of the PI controller. Both control loops are studied for a set point change and for a disturbance in mass flow rate.

For the multi-input multi-output (MIMO) case, two control structures are presented.

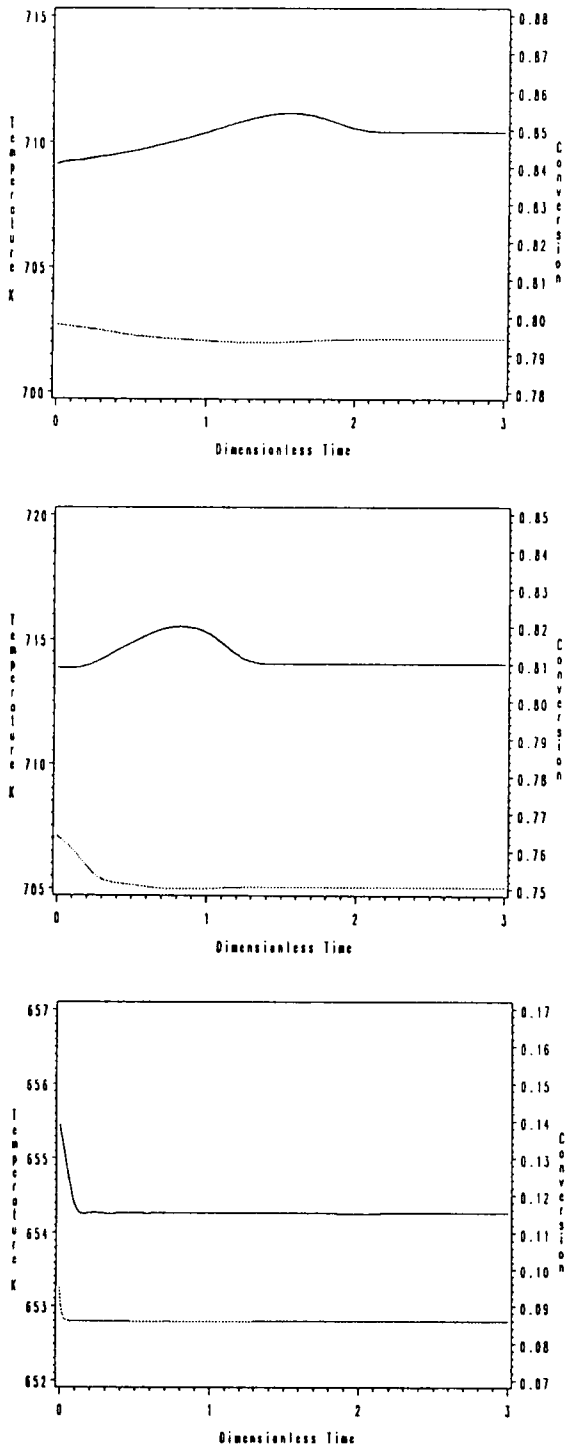

Figure 5.4: The response of reactor temperature to 10 % step change in mass flow rate (solid line: temperature, dotted line: conversion). Top: T20 at z = .99656. Middle: T12 at z = .61389. Bottom: T3 at z = .04388.

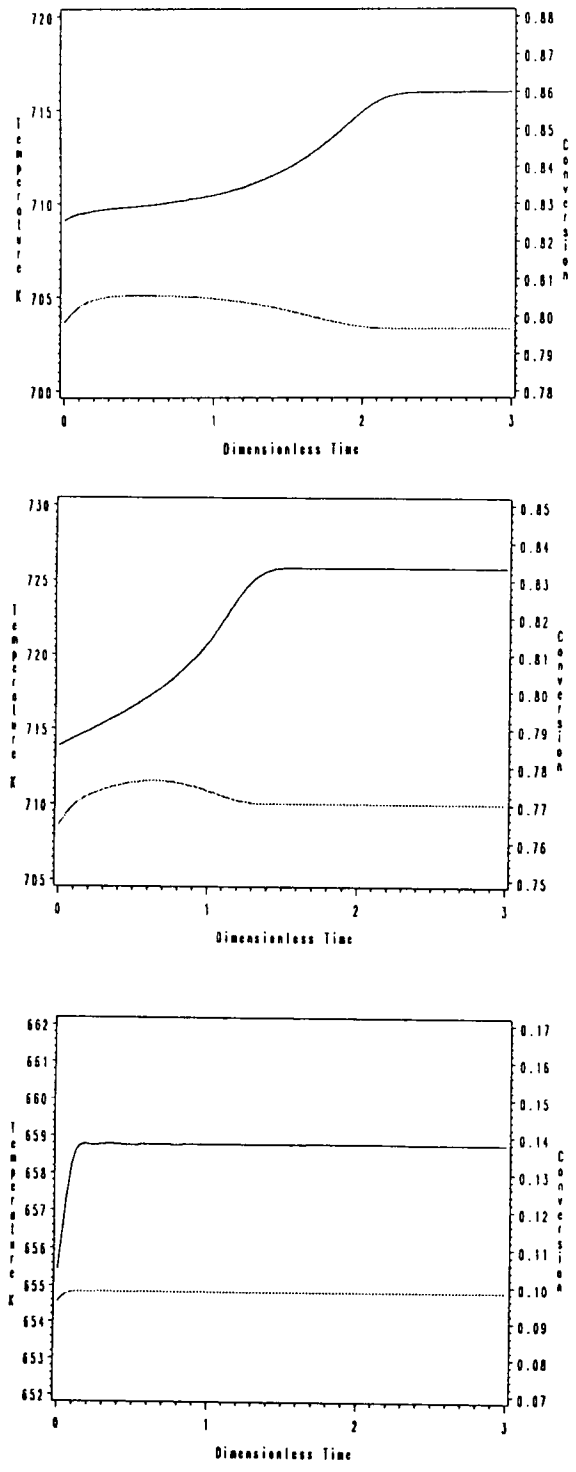

Figure 5.5: The response of reactor temperature to 3 % step change in CO mole fraction (solid line: temperature, dotted line: conversion). Top: T20 at z = .99656. Middle: T12 at z = .61389. Bottom: T3 at z = .04388.

The QDMC algorithm is employed with the feed temperature and wall temperature used as the manipulated variables. In the first case, the QDMC algorithm is used to control the temperatures at T3 ($z = 0.04388$) and T20 ($z = 0.99656$) by manipulating the feed gas temperature and wall temperature simultaneously. This selection of sensor locations and manipulated variables is based on the analysis in Chapter 4. The sensor location of T3 ($z = 0.04388$) was used instead of T1 ($z = 0.0034$) as selected in Chapter 4. This was done to place the measurement in the reactor in consideration of sensor placement difficulty. In the second case, the QDMC algorithm is used to control the temperature at T3 ($z = 0.04388$) and T12 ($z = 0.61389$) by manipulating the feed gas temperature and wall temperature. These two MIMO control structures are simulated for a set point change of 5 K made simultaneously in both controlled temperatures, for a disturbance step change in G of 0.021 $g/sec\ cm^2$ (10 % of the base case value), and for a disturbance step change in the feed CO mole fraction of 3%.

The second MIMO control example controlling the temperatures at T3 and T12 can be viewed from two different aspects. One is the control of the hot spot temperature. Temperature T12 is past but near the hot spot temperature so the control structure could be directed at keeping this temperature from getting to high. Another aspect comes from the observation made in conjunction with the steady state simulation studies. Figures 2.6, 2.9, 2.11, 2.13, and 2.15 all show that very little conversion takes place in the last part of the reactor. This "extra" reactor length may be there for various reasons, one of which, is to make the exit conversion insensitive to reactor disturbances. However, if the exit conversion can be obtained with a shorter reactor by using same control structure, significant reduction in capitol costs could be made.

High and low limits on the feed temperature (Case 1: 643 ± 10 K; and Case 2:

643 ± 20 K) and wall temperature (Case 1: 700 ± 10 K; and Case 2: 700 ± 20 K) are applied as constraints. Upper and lower limits (750 K and 600 K,respectively) is place on the reactor temperature at each sensor location to avoid loss of catalyst activity, but no associate variables are considered.

In the MIMO case, PI controllers are not implemented, since the SISO analysis illustrates as expected that the large time delays deteriorates the controller performance significantly. At the end of the reactor ($z = .99656$) the response time constant to dead time for changes in feed temperature is about seven times, while near the reactor center ($z = 0.61389$) it is four times.

The control studies under taken represented only initial investigations, however, they cover several different control structures (PI, SISO DMC, SISO QDMC, MIMO QDMC) with simulations for both set point changes and disturbance rejection capabilities. An outline of the selected control simulation studies is presented in Table 5.1.

5.4.1 Tuning

The quality of DMC/QDMC algorithm performance depends on several tuning parameters: the number of manipulated variable moves (n) in the control time horizon, the number of projections into the future (p) in the prediction time horizon to account for the future control action, move suppression (λ), selective weighting of controlled variables (γ), and time interval between controller movements.

The following tuning procedures are those of Cutler [28]. He develops a tuning method based on set point tuning using the dynamic vector to simulate the close loop process. As the number of manipulated variable moves (n) increases, the controller has more freedom in matching the output to the set point. In general, the number of future

Table 5.1: The Selected Control Simulation Studies

Type	Manipulated Variable	Controlled Variable	Simulation	Control Algorithm
SISO	T_f	T_3	Set Point	PI, DMC
Case 1			Disturbance (G)	PI, DMC
SISO	T_f	T_{12}	Set Point	PI, QDMC
Case 2			Disturbance (G)	PI, QDMC
MIMO	T_f, T_w	T_3, T_{20}	Set Point	QDMC
Case 1			Disturbance (G, x_{CO})	QDMC
MIMO	T_f, T_w	T_3, T_{12}	Set Point	QDMC
Case 2			Disturbance (G, x_{CO})	QDMC

moves in the manipulated variable is extended to include the dead time plus the time needed for the output response, due to a step change in manipulated variable, to reach 60 % of its steady state value. Then this time is typically divided into 7 to 14 intervals.

Figure 5.6 with generated at T3 ($z = 0.04388$) being controlled by T_f with a prediction horizon (p) of 50 and a control horizon (n) of 14, by changing the move suppression value (λ) from 5 to 12 and ploting the sum of error (Σ ABS(e)) over the time horizon versus λ and the sum of absolute value of the changes in the manipulated variable (Σ ABS(u)) versus λ. The region around $\lambda = 8$ from the plot shows that the absolute value of the error begins to increase rapidly and the absolute value of the change in input begins to decrease rapidly. Figure 5.7 shows the same type of analysis for T12 ($z = .61389$) being controlled by T_f with choosing a prediction horizon (p) of 100 and a control horizon (n) of 14. The region around $\lambda = 16$ from the plot shows that the absolute value of the error begins to increase rapidly and the absolute value of the change in input begins to decrease rapidly. This indicates, that compared to Figure 5.6, that in the presence of large dead time, suppressing the large control movement brings better control performance.

Figure 5.8 is generated at T3 ($z = 0.04388$) controlled by T_f with the value of the move suppression ($\lambda = 8$) determined in Figure 5.6 by changing the number of future moves around the preselected number ($n = 14$) and plotting the size of the change (δu_1) in the input for the first time interval versus the number of future moves used in the closed loop dynamic matrix simulations. The number of future moves for the controller is selected by observing when increasing the number of future moves no longer changes the size of the first move in the manipulated variable. In Figure 5.8, the size of the first move changes only slightly when more than fourteen moves are used. Figure 5.9 shows

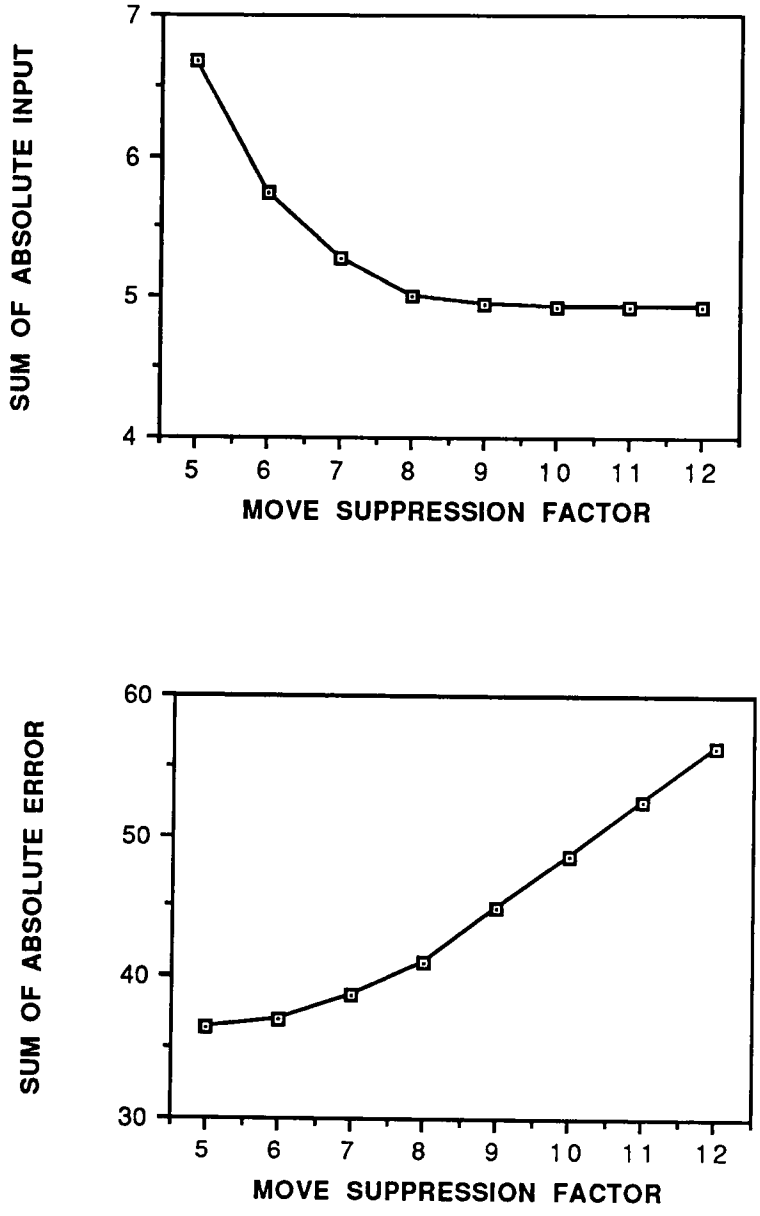

Figure 5.6: The effects of the move suppression factor on the magnitude of the change in the manipulated variable at T3 ($z = 0.04388$). ($p = 50$, $n = 14$)

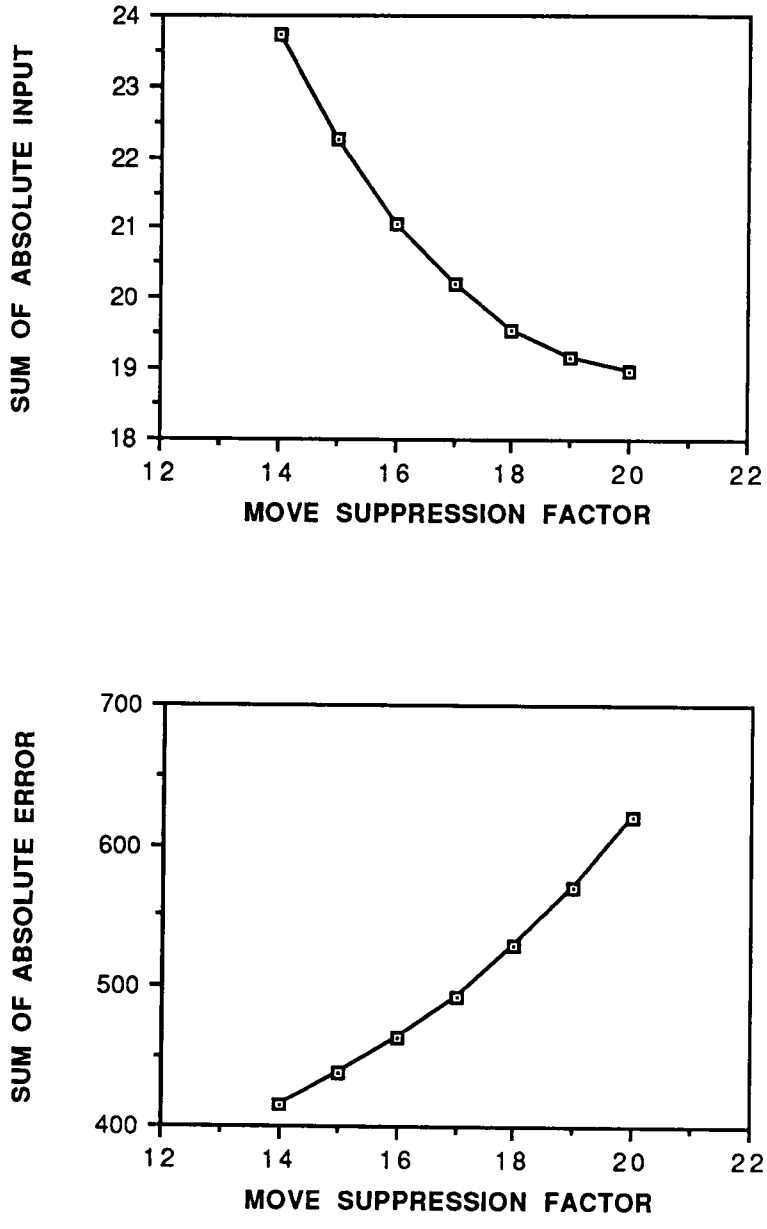

Figure 5.7: The effects of the move suppression factor on the magnitude of the change in the manipulated variable at T12 ($z = 0.61389$). ($p = 100$, $n = 14$)

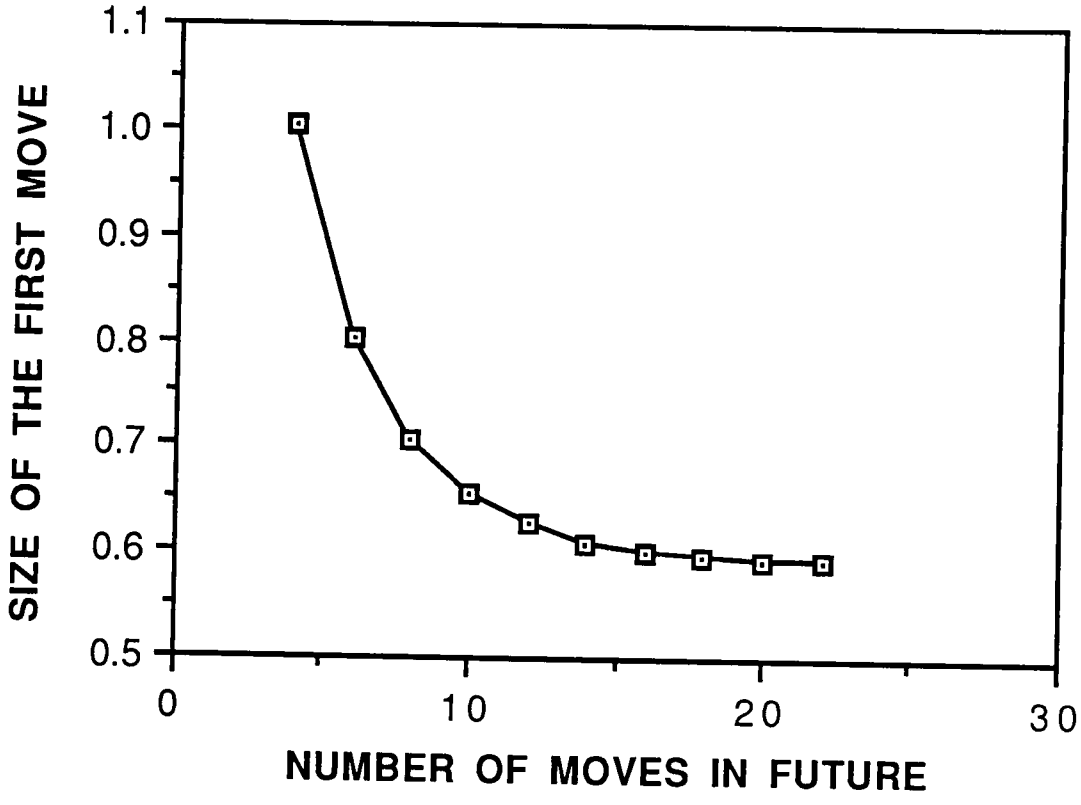

Figure 5.8: The effects of the number of future moves on the size of the first move in the manipulated variable at T3 ($z = 0.04388$). ($p = 50$, $\lambda = 8$)

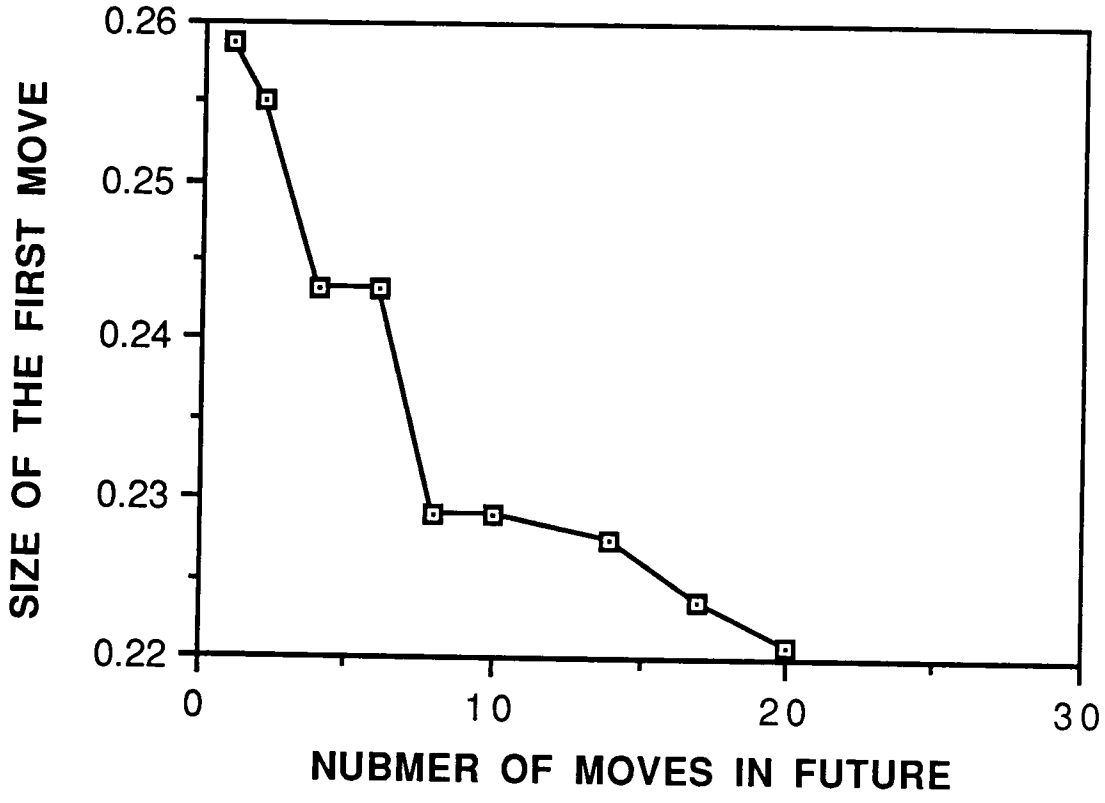

Figure 5.9: The effects of the number of future moves on the size of the first move in the manipulated variable at T12 ($z = 0.61389$). ($p = 100$, $\lambda = 16$)

the same type of analysis for T12 (z = .61389) controled by T_f with the value of the move suppression ($\lambda = 16$) determined in Figure 5.7 by changing the number of future moves around the preselected number ($n = 14$). As expected, it is little different from Figure 5.8 mainly due to the presence of large dead time. The size of the first move shows small changes when more than eight moves are used.

5.5 SISO Simulation Results and Discussions

A series of simulations are presented in this section to evaluate the effectiveness of the SISO (singe-input single-output) DMC and QDMC algorithms on a fixed bed reactor at different sensor location (T3 and T12). In both cases, the temperature of reactor is controlled by manipulating the feed gas temperature. In the following examples, the performances of DMC and QDMC for maintaining temperatures at different locations in the reactor are compared with the conventional PI controller. The comparisons will be made under conditions of step changes in either the set point or the disturbance. Disturbance in the mass flow rate is considered here. The study shows how the controller rejects a certain disturbance with controller parameters obtained from set point tuning instead of tuning for each disturbance. The control parameters for the PI controller are optimized by a pattern search, PATERN [78]. The integral of time multiplied by the absolute error (ITAE) is used as the performance index.

At T3 (z = .04388), a prediction horizon (p) of 50, a control horizon (n) of 14 and a move suppression of 8 are selected by the tuning procedure as outlined in previous section. Thus the matrix A is of dimensions 50×14. At each time interval, a change in the manipulated variable (T_f) is computed which is based on the predicted error over

the time horizon. Figure 5.10 shows a comparison between the DMC and PI controllers in the closed loop simulations for a 5 K set point change. In the case of a process without dead time (see T3 in Figure 5.2), the performance of the PI controller is better than the DMC controller. In this case, the initial tuning parameters for the DMC controller from the previous section was used and the PI controller was optimally tuned using ITAE criteria. If the DMC controller was more tightly tuned, the results of both controller performance should be close to each other.

The behavior of both controllers for disturbances is also considered. Figures 5.11 and 5.12 show the response of DMC compared to the PI controller for a 10 % step change in mass flow rate at $t = 0$. At T3 in Figure 5.4, an increase in the mass flow rate causes a decrease in the rector temperature at T3 immediately. Both of the controllers are able to maintain the set point quite well after the disturbances is introduced. But in spite of the feed temperature control action, the conversion at the exit drops slightly due to changes in the mass flow rate (see Figure 2.13).

The same type of closed loop simulations with QDMC and PI controllers are done at T12 ($z = 0.61389$) with a prediction horizon (p) of 100, a control horizon (n) of 8 and a move suppression of 1. Here the matrix A is of dimensions 100×8. Basically the QDMC tuning parameters are based on the DMC tuning procedure in Figures 5.7 and 5.9, but the move suppression factor has been changed to achieve better control performances. Each move in a manipulated variable is computed and checked for the constraints. Figure 5.13 shows a comparison between QDMC and the PI controller in the closed loop simulations for a 5 K set point change. In the presence of large time delays and inverse response, the performance of QDMC is better than the PI controller due to the prediction capability.

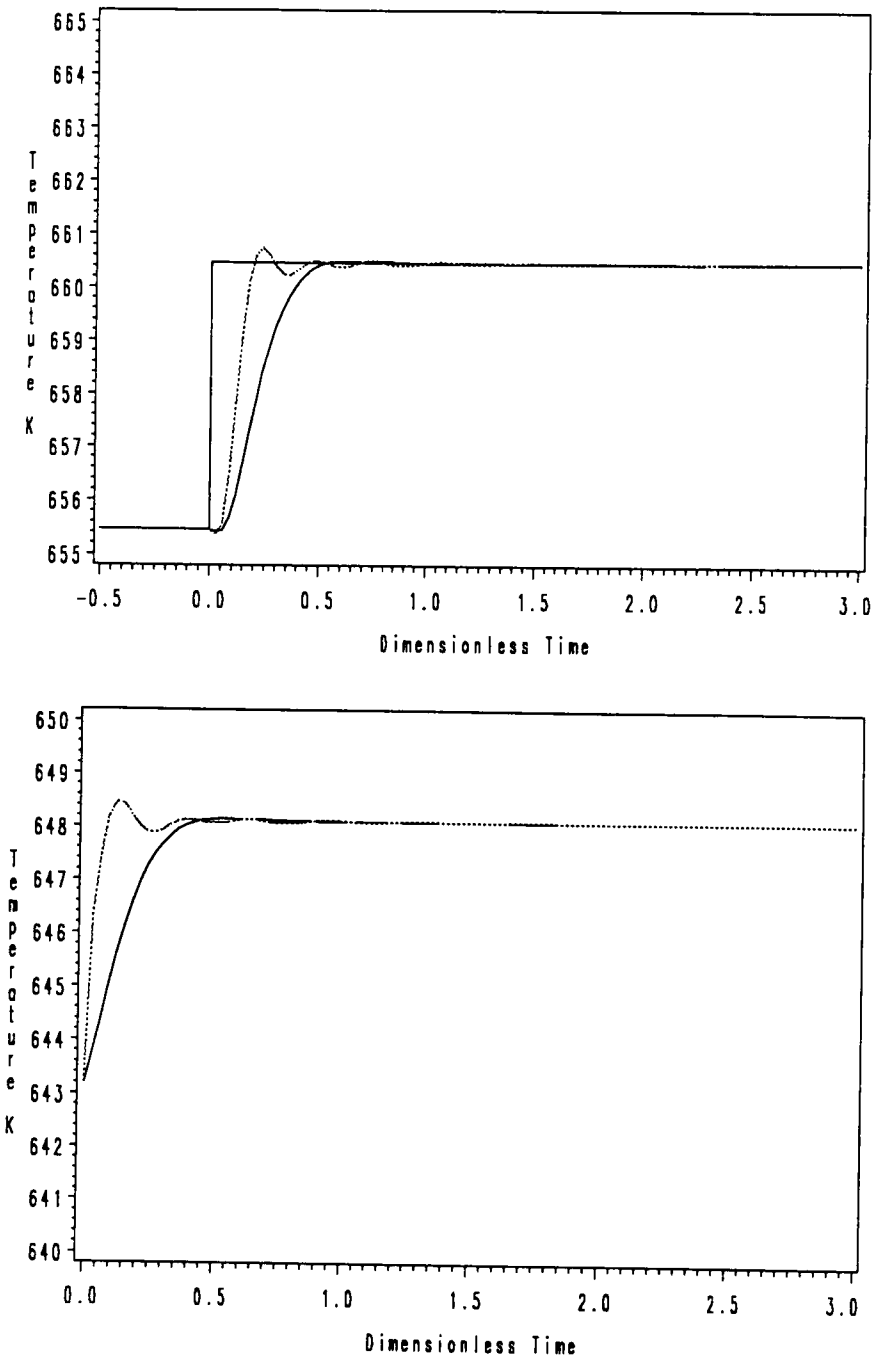

Figure 5.10: The response of reactor temperature at T3 ($z = .04388$) to a 5 K set point change under DMC (solid line, $p = 50$, $n = 14$, $\lambda = 8$) and PI controller (dotted line, $K_c = .4$, $\tau_i = .05$). Top: reactor response. Bottom: controller output.

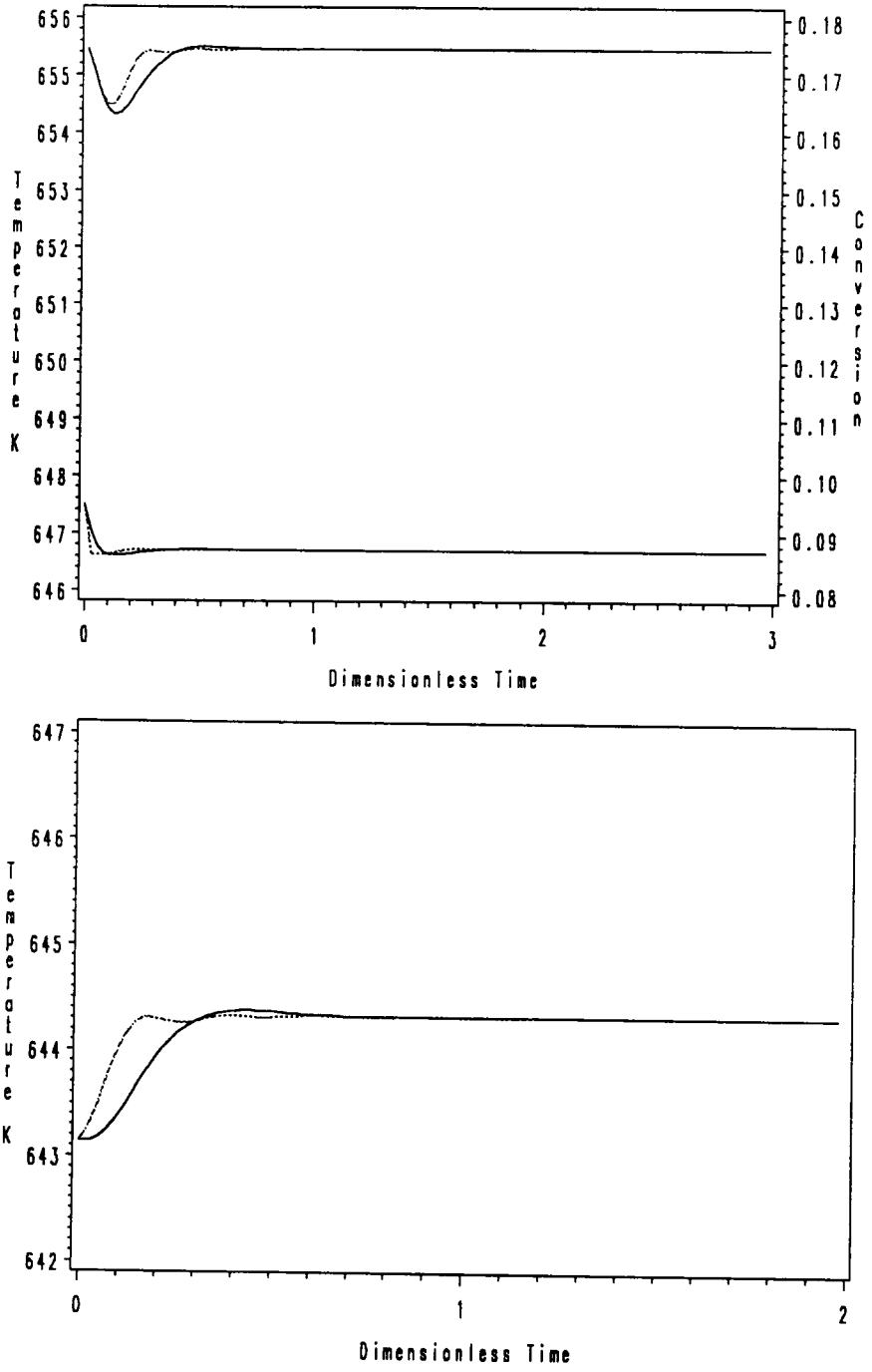

Figure 5.11: The response of reactor temperature at T3 ($z = .04388$) to a 10 % mass flow rate step change under DMC (solid line, $p = 50$, $n = 14$, $\lambda = 8$) and the PI controller (dotted line, $K_c = .4$, $\tau_i = .05$). Top: reactor response. Bottom: controller output.

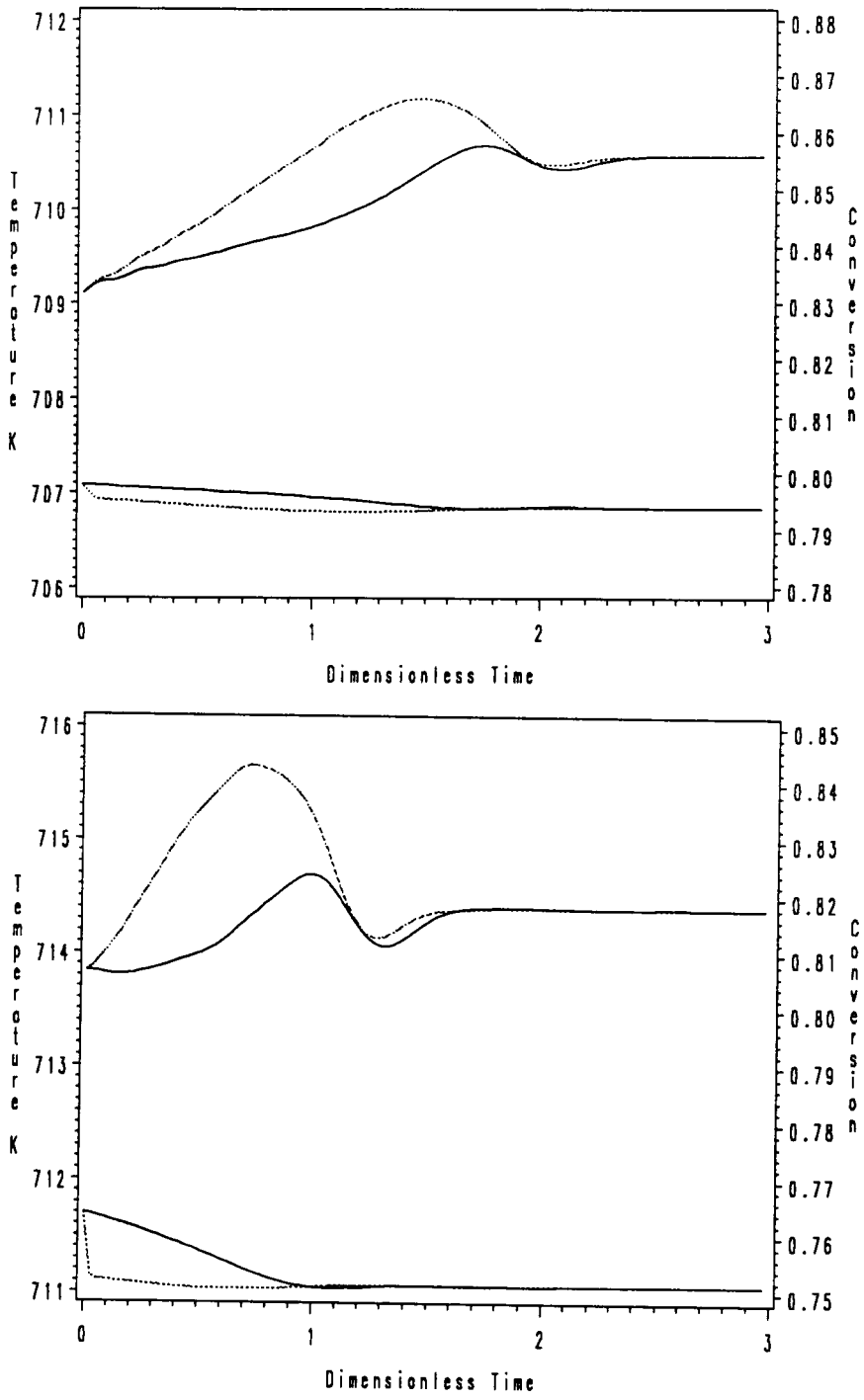

Figure 5.12: The response of reactor temperature to 10 % mass flow rate step change under DMC (solid line, $p = 50$, $n = 14$, $\lambda = 8$) and the PI controller (dotted line, $K_c = .4$, $\tau_i = .05$). Top: T20 at $z = .99656$. Bottom: T12 at $z = 0.61389$.

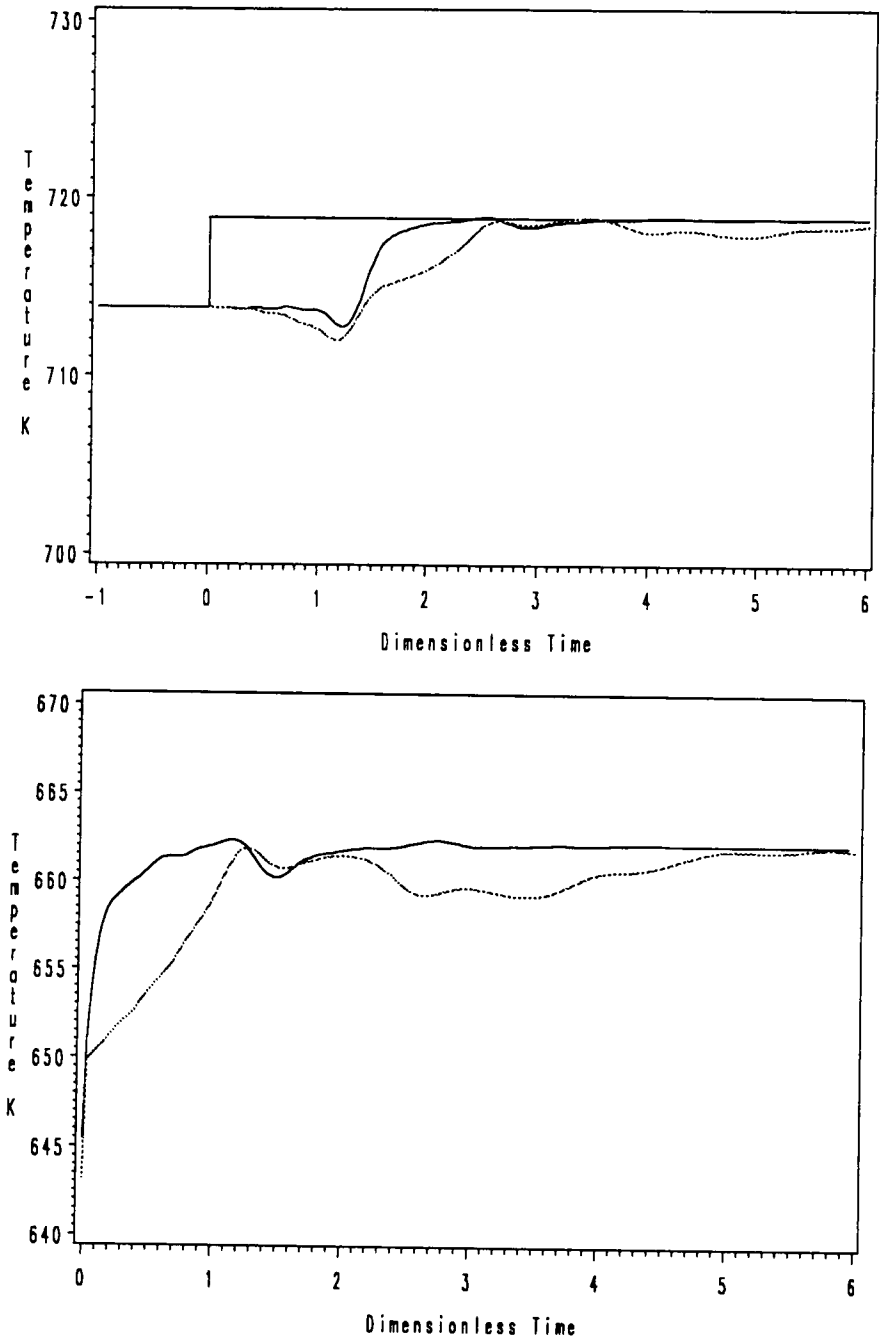

Figure 5.13: The response of reactor temperature at T12 ($z = .61389$) to a 5 K set point change under QDMC (solid line, $p = 100$, $n = 8$, $\lambda = 1$) and the PI controller (dotted line, $K_c = 1.3$, $\tau_i = .9$). Top: reactor response. Bottom: controller output.

Figures 5.14 and 5.15 show another comparison between QDMC and the PI controller for a disturbance. At $t = 0$, a 10 % increase in the mass flow rate was made. DMC is able to maintain the set point against such a disturbance, while the PI controller is quite oscillatory after the disturbance is introduced. In the presence of large dead time and inverse response, the performance of QDMC to reject the disturbance is better than those of the PI controller due to its prediction capability. But when there is a disturbance in the mass flow rate, controlling the reactor temperature right after the hot spot causes large oscillations at the front and the end of the reactor. Again, the conversion at the exit drops slightly due to changes in mass flow rate.

These types of SISO simulations demonstrate that DMC handles systems with difficult dynamic characteristics, such as dead time and inverse response better than the PI controller. It is obvious that alternative PI structures, such as the Smith Predictor [83,97], can help the controller performance on systems with a large dead time, but it has not been tried in this study. The results of both SISO case studies indicate that controlling the reactor temperature at the front using the feed temperature is better than controlling the reactor temperature right after the hot spot. An outline of the SISO simulation studies is presented in Table 5.2.

5.6 Multivariable QDMC Simulation Results and Discussion

In Case 1, a prediction horizon (p) of 130, and a control horizon (n) of 14 are selected. Then the matrix A is of dimensions 260×28. Both output weighting parameters are selected as $\gamma_i = 1$, because both of the controlled variables are temperatures while the move suppression parameters λ_i are 8 and 4, respectively, for the two manipulated

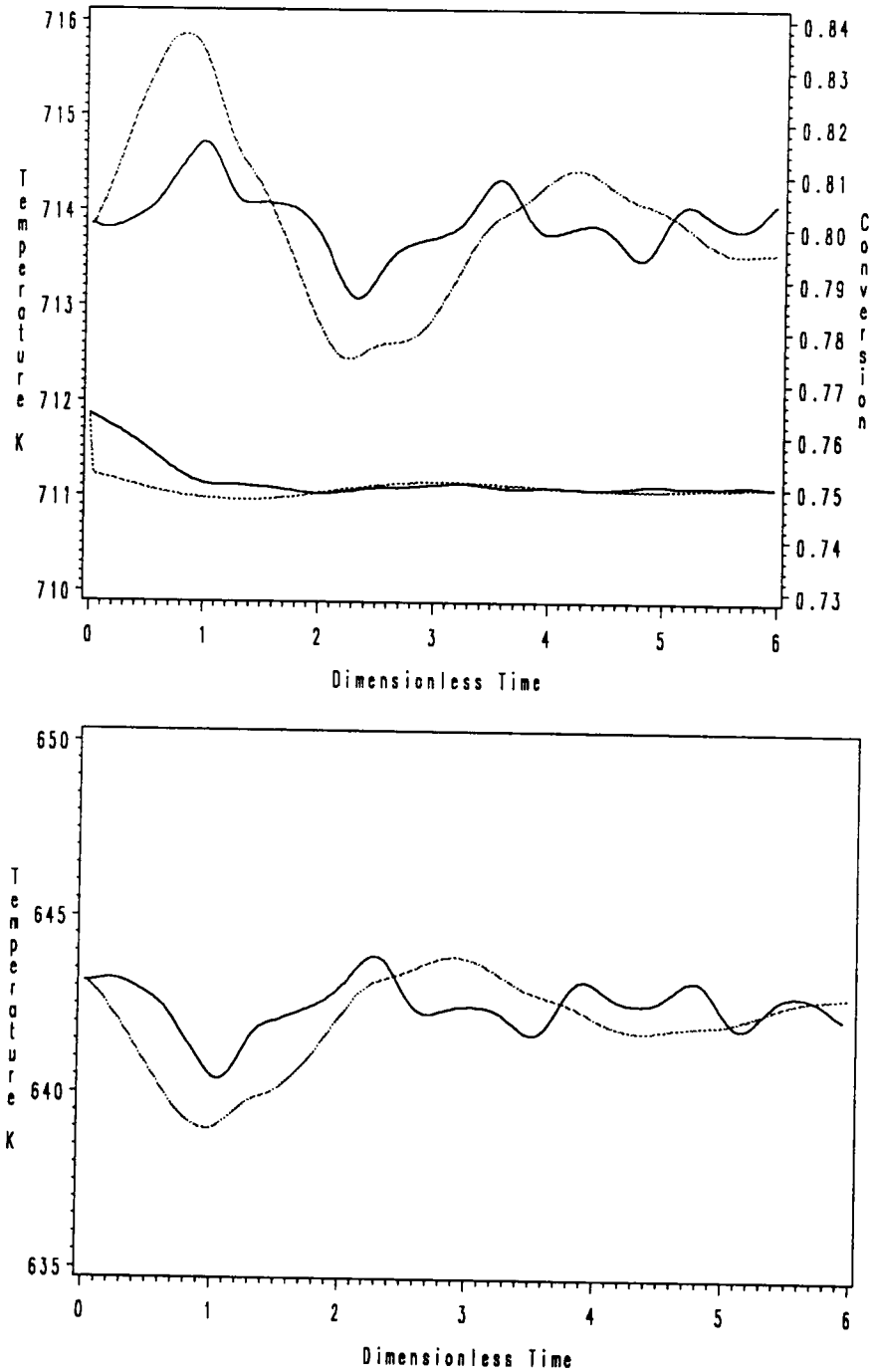

Figure 5.14: The response of reactor temperature at T12 ($z = .61389$) to a 10 % mass flow rate step change under QDMC (solid line, $p = 100$, $n = 8$, $\lambda = 1$) and the PI controller (dotted line, $K_c = 1.3$, $\tau_i = .9$). Top: reactor response. Bottom: controller output.

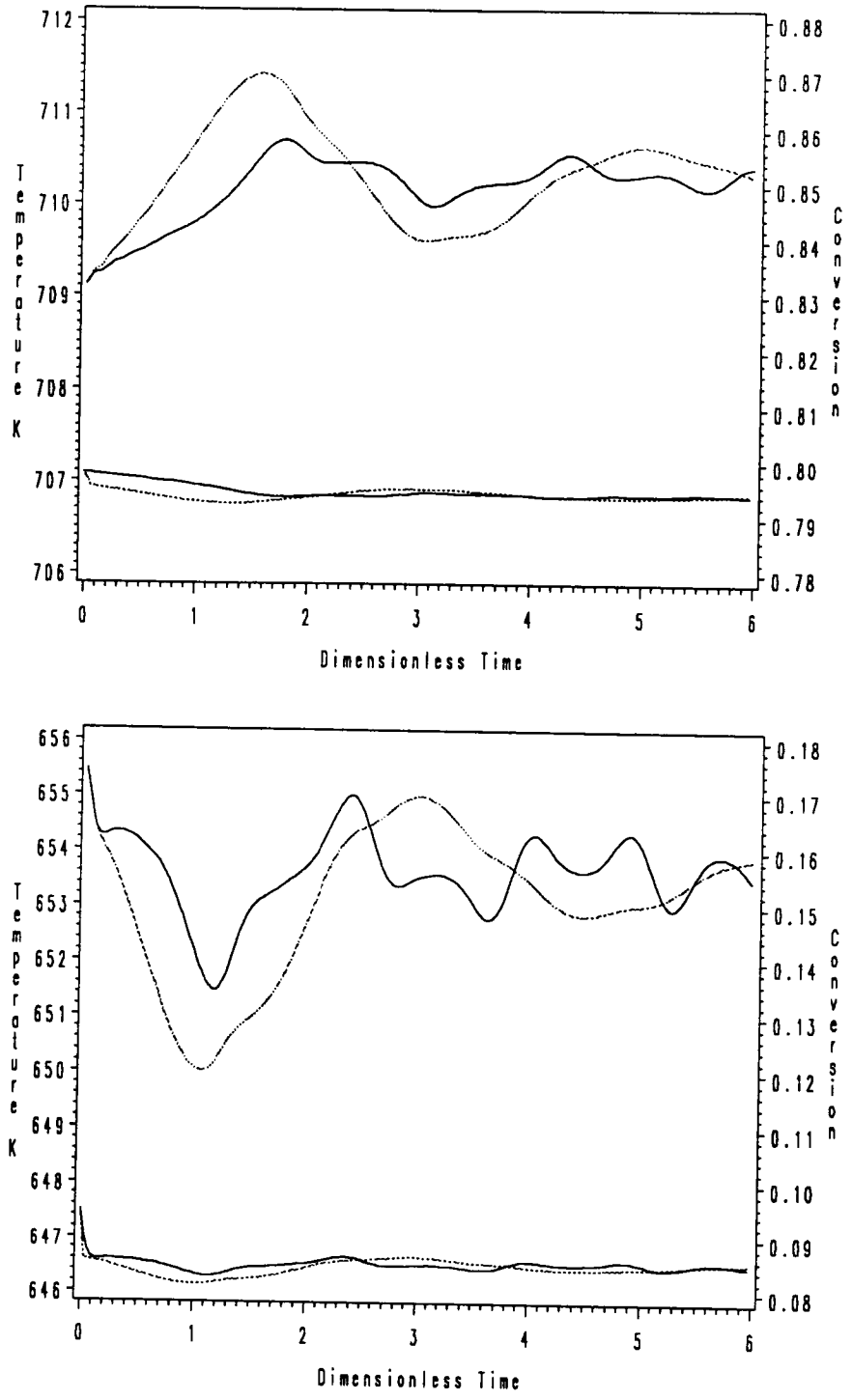

Figure 5.15: The response of reactor temperature to a 10 % mass flow rate step change under DMC (solid line, $p = 100$, $n = 8$, $\lambda = 1$) and the PI controller (dotted line, $K_c = 1.3$, $\tau_i = .9$). Top: T20 at $z = .99656$. Bottom: T3 at $z = .04388$.

Table 5.2: A Summary of the SISO Simulation Studies in terms of the Maximum Temperature Deviation (ΔT in K) at z_3, z_{12} and $z20$ and the Maximum Conversion Deviation (Δx in Conversion) at $z20$ (Manipulated Variable: T_f)

Type	Simulation	Control Algorithm	z_3 (ΔT)	z_{12} (ΔT)	z_{20} (ΔT)	z_{20} (Δx)	Comments
SISO Case 1	Set Point (5 K)	PI	5.0	–	–	–	good
		DMC	5.0	–	–	–	good
	Disturbance (10 % ΔG)	PI	1.0	1.8	2.0	0.47	sensitive
		DMC	1.2	0.9	1.6	0.4	good
SISO Case 2	Set Point (5 K)	PI	–	5.0	–	–	good
		QDMC	–	5.0	–	–	good
	Disturbance (10 % ΔG)	PI	5.4	3.4	2.3	0.54	very oscillatory
		QDMC	4.0	1.6	1.6	0.40	oscillatory

variables (T_f and T_w).

Figures 5.16 and 5.17 show the response of the reactor to set point changes of 5 K in both loops for T3 and T20 when the feed gas temperature and wall temperature are used as the manipulated variables. In this case, at $t = 0$ both set points (T3 and T20) are increased by 5 K. As shown in Figures 5.16 and 5.17, both temperatures track their set points quite well and interactions are small. Due to a distinctively different response times to each manipulated variable, T20 ($z = .99656$) exhibits interesting behavior as the result of the superposition of the two step responses. Since response to the wall temperature is fast, T20 changes immediately, and then, later T20 shows the effect of the feed temperature.

Next, disturbances are introduced to the system. Figures 5.18 and 5.19 show the response of the system to the disturbance using QDMC. In this case, at $t = 0$, the mass flow rate is increased by 10 %. As shown in Figure 5.18, both reactor temperatures are able to maintain their set points. The effect of the wall temperature control action, see the steady state effect of changes in the wall temperature on concentration in Figure 2.11, compensates for the conversion drop at the exit due to changes in the mass flow rate.

In another disturbance test, at $t = 0$, the CO mole fraction is increased by 3 %. As shown in Figures 5.20 and 5.21, the temperatures are also able to maintain their set points under this disturbance. Again, the effect of the wall temperature control action compensates for the conversion increase at the exit due to changes in CO mole fraction, but eventually the conversion is increased about 0.6 %.

The same type of control application is carried out in another configuration, Case 2 in which, the second sensor is placed in the middle of the reactor, T3 and T12, but the same manipulated variables are used, the feed temperature and the wall temperature.

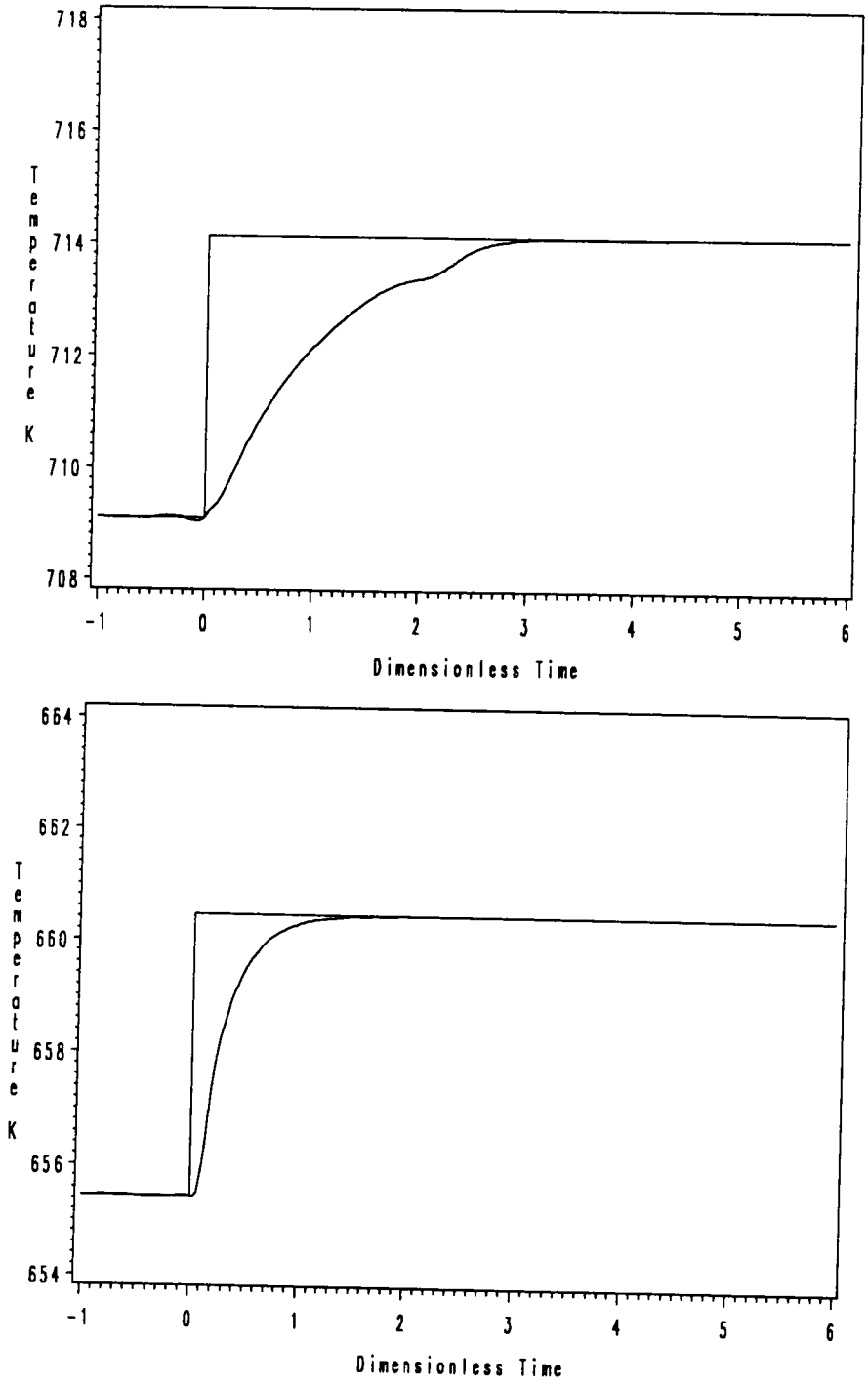

Figure 5.16: The response of reactor temperature to 5 K set point changes at T3 (z = .04388) and T20 (z = .99656) using T_f (p = 130, n = 14, λ = 8) and T_w (p = 130, n = 14, λ = 4) as manipulated variables (solid line: temperature, dotted line: conversion). Top: T20. Bottom: T3.

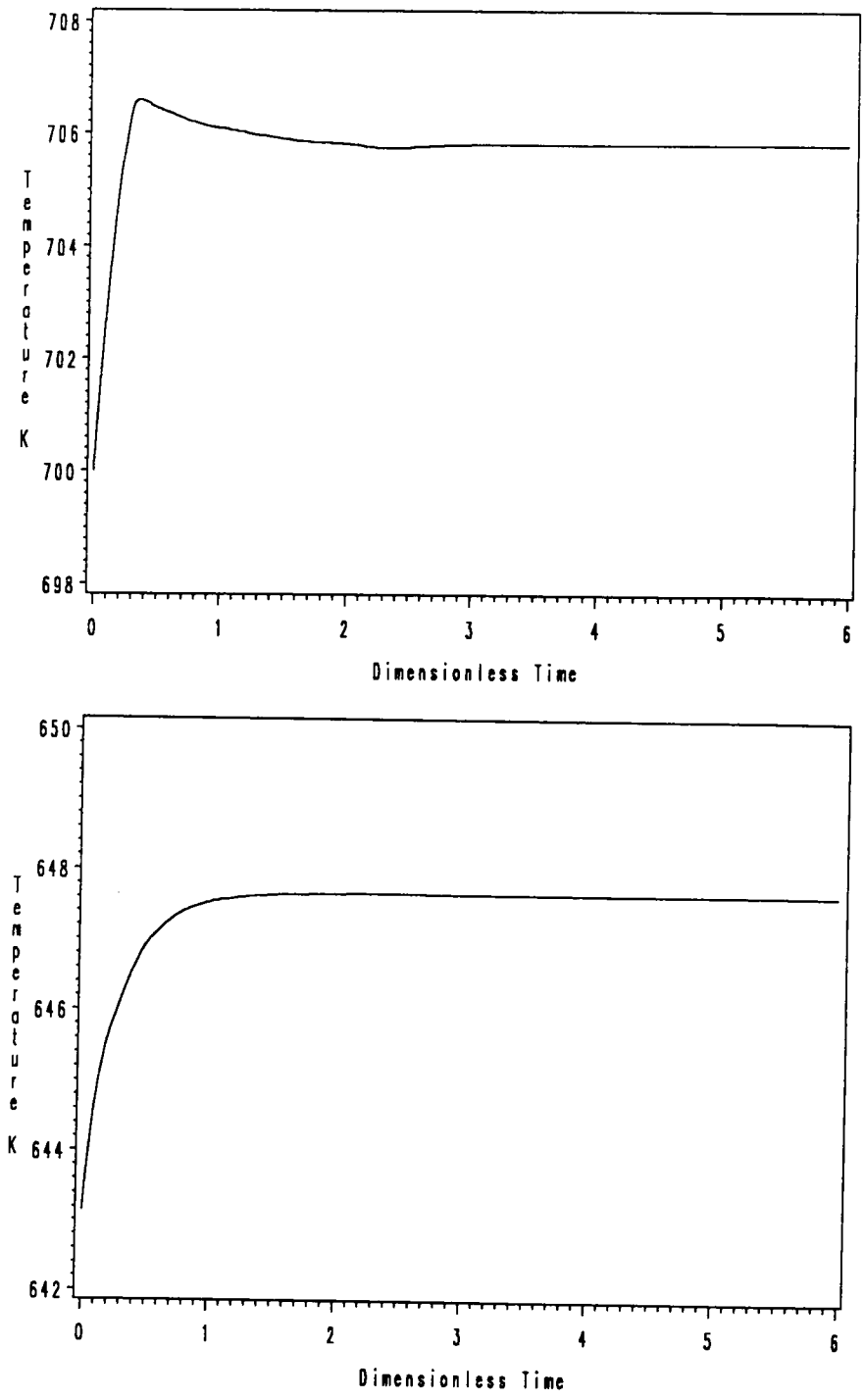

Figure 5.17: The controller output for 5 K set point changes at T3 (z = .04388) and T20 (z = .99656) using T_f (p = 130, n = 14, λ = 8) and T_w (p = 130, n = 14, λ = 4) as manipulated variables. Top: wall temperature. Bottom: feed temperature.

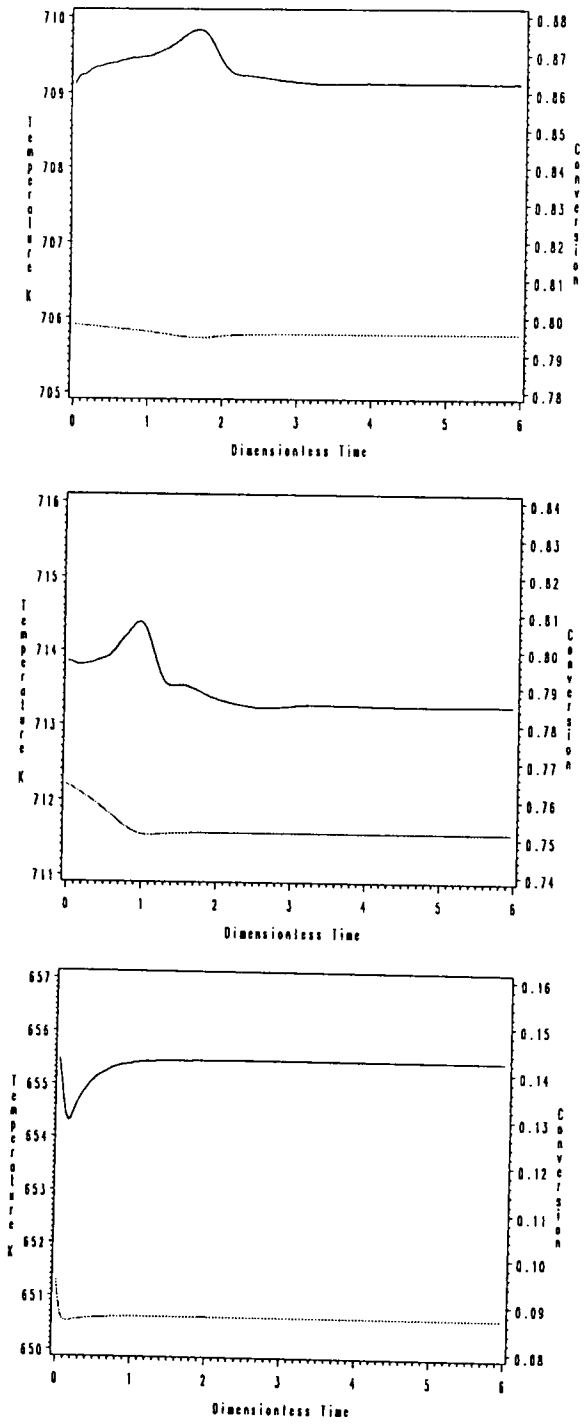

Figure 5.18: The response of reactor temperature to a 10 % mass flow rate step change at T3 (z = .04388) and T20 (z = .99656) using T_f (p = 130, n = 14, λ = 8) and T_w (p = 130, n = 14, λ = 4) as manipulated variables (solid line: temperature, dotted line: conversion). Top: T20. Middle: T12. Bottom: T3.

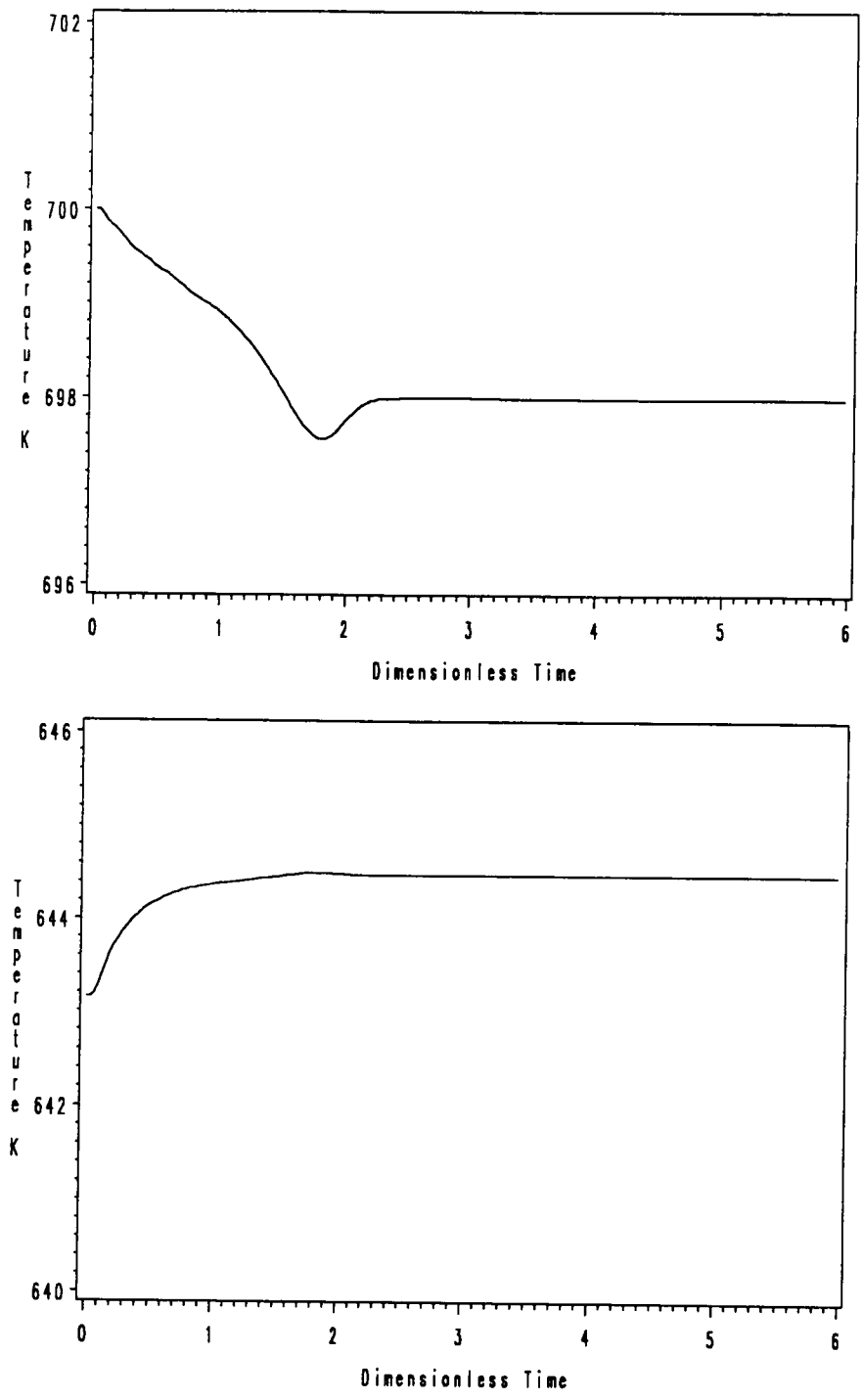

Figure 5.19: The controller output for a 10 % mass flow rate step change at T3 (z = .04388) and T20 (z = .99656) using T_f (p = 130, n = 14, λ = 8) and T_w (p = 130, n = 14, λ = 4) as manipulated variables. Top: wall temperature. Bottom: feed temperature.

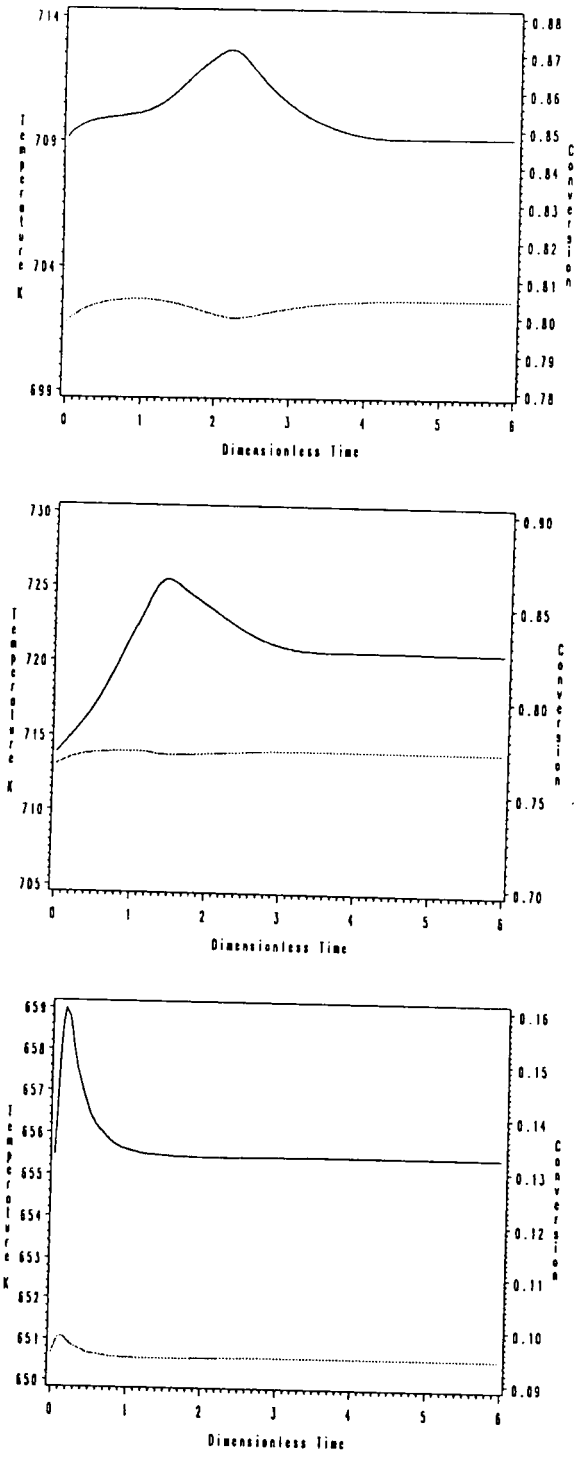

Figure 5.20: The response of reactor temperature to a 3 % CO mole fraction step change at T3 ($z = .04388$) and T20 ($z = .99656$) using T_f ($p = 130$, $n = 14$, $\lambda = 8$) and T_w ($p = 130$, $n = 14$, $\lambda = 4$) as manipulated variables (solid line: temperature, dotted line: conversion). Top: T20. Middle: T12. Bottom: T3.

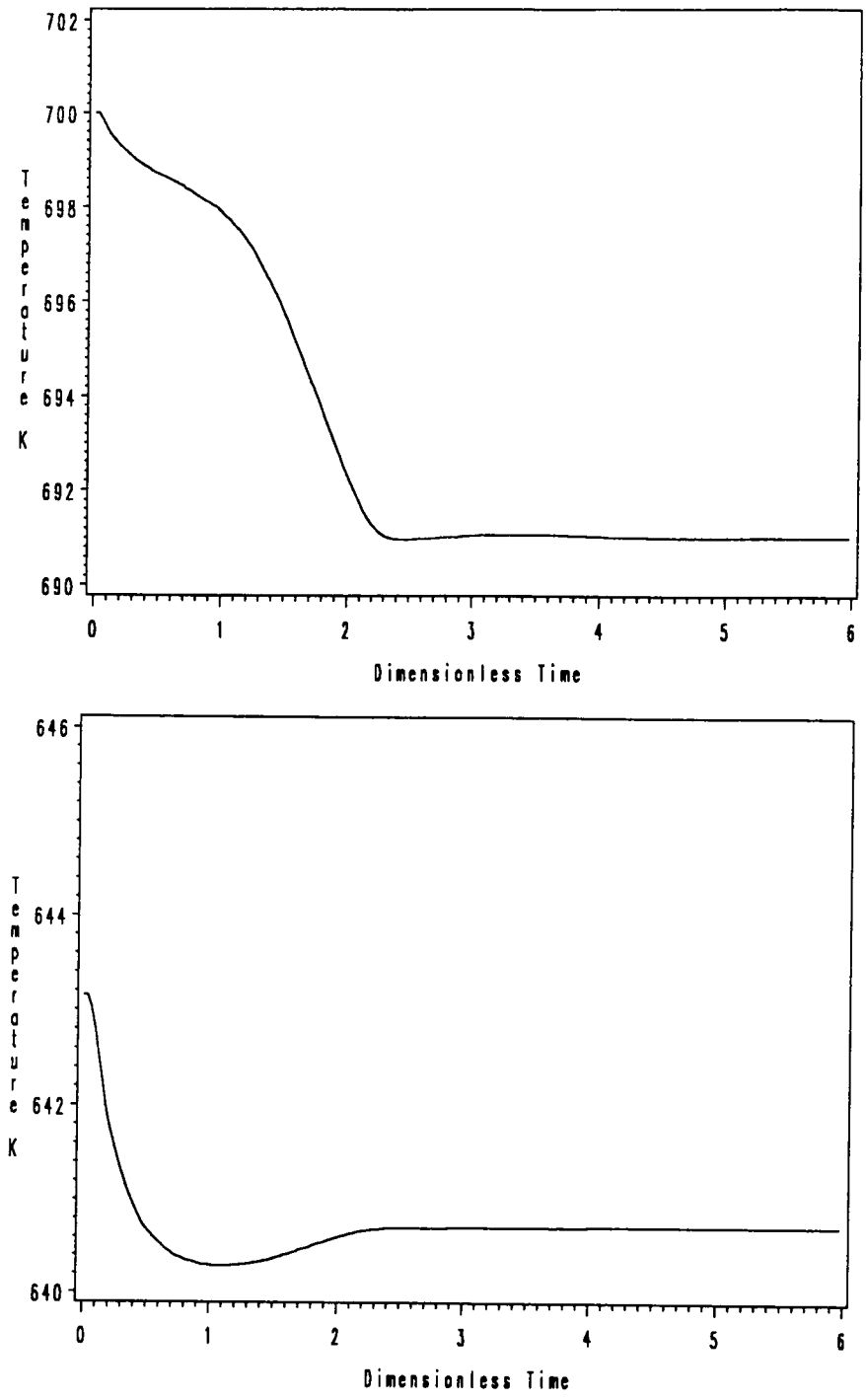

Figure 5.21: The controller output for a 3 % CO mole fraction step change at T3 ($z = .04388$) and T20 ($z = .99656$) using T_f ($p = 130$, $n = 14$, $\lambda = 8$) and T_w ($p = 130$, $n = 14$, $\lambda = 4$) as manipulated variables. Top: wall temperature. Bottom: feed temperature

In Case 2, a prediction horizon (p) of 100 and control horizon (n) of 14 are selected. Then, matrix A is of dimensions 200×28. The output weighting parameters are again selected as $\gamma_i = 1$ while the move suppression parameters λ_i are 8 and 4, respectively, for the two manipulated variables.

Figures 5.22 and 5.23 show the response of the system to set point changes using QDMC. In this case, at $t = 0$, both set points (T1 and T12) are increased by 5 K. As shown in Figure 5.22, both temperatures are able to track their set points quite well. Again, due to a distinctive response time difference to each of the manipulated variables, T12 ($z = .61389$) shows the same behavior like adding two step response even more clearly than Figure 5.16. Since T12 responds relatively fast to the wall temperature, T12 changes immediately, and then later T12 show the effects of its response to the feed temperature which is faster than T20.

Next, the same disturbances are introduced to the system as in Case 1. Figures 5.24 and 5.25 shows the system response to the disturbance using QDMC. In this case, at $t = 0$, the mass flow rate increased by 10 %. Figure 5.24 shows that both temperatures are able to maintain their set points and reject the disturbance. In another disturbance rejection test, at $t = 0$, the CO mole fraction is increased by 3 %. Figures 5.26 and 5.27 show that both temperatures are able to maintain their set points under such a disturbance. In both disturbance rejection tests, the effect of the wall temperature control action compensates for the conversion changes at the exit due to changes in the mass flow rate and CO mole fraction.

In both MIMO control cases, the QDMC algorithm demonstrated excellent set point tracking and disturbance rejection properties even in the face of large time delays, nonlinearity and inverse response. Since Case 2 has more loop interaction than Case 1

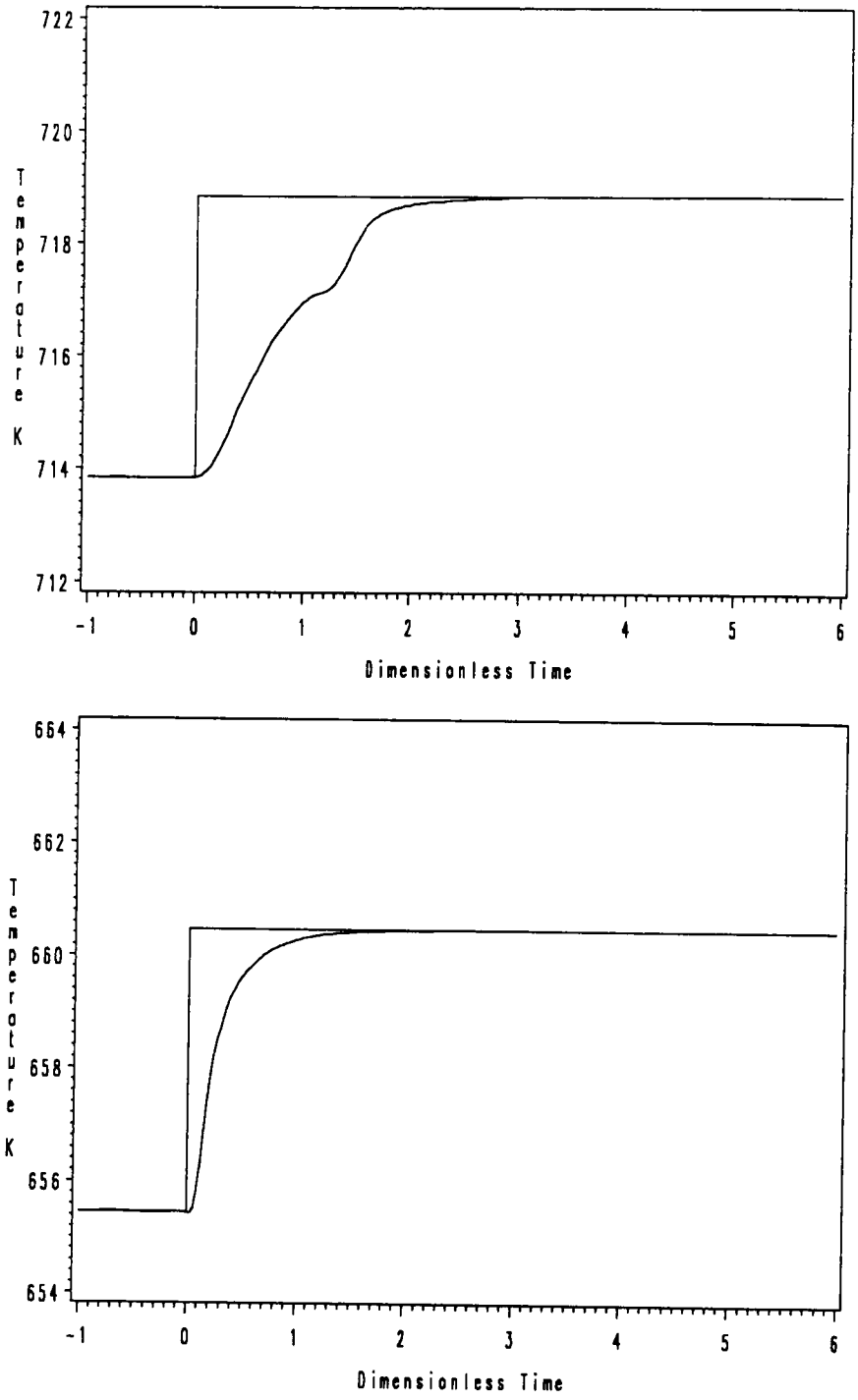

Figure 5.22: The response of reactor temperature to 5 K set point changes at T3 ($z = .04388$) and T12 ($z = .61389$) using T_f ($p = 100$, $n = 14$, $\lambda = 4$) and T_w ($p = 100$, $n = 14$, $\lambda = 4$) as manipulated variables. Top: T12. Bottom: T3.

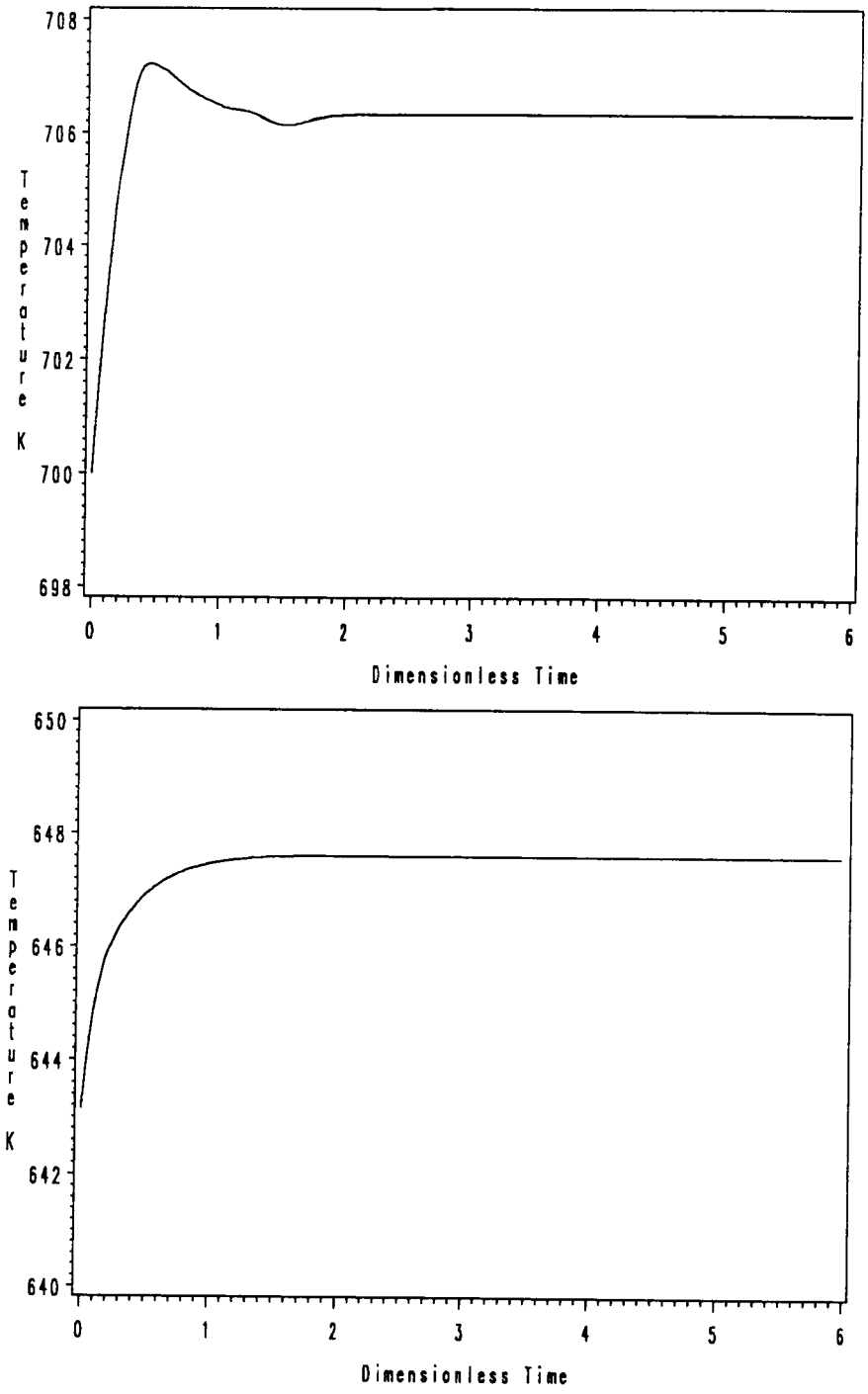

Figure 5.23: The controller output to 5 K set point changes at T3 ($z = .04388$) and T12 ($z = .61389$) using T_f ($p = 100$, $n = 14$, $\lambda = 4$) and T_w ($p = 100$, $n = 14$, $\lambda = 4$) as manipulated variables. Top: wall temperature. Bottom: feed temperature.

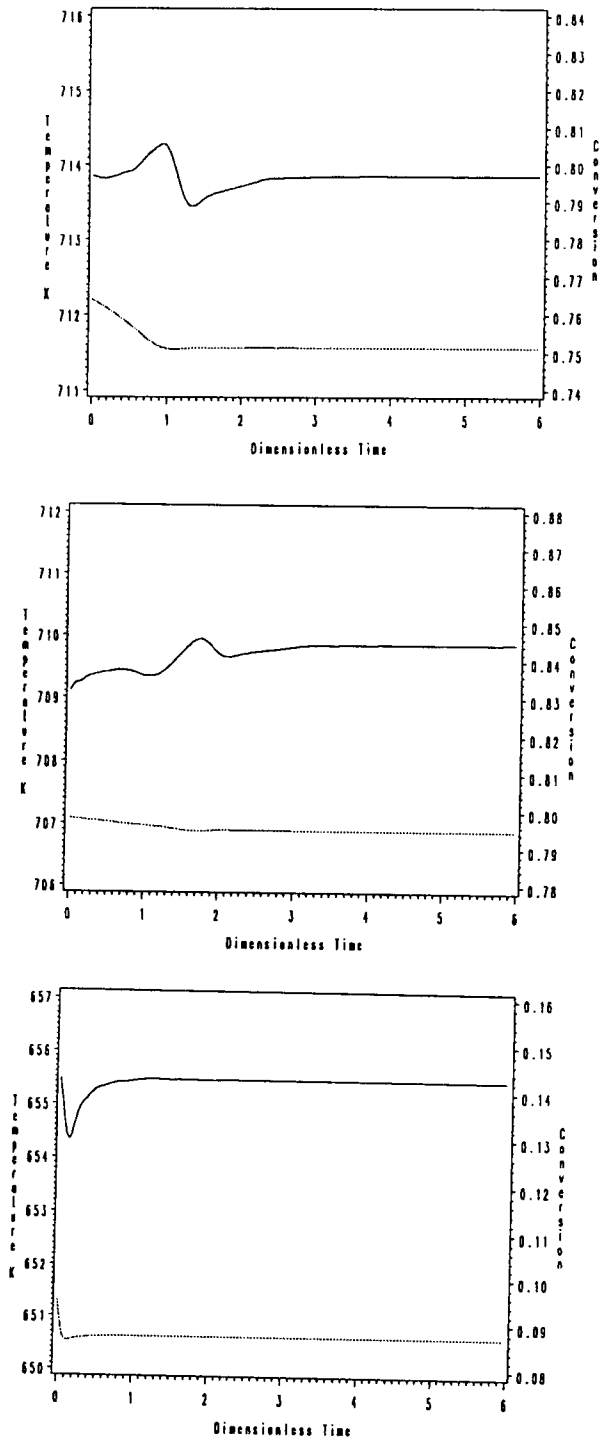

Figure 5.24: The response of reactor temperature to a 10 % mass flow rate step change at T3 (z = .04388) and T12 (z = .61389) using T_f (p = 100, n = 14, λ = 4) and T_w (p = 100, n = 14, λ = 4) as manipulated variables (solid line: temperature, dotted line: conversion). Top: T20. Middle: T12. Bottom: T3.

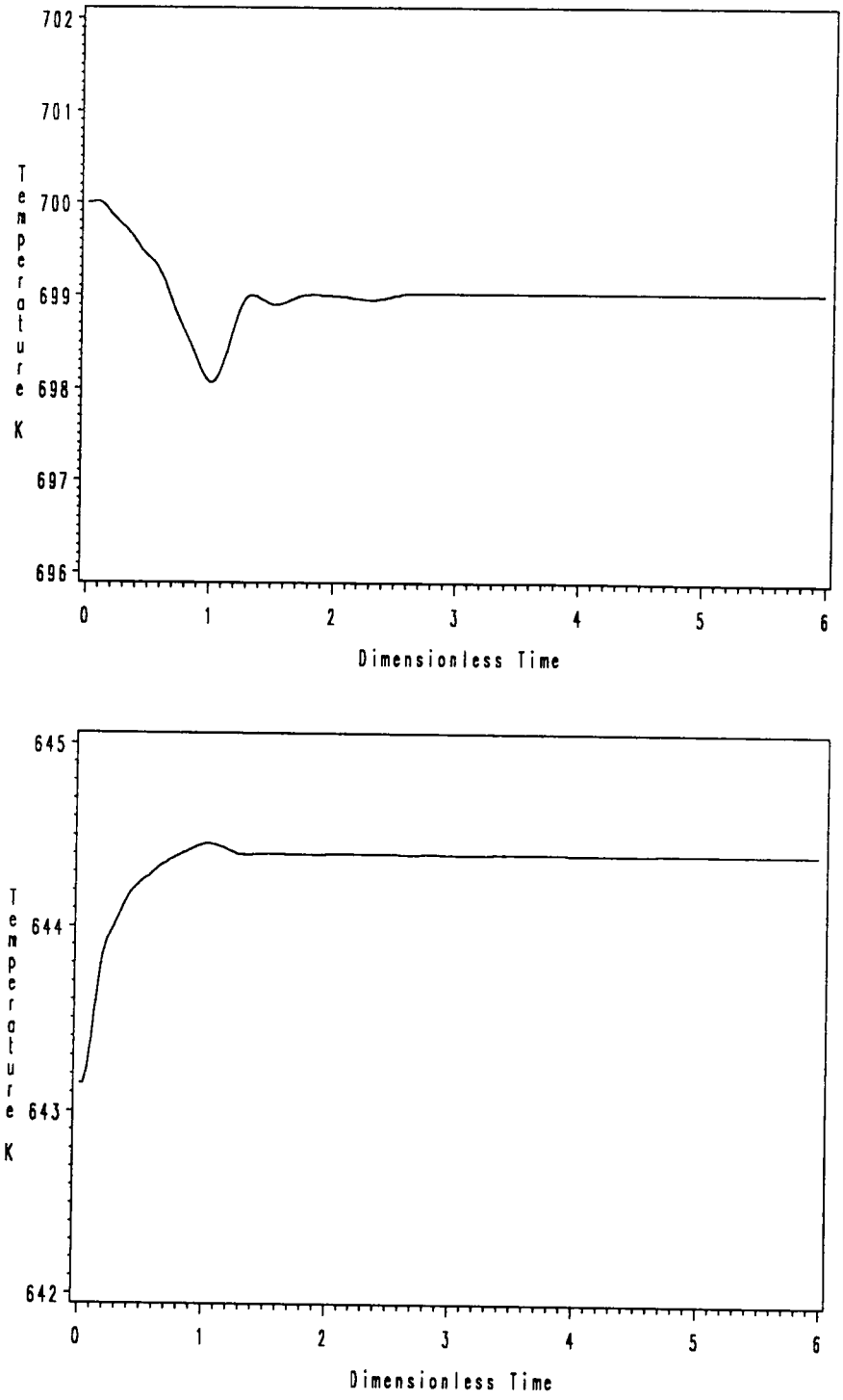

Figure 5.25: The controller output for a 10 % mass flow rate step change at T3 (z = .04388) and T12 (z = .61389) using T_f (p = 100, n = 14, λ = 4) and T_w (p = 100, n = 14, λ = 4) as manipulated variables. Top: wall temperature. Bottom: feed temperature.

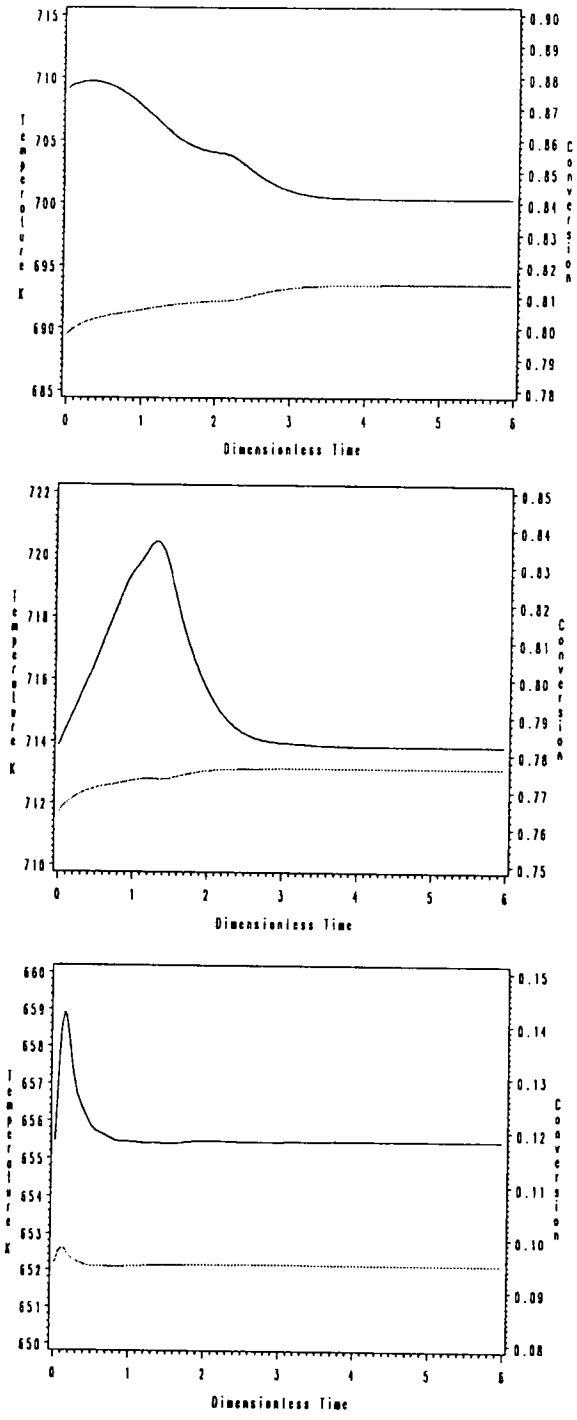

Figure 5.26: The response of reactor temperature to a 3 % CO mole fraction step change at T3 (z = .04388) and T12 (z = .61389) using T_f (p = 100, n = 14, λ = 4) and T_w (p = 100, n = 14, λ = 4) as manipulated variables (solid line: temperature, dotted line: conversion). Top: T20. Middle: T12. Bottom: T3.

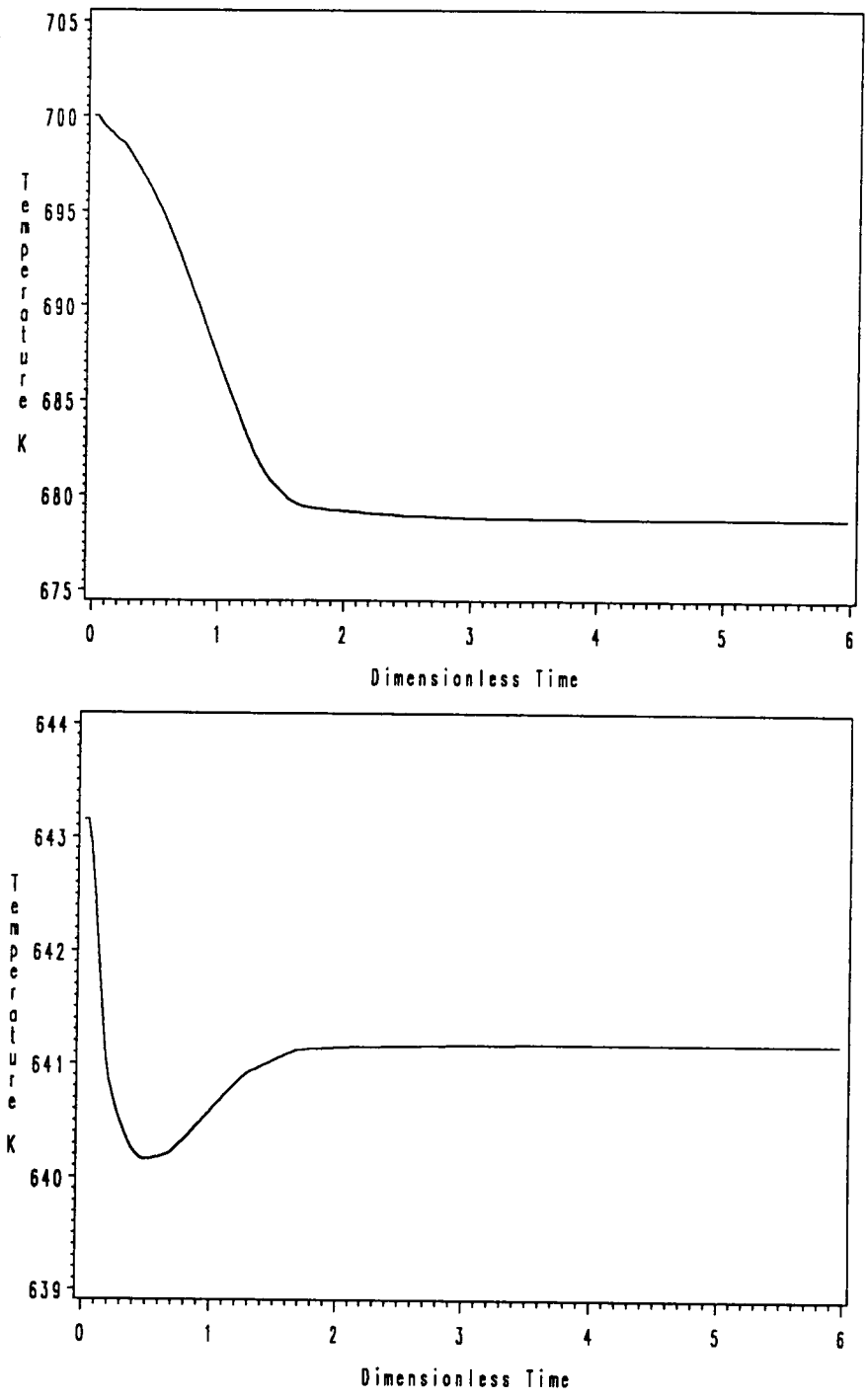

Figure 5.27: The controller output for a 3 % CO mole fraction step change at T3 ($z = .04388$) and T12 ($z = .61389$) using T_f ($p = 100$, $n = 14$, $\lambda = 4$) and T_w ($p = 100$, $n = 14$, $\lambda = 4$) as manipulated variables. Top: wall temperature. Bottom: feed temperature.

(See Table 4.1) and the second sensor location is right after the hot spot, the control configuration of Case 2 requires larger control actions in the manipulated variables, especially the wall temperature when the disturbances are introduced to the reactor. The results of both MIMO case studies indicate that Case 1, controlling the reactor temperatures close to the entrance and the exit, is a better control strategy than Case 2, controlling the reactor temperature close to the entrance and right after the hot spot with same manipulated variables. An outline of the MIMO QDMC simulation studies is presented in Table 5.3.

5.7 Conclusion

Implementation of the DMC/QDMC algorithm to a fixed-bed reactor with the water-gas shift reaction has been demonstrated. Simulation results using a 20-th order nonlinear ODE model at the nominal operating conditions have been presented for single-input single-output and multi-input multi-output (2×2) control case.

For the single-input/single-output cases, two control configurations, one close to the entrance and the other right after the hot spot, were manipulated by feed gas temperature. The performance of DMC was not much different than from PI controller when there are small time delays in the process. But in the presence of large time delays and inverse response, QDMC considerably showed better performance than the PI controller. At both sensor locations, DMC/QDMC showed excellent set point tracking responses and disturbance rejection characteristics by manipulating the feed gas temperature under inverse response and nonminimum phase characteristics. The results of both SISO case studies indicate that controlling the reactor temperature at the front

Table 5.3: A Summary of the MIMO QDMC Simulation Studies in terms of the Maximum Temperature Deviation (ΔT in K) at z_3, z_{12} and $z20$ and the Maximum Conversion Deviation (Δx in Conversion) at $z20$ (Manipulated Variables: T_f and T_w; Controlled Variables: T3 and T20 in Case 1; and T3 and T12 in Case 2)

Type	Simulation	z_3 (ΔT)	z_{12} (ΔT)	z_{20} (ΔT)	z_{20} (Δx)	Comments
MIMO Case 1	Set Point (5 K)	5.0	–	5.0	–	good
	Disturbance (10 % ΔG)	1.2	1.2	0.8	0.33	good
	Disturbance (3 % Δx_{CO})	3.6	12.6	3.6	0.64	good
MIMO Case 2	Set Point (5 K)	5.0	5.0	–	–	good
	Disturbance (10 % ΔG)	1.1	0.8	0.8	0.33	good
	Disturbance (3 % Δx_{CO})	3.5	6.6	9.4	1.59	large control action

using the feed temperature is better than controlling the reactor temperature right after the hot spot.

For the multivariable cases, two control configurations with different sensor locations were tried. The first case used the feed gas temperature and the wall temperature to control the reactor temperature close to the entrance and close to the exit. The second scheme used the feed gas temperature and the wall temperature to control the reactor temperature close to the enterance and right after the hot spot. In both control configurations, multivariable QDMC demonstrated excellent set point tracking responses and disturbance rejection characteristics by manipulating the feed gas temperature and wall temperature in the face of large time delays, nonlinearities and inverse response. The results of both MIMO case studies indicate that Case 1, controlling the reactor temperatures close to the entrance and the exit, is a better control strategy than Case 2, controlling the reactor temperature closed the entrance and right after the hot spot with the same manipulated variables.

When the reactor is subjected to disturbances such as mass flow rate and CO mole fraction, the controllers are able to maintain the temperature set points but they have difficulties in maintaining the exit conversion in most cases. The effect of wall temperature on the conversion at the exit shows promising results. In general, both MIMO control cases show better control performances than the SISO cases in this study. Overall, the Case 1 MIMO structure, controlling the reactor temperatures close to the entrance and the exit using the feed temperature and the wall temperature, shows the best control performance.

5.8 Nomenclature

a_c	associcated variable projection vector
a_i	unit step-response coefficient
a_m	measured vector of associated variable
a^*	effect of the past input on the projection of a
A	dynamic matrix of controlled variable step-response coefficients
A^+	pseudoinverse of A
B	dynamic matrix of associated variable step-response coefficients
c	vector of projected deviations of constrained variables
C	LHS matrix of QP linear inequalities
d	unmodeled disturbance
e	projected set point error vector
g	Quadratic Program gradient vector
H	Quadratic Program Hessian vector
n	number of input moves
p	prediction horizon
P	prediction of controlled variable
x	vector of present and future move
Γ	matrix of controlled variable weight γ_i
Λ	matrix of move suppression factors λ_i

Superscripts

$*$	projection based on moves up to present time

Subscripts

m	measurement
max	maximum bound
min	minimum bound
s	set point

CHAPTER 6

Conclusions and Future Work

6.1 Conclusions

The dynamic modeling and simulation, selection of sensor locations and manipulated variables, control loop pairing for SISO design, and implementation of DMC/QDMC algorithm to a fixed bed tubular reactor have been investigated in this study.

A two dimensional dynamic model and simulation of fixed bed reactor was first studied. Many factors have been considered in the modeling and simulation of the water-gas shift tubular reactor system; for example, the operating characteristics of the catalyst to be used, temperature limits on their operation, the kinetics of the catalyzed reaction, and the operating conditions in industrial water-gas shift reactors. In general, whenever possible, the parameters and operating conditions have been selected to be close to those stated for the industrial case. Large portions of this study are focused on the modeling and simulation of the water-gas shift reaction. Rigorous steady state and dynamic simulations are presented for a comprehensive analysis of the reactor behavior under different operating conditions. Detailed steady state and dynamic simulations yielded important results.

- Steady state simulations are presented that show the steady state responses of process variables with a small number of collocation points.

- Dynamic simulations showed that the selection of the number of collocation points

was important to obtain an accurate simulation. Unlike steady state simulation, dynamic simulations require more collocation points to assure an accurate simulation. The error criteria (below 10^{-6}) used in the Gear variable time step size integration subroutine is able to yield reliable simulation results.

Control structure from single-input single-output DMC to multivariable QDMC were sucessfully implemented on a fixed bed reactor with the water-gas shift reaction. This reactor exhibits inverse response and nonminimum phase characteristics. Due to the nature of distributed parameter systems, there is an infinite number of potential controlled variables, e.g. reactor temperatures at different locations down the length of the reactor. The potential manipulated variables for this reactor are the feed gas temperature, mass flow rate, CO mole fraction and the wall temperature. Information for controller design used in this study required steady state gains. The steady state gains were obtained from the nonlinear steady state or dynamic simulations. Steady state gains was determined by step changes in the manipulated variables including positive and negative steps and then an average value was used. From the steady state gain matrix, the sensor location and possible pairing between the controlled and manipulated variables were decided by SVA and RGA. The most effective control configuration is to control the reactor temperature T1 ($z = .34357e - 2$), using the feed gas temperature, and to control the reactor temperature T20 ($z = .99656$), using the wall temperature.

A single-input/single-output DMC/QDMC algorithm was implemented on two different control configurations, one close to entrance (T3) and the other right after hot spot (T12), by manipulating feed gas temperature. Both cases yielded an excellent set point tracking response and disturbance rejection properties by manipulating the feed gas temperature under difficult dynamic characteristics, such as inverse response and

large time delays.

The multivariable QDMC was sucessfully implemented for the fixed bed reactor. Two different control configurations were used. The first control case used the feed gas temperature and the wall temperature to control the temperatures close to the entrance (T3) and close to the exit (T20). The second control case used the feed gas temperature and the wall temperature to control the temperature close to the enterance (T3) and right after the hot spot (T12). Both configurations showed excellent performance in set point tracking and disturbance rejection by manipulating feed gas temperature and wall temperature in the face of inverse response, nonlinearities, and large time delays.

6.2 Future Work

In this work several problems associated with the design of the reactor control system and their implementation require further investigation in subsequent research efforts.

With the development of an on-line compostion senor, control system based on compostion requires further research efforts. Little attention was paid to the importance of process disturbances and noise in the control system development. Noise and disturbances are common features of industrial reactors and, therefore, their effects on the performance of control system should be investigated.

With increasing demands for higher performance from control systems, the concept of control system design should be expanded to plant-wide instead of addressing individual unit operations. Thus, the heat integration, such as the Heat Economizer which is introduced in this study, and material recycle require plant-wide developments of mathematical modeling, software, and control system design.

BIBLIOGRAPHY

BIBLIOGRAPHY

[1] Alvarez, J., J. A. Romagnoli and G. Stephanopoulos, *Variable Measurement Structures for The Control of a Tubular Reactor*, Chem. Eng. Sci., 36, 10, 1695-1712 (1981).

[2] Ampaya, J. P. and R. G. Rinker, *Design Correlation for Autothermal reactors with Internal Countercurrent Heat Exchange*, Ind. Eng. Chem. Pro. Des. Dev., 16, 63-69 (1977).

[3] Ampaya, J. P. and R. G. Rinker, *Autothermal Reactor with Internal Heat Exchange: Numerical and Experimental Studies in the Multiple Steady State Region*, Chem. Eng. Sci., 32, 1327-1338 (1977).

[4] Ampaya, J. P. and R. G. Rinker, *Autothermal Reactor with Internal Heat Exchange: Numerical and Preliminary Experimental Studies of Transient Behavior Including Startup in the Multiple Steady State Region*, Chem. Eng. Sci., 32, 1327-1338 (1977).

[5] Aris, R. and N. R. Amundson, *An Analysis of Chemical Reactor Stability and Control-I. The Possibility of Local Control with Perfect or Imperfect Control Mechanisms*, Chem. Eng. Sci., 7, 121-131 (1958).

[6] Aris, R. and N. R. Amundson, *An Analysis of Chemical Reactor Stability and Control-II. The Evolution of Proportional Control*, Chem. Eng. Sci., 7, 132-147 (1958).

[7] Baddour, R. F., P.L.T. Brian, B.A. Logeais and P. Emery, *Steady State Simulation of an Ammonia Synthesis Converter*, Chem. Eng. Sci., 20, 281-292 (1965).

[8] Baddour, R. F., P.L.T. Brian, B.A. Logeais and P. Emery, *Transient Behavior of an Ammonia Synthesis Reactor*, Chem. Eng. Sci., 20, 297-310 (1965).

[9] Baker, A. J., *Finite Element Computational Fluid Mechanics*, McGraw-Hill, New York (1983).

[10] Bilous, Olegh and N. R. Amundson, *Chemical Reactor Stability and Sensitivity*, AIChE J.. Vol 1, 513-522 (1955).

[11] Bohlbro H., *The Kinetics of the Water Gas Conversion at Atmospheric Pressure*, Acta Chem. Scand., 15, 502-520 (1961).

[12] Bohlbro H., *The Kinetics of the Water Gas Conversion at Atmospheric Pressure: II. Investigation at Elevated Pressure.*, Acta Chem. Scand., 16, 431-438 (1962).

[13] Bonvin, D., R.G. Rinker and D. A. Mellichamp, *Dynamic Analysis and Control Structures for a Tubular Autothermal Reactor at an Unstable State*, Chem. Eng. Sci., 35, 603-612 (1980).

[14] Bonvin, D., R.G. Rinker and D. A. Mellichamp, *On Controlling an Autothermal Fixed-Bed Reactor at an Unstable State-I. Steady State and Dynamic Modeling*, Chem. Eng. Sci., 38, 233-244 (1983).

[15] Bonvin, D., R.G. Rinker and D. A. Mellichamp, *On Controlling an Autothermal Fixed-Bed Reactor at an Unstable State-II. Discrimination among Rival Models to Achieve Suitable Internal Structure*, Chem. Eng. Sci., 38, 245-256 (1983).

[16] Bonvin, D., R.G. Rinker and D. A. Mellichamp, *On Controlling an Autothermal Fixed-Bed Reactor at an Unstable State-III. Model Reduction and Control Strategies which avoid State Estimation*, Chem. Eng. Sci., 38, 607-618 (1983).

[17] Bonvin, D., C. Wong, R.G. Rinker and D. A. Mellichamp, *On Controlling an Autothermal Fixed-Bed Reactor at an Unstable State-IV. Model Fitting and Control of the Laboratory Reactor*, Chem. Eng. Sci., 38, 619-634 (1983).

[18] Bonvin, D. and Mellichamp, D. A., *Rescaling State and Input Variables for the Purpose of Analyzing Process Models*, Amer. Control Conf. (1985).

[19] Borgars D. J. and J. S. Campbell, *Design and Operation of CO Shift, Naptha, and Natural Gas*, Ammonia, Fertilizer Sci. and Tech. Ser., Vol. 2., 25-72 (1974).

[20] Bristol, E. H., *On a New Measure of Interaction for Multivariable Process Control*, IEEE Transactions on Automatic Control, 133-134 (1966).

[21] Bruns, D. D. and J. E. Bailey, *Process Operation Near an Unstable State Using Nonlinear Feedback Control*, Chem. Eng. Sci., 30, 755-762 (1975).

[22] Bruns, D. D. and J. E. Bailey, *Nonlinear Feedback Control for Operating a Nonisothermal CSTR near an Unstable Steady State*, Chem. Eng. Sci., 32, 257-264 (1977).

[23] Carberry, J. J., *Chemical and Catalytic Reactor Engineering*, McGraw-Hill, New York (1976).

[24] Chang, M. and R. A. Schmitz, *An Experimental Study of Oscillatory States in a Stirred Reactor*, Chem. Eng. Sci., 30, 21-34 (1975).

[25] Chang, M. and R. A. Schmitz,*Feedback Control of Unstable States in a Laboratory Reactor*, Chem. Eng. Sci., 30, 837-846 (1975).

[26] Chang, S. H., *Nonlinear Feedback Control and Dead Time Compensation for Systems with Dead Time*, Master Thesis, UT Knoxville (1984).

[27] Crier, J. E. and A. S. Foss, *Computational Studies of Transient in Packed Tubular Chemical Reactors*, AIChE J., 514-522 (1966).

[28] Cutler, C. R., *Dynamic Matrix Control: An Optimal Multivariable Control Algorithm with Constraints*, Ph.D. Thesis, U. of Houston, Houston, TX (1983).

[29] Cutler, C. R., and B. L. Remaker, *Dynamic Matrix Control - A Computer Control Algorithm*, AIChE 86th National Meeting, Houston, TX, April 1979.

[30] Cutler, C. R., *Dynamic Matrix Control of Imbalanced Systems* , ISA Transactions, 21, 1 (1982).

[31] Davison, E. J., *Multivariable Tuning Regulators: the feedforward and robust control of a general servomechanism problem*, IEEE Trans. Automat. Contr. AC-21: 35-47 (1976).

[32] De Wasch, A. P. and G. F. Froment, *A two dimensional heterogeneous model for fixed bed catalytic reactors*, Chem. Eng. Sci., 26, 629-634 (1971).

[33] Degnan, T. F. and J. Wei, *The Co-current Reactor Heat Exchanger:Part I Theory*, AIChE J., 25,338-344 (1979).

[34] Degnan, T. F. and J. Wei, *The Co-current Reactor Heat Exchanger:Part II. Experimental Results*, AIChE J., 26, 60-67 (1980).

[35] Dyer, C. W.,*The Effect of Matrix Scaling on the Design and Control of Multivariable Processes*, Master Thesis, UT Knoxville (1987).

[36] Downs, J. J., *The Control of Azeotropic Distillation Columns*, Ph.D. Thesis, UT Knoxville (1982)

[37] Finlayson, B. A., *The Method of Weighted Residuals and Variational Principles*, Academic Press, New York (1972).

[38] Finlayson, B. A., *Packed Bed Reactor Analysis by Orthogonal Collocation*, Chem. Eng. Sci., 26, 1081-1091 (1971).

[39] Froment, G. F. and K. B. Bischoff, *Chemical Reactor - Analysis and Design*, Wiley, New York (1979)

[40] Foss, A. S., J. M. Edmunds and B. Kouvarltakis, *Multivariable Control System for Two-Bed Reactors by the Characteristic Locus Method*, Ind. Eng. Chem. Fundam., 19, 109-117 (1980).

[41] Garcia, C. E. and Morari, M., *Internal Model Control: A Unifying Review and Some New Results*, Ind. Eng. Chem. Process Des. Dev., (1981).

[42] Garcia, C. E. and Morshedi, A. M., *Quadratic Programming Solution of Dynamic Matrix Control (QDMC)*, Submitted to Chemical Engineering Communications (1985).

[43] Georgakis, C., R. Aris, and N. R. Amundson, *Studies in The Control of Tubular Reactors -I.*, Chem. Eng. Sci., 1359-1369 (1977).

[44] Georgakis, C., R. Aris, and N. R. Amundson, *Studies in The Control of Tubular Reactors -II.*, Chem. Eng. Sci., 1371-1379 (1977).

[45] Georgakis, C., R. Aris, and N. R. Amundson, *Studies in The Control of Tubular Reactors -III.*, Chem. Eng. Sci., 1381-1387 (1977).

[46] Gerstle, J. G., J. M. Keeton, C. F. Moore,and D. D. Bruns, *Singular Value Decomposition Controller Design using a Reduced Order Model*, A. C. C., San Diego, June 1983.

[47] Giger G. K., R. Mutharasan and D. R. Coughanowr, *Control of Temperature Peaks in Adiabatic Fixed-Bed Tubular Reactors*, Ind. Eng. Chem. Fundam., 19, 389 (1980).

[48] Gilles, E. D., *Application of Modeling, Estimation, and Control to Chemical Process*, Eng. Found. Conf. ChE. Pro. Control, 1981, Sea Island, Georgia.

[49] Gilles, E. D., *Some New Approaches Controlling Complex Processes in Chemical Engineering*, Chemical Process Control - CPC III (1986).

[50] Goldfarb, D. and A. Idnani, *A Numerically Stable Dual Method for Solving Strictly Convex Quadratic Programs*, Mathematical Programming, 27,1-33 (1983).

[51] Hackney, J. E.,*Control Studies of an Ethanol-Water Distillation Column*, Ph.D. Proposal (1987).

[52] Harris T. J., J. F. MacGregor and J. D. Wright, *An Application of Self-Tuning Regulators to Catalytic Reactor Control*, Proc. JACC, Philadelphia, 43-55 (1978).

[53] Harris T. J., J. F. MacGregor and J. D. Wright, *Optimal Sensor Location with an Application to a Packed Bed Tubular Reactor*, AIChE J., 26, 6, 910-916 (1980). Proc. JACC, Philadelphia, 43-55 (1978).

[54] Hindmarsh, A. C., ODEPACK:The Livermore Solvers for Ordinary Differential Equations, (1987).

[55] Hoiberg, J. A., B. C. Lyche and A. S. Foss, *Experimental Evaluation of Dynamic Models for a Fixed Bed Catalytic Reactor*, AIChE J., 17, 1434-1447 (1971).

[56] IMSL MATH/LIBRARY, International Mathematical & Statistical Libraries, Inc., NBC Building, 7500 Belair Boulevard, Houston, Texsas.

[57] Joffe, B. L. and R. W. H. Sargent, *The Design of an On-Line Control Scheme for a Tubular Catalytic Reactor*, Trans. Instn. Chem. Engrs., 50, 270-282 (1972).

[58] Jutan, A., J. P. Tremblay, J. F. MacGregor, and J. D. Wright, *Multivariable Computer Control of a Butane Hydrogenolysis Reactor - I. State Space Reactor Modeling*, AIChE J., 23, 732-741 (1977).

[59] Jutan, A., J. P. Tremblay, J. F. MacGregor, and J. D. Wright, *Multivariable Computer Control of a Butane Hydrogenolysis Reactor - II. Data Collection, Parameter Estimation, and Stochastic Disturbance Identification*, AIChE J., 23, 742-750 (1977).

[60] Jutan, A., J. P. Tremblay, J. F. MacGregor, and J. D. Wright, *Multivariable Computer Control of a Butane Hydrogenolysis Reactor - III. On-Line Linear Quadratic Stochastic Control Studies*, AIChE J., 23, 751-758 (1977).

[61] Jutan, A., J. F. MacGregor, and J. D. Wright,*Design and On-Line Implementation of a Stochastic Controller Using an Identified Multivariable Noise Model*, Proc. Joint Auto. Control Conf., San Francisco (1980).

[62] Jutan, A., J. D. Wright and J. F. MacGregor, *Multivariable Computer Control of a Butane Hydrogenolysis Reactor, Part II: Design and On-line Implementation of a Stochastic Controller Using an Identified Multivariable Noise Model*, AIChE J., 30, 2, 220-226 (1984).

[63] Kelma, V.C. and A. J. Laub, *Singular Value Decomposition: Its Computation and Some Applications*, IEEE Trans. Auto. Contro., AC-25, 164 (1980).

[64] Khanna R. and J. H. Seinfeld, *Mathematical Modeling of Packed Bed Reactors: Numerical Solutions and Control Model Development*, Advanced Chem. Eng., 13, 113-191 (1987).

[65] Kheshgi, H. S., P. S. Hagan, S. C. Reyes and J. C. Pirkle, Jr., *Transients in tubular reactors: comparision of one- and two-dimnesional models*, AIChE J., 34, 8, 1373-1375 (1988).

[66] Lappinga, A. and A. Foss *Rapid Set Point Attainment of a Reactor Feed Preheat System and Coordination with Reactor Control*, Proc. Amer. Chem. Control Conf, San Diego, 3, 1602-1607 (1984).

[67] Lau, H. and Jensen K. F., *Evaluation of Changeover Control Policies by Singular Value Analysis-Effects of Scaling*, AIChE J., 31, 135-146, (1985).

[68] Lee, K. S. and W. K. Lee, *Discrete-Time Multivariable Adaptive Control of a Nonadiabatic Fixed Bed Reactor*, 3rd Proc. Pacific. Chem. Eng. Congress, 147-152 (1983).

[69] Lee, K. S. and W. K. Lee, *On-line Optimizing Control of a Nonadiabatic Fixed Bed Reactor*, AIChE J., 31, 667 (1985).

[70] Lee, W. and Weekman, *Advanced Control Practice in the Chemical Process Industry: A View from Industry*, AIChE J., 22, 27-38 (1976).

[71] Mandler, J. A., D. M. Strand, R. Khanna and J. H. Seinfeld, *Control of a Packed Bed Reactor with Feed-Effluent Heat Exchange*, Proc. Amer. Control Conf., San Diego, 3, 1608-1613 (1984).

[72] Mandler, J. A., M. Morari and J. H. Seinfeld, *Control System Design for a Fixed-Bed Mathanation Reactor*, Chem. Eng. Sci., 41, 6, 1577-1597 (1986).

[73] McDermott, P. E., R. G. Rinker and D. A. Mellichamp, *Multivariable Self-Tuning Control of a Tubular Autothermal Reactor*, Proc. Amer. Control Conf., San Diego, 3, 1614-1620 (1984).

[74] McDermott, P. E., R. G. Rinker and D. A. Mellichamp, *Pole Placement Self-Tuning Control of a Fixed-Bed Autothermal Reactor Part I: Single Variable Control*, AIChE J., 32, 6, 1004-1014 (1986).

[75] McDermott, P. E., R. G. Rinker and D. A. Mellichamp, *Pole Placement Self-Tuning Control of a Fixed-Bed Autothermal Reactor Part II: Multivariable Control*, AIChE J., 32, 6, 1015-1024 (1986).

[76] J. M. Moe, *Design of Water-Gas Shift Reactors*, Chem. Eng. Progr., 58, 33-36, (1962).

[77] Moore, C. F., Hackney, J. E. and Canter, D. L., *Selecting Sensor Location and Type for Multivariable Processes*, Shell Control Workshop (1986).

[78] Moore, C. F., C. L. Smith, and P. W. Murill, *Multi-dimensional Optimization Using Patern Search*, IBM Share Library, PID No. 6448 (1968).

[79] Morari, M. and K. W. Fung, *Nonlinear Inferential Control*, Computers and Chem. Eng., 6, 4, 271-281 (1982).

[80] Murase, A., H. L. Roberts and A. O. Converse, *Optimal Thermal Design of an Autothermal Ammonia Synthesis Reactor*, Ind. Chem. Eng. Pro. Des. Dev., 9, 503-513 (1970).

[81] Niederlinski, A., *A Heuristic Approach to the Design of Linear Multivariable Control Systems*, Automatica, 7, 691, (1971).

[82] Nisenfeld, A. E. and H. M. Schlutz, *Interaction Analysis Applied to Control System Design*, Instrumentation Technology, April (1971).

[83] Ogunnaike, B. A. and H. W. Ray, AIChE J., *Multivariable Time Delay Control Systems Design for Linear Systems having Multiple Time Delays*, AIChE J., 25, 1043 (1979).

[84] Paradis, W. O. and D. D. Perlmuter, *Feedback Control of a Distributed Parameter Process*, AIChE J., 883-890 (1966).

[85] Patnaik, L. M. , I. G. Sarma, and N. Viswnadham,*Design of single Variable Controller for Ammonia Reactors*, Chem. Eng. Sci., 35, 754-756 (1980).

[86] Penttinen, J. and H. N. Koivo, *Multivariable Tuning Regulators for Unknown Systems*, Automatica , 16, 393-398 (1980).

[87] Perlmutter, D. D., *Stabilities of Chemical Reactors*, Prentice Hall, Englewood Cliffs, New Jersey (1972).

[88] PRO-MATLAB, The MathWorks, Inc., 20 North Main St., Suite 250, Sherborn, MA 01770.

[89] Prett, D. M. and R. D. Gillete, *Optimization and Constrained Multivariable Control of a Catalytic Cracking Unit*, AIChE 86th Meeting, April 1979, Houston, Texas.

[90] Powell, M. J. D. *On the Quadratic Programming Algorithm of Goldfarb and Idnani*, DAMTP Report NA19, Cambridge, England (1983).

[91] Ray, W. H. , *Fixed-Bed Reactors:Dynamics and Control*, 5th Eur./2nd Int. Symp. Chem. Reaction Eng., Amsterdam (1972).

[92] Ray, H. W., *Advanced Process Control*, McGraw-Hill (1981).

[93] Roat,S. D., J. J. Downs, E. F. Vogel, and J. E. Doss, *The Integration of Roigorous Dynamic Modeling and Control System Synthesis for Distillation Columns: An Industiral Approach*, Chemical Process Control - CPC III, (1986).

[94] Sabo, D. S. and J. S. Dranoff, *Stability Analysis of a Continuous Flow Stirred Tank Reactor with Consecutive Reactions*, AIChE J., 16, 2, 211-217 (1970).

[95] Shinskey, F. G., *Process Control Systems*, McGraw-Hill Co., New York (1977).

[96] Smith, C. A. and Corripio, A. B., *Principles and Practice of Automatic Process Control*, John Wiley & Sons, New York (1985).

[97] Smith, O. J. M., *Closer Control of Loops with Dead Time*, Chem. Eng. Progr., 53, 5, 217-219 (1957).

[98] Smith, R. C., C. F. Moore and D. D. Bruns, *A Structural Framework for Multivariable Control Applications*, Joint Auto. Control Conf., Charlotteville, Virginia, June 1981.

[99] Smith, R. C. and D. D. Bruns, *Singular Value Analysis: A Geometrical Structure for Multivariable Process Control*, AIChE Winter Meeting, 1982, Orlando, Florida.

[100] Sorensen, J. P., *Experimental Investigation of the Dynamics of a Fixed-Bed Reactor*, Chem. Eng. Sci., 31, 719-725 (1976).

[101] Sorensen, J. P., *Experimental Investigation of the Optimal Control of a Fixed-Bed Reactor*, Chem. Eng. Sci., 32, 763-774 (1977).

[102] Sorensen, J. P., S. B. Jorgensen and K. Clement, *Fixed-Bed Reactor Kalman Filtering and Optimal Control-I. Computational Comparison of Discrete vs Continuous Time Formulation*, Chem. Eng. Sci., 35, 1223-1230 (1980).

[103] Sorensen, J. P., S. B. Jorgensen and K. Clement, *Fixed-Bed Reactor Kalman Filtering and Optimal Control-II. Experimental Investigation of Discrete Time Case with Stochastic Disturbances*, Chem. Eng. Sci., 35, 1231-1236 (1980).

[104] Stephens, A. D., *Stabilities and Optimization of a Methanol Convertor*, Chem. Eng. Sci., 30, 1619 (1975).

[105] Stephanopoulous, G., *Chemical Process Control: An Introduction to Theory and Practice*, Prentice-Hall, Englewood Cliffs, New Jersey (1984).

[106] Strangeland, B. E. and A. S. Foss, *Control of a Fixed Bed Chemical Reactor*, I & EC Fundamentals, 9, 38-48 (1970).

[107] Van Doesburg, H. and W. A. de Jong, *Dynamic Behavior of an Adiabatic Fixed Bed Methanator*, Proc. of the 3rd Int. Sym. Chem. Reaction Eng., Evanston, Illinois, 489 (1974).

[108] Vakil, H. B., M. L. Michelsen, and A. S. Foss, *Fixed-Bed Reactor Control with State Estimation*, Ind. Eng. Chem. Fundam., 12, 328-335 (1973).

[109] Van Heerdeen, C., *Autothermic Processes. Properties and Reactor Design*, Ind. Eng. Chem., 45, 1242-1247 (1953).

[110] Van Heerdeen, C., *The Character of the Stationary State of Exothermic Processes*, Chem. Eng. Sci., 8, 133-145 (1958).

[111] Villadsen, J. V. and W. E. Stewart, em Solution of Boundary-Value Problems By Orthogonal Collocation, Chem. Eng. Sci., 22, 1483-1501 (1967).

[112] Villadsen, J. V. and M. L. Michelsen, em Solution of Differential Equation Models By Ploynomial Approximation, Prentice-Hall, Englewood Cliffs, New Jersey (1978).

[113] Wallman, P. H., J. M. Silva and A. S. Foss, *Multi-Bed Catalytic Reactor Control Systems: Configuration Development and Experimental Testing*, Ind. Eng. Fundam., 18, 383-391 (1979).

[114] Wallman, P. H., J. M. Silva, and A. S. Foss, *Multivariable Integral Controls for Fixed-Bed Reactors*, Ind. Eng. Fundam., 18, 392-399 (1979).

[115] Wandrey, C. and A. Renken, *Ignition and Extinction of Autothermal Reactors at Periodic Operation*, Chem. Eng. Sci., 32, 448-451 (1977).

[116] Wright J. D., J. F. MacGregor, A. Jutan, J. P. Tremblay and A. Wong *Inferential Control of an Exothermic Packed-Bed Tubular Reactor*, Proc. Joint Auto. Control Conf., San Francisco (1980).

VITA

Moon Kyu Ko was born in Daejon, Korea on February 25, 1955. He graduated from Daejon High School in February 1974. The following March he entered Sung Kyun Kwan University, and in February 1978 he received a Bachelor of Science degree in Chemical Engineering. In the spring of 1978 he entered graduate school at Korea University, Seoul pursuing a Master of Science degree in Chemical Engineering. This degree was awarded in February 1980. In the fall of 1981 he entered graduate school at the University of Tennessee, Knoxville pursuing Master of Science degree in Chemical Engineering. This degree was awarded in December 1986. In August 1991 the author received the Doctor of Philosophy degree in Chemical Engineering.